

University of Alberta

**Multi-dimensional Water Flow and Solute Transport in Heterogeneous,
Layered Soils**

by

Yanyan Sunny Song

A thesis submitted to the Faculty of Graduate Studies and Research
in partial fulfillment of the requirements for the degree of

**Master of Science
in
Soil Science**

Department of Renewable Resources

© Yanyan Sunny Song

Fall 2012
Edmonton, Alberta

Permission is hereby granted to the University of Alberta Libraries to reproduce single copies of this thesis and to lend or sell such copies for private, scholarly or scientific research purposes only. Where the thesis is converted to, or otherwise made available in digital form, the University of Alberta will advise potential users of the thesis of these terms.

The author reserves all other publication and other rights in association with the copyright in the thesis and, except as herein before provided, neither the thesis nor any substantial portion thereof may be printed or otherwise reproduced in any material form whatsoever without the author's prior written permission.

Dedication

I would like to dedicate this to my mom and Dad, Guizhen Lu and Junping Song for their lifetime of support.

Abstract

Onsite, at-grade wastewater treatment systems have the task of the remediation of wastewater for people living in remote areas. The design of efficient onsite wastewater treatment systems is very important to environmental safety and human health. The efficiency of the wastewater treatment depends on the travel time and the contact length of the wastewater through the vadose zone. Therefore, understanding and accurately modeling the hydraulic process of the system is very important for designing the system and quantifying the environmental risks of the system. The hydraulic processes occurring in an onsite at-grade wastewater treatment system are similar to those of a layered field soil under a surface line source boundary condition. Water flow and solute transport under these conditions has been investigated in simplified, homogeneous soils, but field soils are more complex with spatially variable hydraulic properties and soil horizons/layers. The overall objective of the research is to increase our understanding of, and develop methods to predict, the infiltration of water and solutes into field soils for boundary conditions typical of surface at-grade (on-site) wastewater treatment systems with the use of a numerical hydrological model (HYDRUS). Specially, the

influence on the spatial variability, horizonation (layering) and spatial correlation of soil hydraulic properties on flow and transport behavior under surface line sources was quantified.

The influence of the spatial correlation of the hydraulic variability in each horizon and the cross-correlation across the horizon interface was introduced into soil hydrological models and investigated in two ways: 1) assuming Miller-similar media and simulating scaling factors continuously across the domain using a spatially correlated random field generator; different average values of the scaling factors were assigned to each horizon simulate the differences of the hydraulic properties in two horizons; and 2) using the spatial pattern of the laboratory-measured hydraulic properties of a non-Miller-similar layered field soil to generate a more realistic three-dimensional soil domain. Results indicate that in a Miller-similar media, the hydraulic response was sensitive to the variability of the hydraulic properties, and more sensitive to the variability close to the surface line source than at greater depths. The magnitude of the variance and spatial correlation of the soil hydraulic properties significantly influenced the vertical solute travel time directly underneath the surface line source. The difference between the

maximum and minimum solute travel time (10 days) was expected to have significant influence on the remediation of the pathogenic bacteria and potentially, viruses. The simulated hydraulic outputs (average and variance of the water storage) were also found to be sensitive to the variation of the input hydraulic properties for the non-Miller-similar field soil. These results indicate that soil type and soil heterogeneity should be considered for risk-based designs of on-site at-grade wastewater disposal systems.

Acknowledgement

This would not have been possible without the help of my supervisors, Dr. Miles Dyck and Dr. Gary Kachanoski. I am indebted to the knowledge, patience, and encouragement of both of them. I'd like to thank Gary for accepting me as his graduate student when I was not sure where to go for my future. His knowledge of soil physics and enthusiasm was the first thing that made me attracted by soil physics. He has always been very responsible to me. Miles is always very kind and patient to me. He treated me with the respect of an older and wiser sibling. He has guided me through my entire M.Sc studies, and helped me solve lots of problems. I could not have wished for better supervisors than Gary and Miles.

I also would like to thank my external examiner, Dr. Juliana Leung for her advice and critical review.

Other professors, supporting staff in the renewable resources department, also supported me with their knowledge.

And finally, a big thank you to all my friends, family members, and all my lab group members for their support and friendship.

Table of Contents

1. General Introduction	1
1.1 Background	1
1.2 Analytical Models of water flow and solute transport in soils	4
1.2.1. Analytical solutions of steady state infiltration from a surface line source	4
1.2.2 Solute travel time as a function of average water content and Gardner's parameter α	10
1.2.3 Analytical solution for infiltration in heterogeneous soil.....	11
1.3. Numerical models for predicting infiltration in heterogeneous model	14
1.4. Onsite pressurized At-grade Waste Water Treatment System.....	20
1.5. Modeling of heterogeneous layered soil.....	23
1.6. Objective of the Study.....	24
1.7. References	25
2. Sensitivity of vertical flux, volumetric water content, velocity and conservative solute travel time directly underneath surface line source at steady state	31
2.1 Introduction	31
2.2. Theory	33
2.3. Methods.....	35
2.3.1. Model construction.....	35
2.3.2. Miller-Miller scaling factors	37
2.3.3. Calculations	41
2.4. Results and Discussion	42
2.5. Conclusion.....	54
2.6. References	55
3. Simulation of three-dimensional flow under surface line sources: sensitivity analysis and model calibration.....	76
3.1. Introduction	76
3.2. Methods.....	78
3.2.1. Data from 2-D surface infiltration on layered field soil.....	78
3.2.2. Hydraulic Property Model and Parameterization of Flow Model	81

3.2.3.	Three-dimensional random field generation hydraulic properties for the numerical model.....	82
3.2.4.	Model selection and description	89
3.2.5.	Calibration of the numerical model	90
3.2.6.	Initial condition	93
3.2.7.	Error Analysis-Least Square Method.....	93
3.2.8.	Scale-dependent variance.....	94
3.2.9.	Sensitivity Analysis for VG parameters.....	95
3.3.	Results and Discussion	97
3.3.1.	Calibration.....	97
3.3.2.	Sensitivity Analysis.....	98
3.3.3.	Mean and variance of transient soil water storage	100
3.3.4.	Least Square Error Contour Map	102
3.3.5.	Limitations of the numerical model	103
3.4.	Conclusion.....	107
3.5.	References	110
4.	General Discussion and Conclusion.....	149
4.1.	Summary and contribution of this M.sc thesis	149
4.2.	Future research	152
4.3.	References	152
	APPENDIX A: HYDRUS software package for simulating two and three-dimensional water flow, heat and solute transport.....	154

List of Tables

Table 2-1: Scaling factors and related parameters and corresponding conservative travel time	58
Table 3-1: Parametric variogram model parameters	112
Table 3-2: Simulated average water storage with initial condition h=-20 cm and followed by 20 days drainage	113
Table 3-3: Ranges of the parametric variogram models and the corresponding empirical variogram of the each simulated van Genuchten parameter	114

List of Figures

Figure 2-1: (a) Illustration of finite element size distribution and (b) Boundary conditions of two dimensional numerical model in HYDRUS 2D	59
Figure 2-2 : HYDRUS model output of soil water content at steady state (1000 days) corresponding to uniform loam soil.....	60
Figure 2-3: Hydrus model output of soil water content at steady state (1000 days) corresponding to 0 cm correlation range, 10% CV, and $A_{ave}=0.75$ $B_{ave}=1.318$ (maximum travel time)	61
Figure 2-4: : HYDRUS model output of soil water content at steady state corresponding to 15 cm correlation range, 100% CV, and $A_{ave}=1.236$ $B_{ave}=0.7$ (minimum travel time)	62
Figure 2-5: HYDRUS model output of soil water matric potential at steady state (1000 days) corresponding to uniform loam soil.....	63
Figure 2-6: HYDRUS model output of soil water matric potential at steady state (1000 days) corresponding to 0 cm correlation range, 10% CV, and $A_{ave}=0.75$ $B_{ave}=1.318$ (maximum travel time).....	64
Figure 2-7: HYDRUS model output of soil water matric pressure head at steady state (1000days) corresponding to 15 cm correlation range, 100% CV, and $A_{ave}=1.236$ $B_{ave}=0.7$ (minimum travel time)	65
Figure 2-8: Soil water retention curve (θ versus h) with average of matric potential scaling factors equals 1, 0.7, 0.75, 0.9, 1.127, 1.236, 1.318.....	66
Figure 2-9: Soil water hydraulic conductivity (K_s) versus soil water content (θ) average of matric potential scaling factors equals 1, 0.7, 0.75, 0.9, 1.127, 1.236, 1.318	67
Figure 2-10: Soil water matric potential scaling factor ($A_{ave}=B_{ave}=1$).....	68

Figure 2-11: Volumetric water content directly beneath the surface line source at steady state	69
Figure 2-12: Vertical flux density directly beneath the surface line source at steady state	70
Figure 2-13: Vertical flux density (log scale) directly beneath the surface line source at steady state	71
Figure 2-14: Vertical velocity directly beneath the surface line source at steady state	72
Figure 2-15: Vertical velocity directly beneath the surface line source within top 10 cm at steady state	73
Figure 2-16: Vertical velocity (log scale) directly beneath the surface line source at steady state	74
Figure 2-17: Conservative travel time versus Range of correlation in vertical direction directly beneath the surface line source at steady state	75
Figure 3-1: Estimated empirical variogram for K_s.....	115
Figure 3-2: Estimated empirical variogram for α	116
Figure 3-3: Estimated empirical variogram for n.....	117
Figure 3-4: Estimated empirical variogram for θ_s.....	118
Figure 3-5: parametric variogram model for K_s	119
Figure 3-6: Parametric variogram model for α.....	120
Figure 3-7: Parametric variogram model for n.....	121
Figure 3-8: Parametric variogram model for saturated water content θ_s	122
Figure 3-9: Boundary condition of the numerical model (HYDRUS)	123
Figure 3-10: Output results after 10 days of simulation (HYDRUS)	124
Figure 3-11: Comparison of average water in top 25 cm and 60 cm of simulated output versus field measurement.....	125
Figure 3-12: Comparison of water storage variance in top 25 cm and 60 cm of simulated output versus field measurement	126
Figure 3-13: Soil water storage from numerical simulations with input VG parameter $\theta_s \pm 20\%$, and TDR measured	

	field data. The simulation corresponding to unmodified VG parameters is utilized as a reference	127
Figure 3-14:	Soil water storage from numerical simulations with input VG parameter $\pm 20\%$, and TDR measured field data. The simulation corresponding to unmodified VG parameters is utilized as a reference	128
Figure 3-15:	Soil water storage from numerical simulations with input VG parameter $\pm 20\%$, and TDR measured field data. The simulation corresponding to unmodified VG parameters is utilized as a reference	129
Figure 3-16:	Soil water storage from numerical simulations with input VG parameter $K_s \pm 20\%$, and TDR measured field data. The simulation corresponding to unmodified VG parameters is utilized as a reference	130
Figure 3-17:	Soil water storage from numerical simulations with CV of the input VG parameter K_s decreased by 10%, and TDR measured field data. The simulation corresponding to unmodified VG parameters is utilized as a reference	131
Figure 3-18:	Soil water storage from numerical simulations with CV of the input VG parameter $n \pm 10\%$, and TDR measured field data. The simulation corresponding to unmodified VG parameters is utilized as a reference	132
Figure 3-19:	Soil water storage from numerical simulations with CV of the input VG parameter $\alpha \pm 10\%$, and TDR measured field data. The simulation corresponding to unmodified VG parameters is utilized as a reference	133
Figure 3-20:	Soil water storage from numerical simulations with CV of the input VG parameter $\theta_s \pm 10\%$, and TDR measured field data. The simulation corresponding to	

unmodified VG parameters is utilized as a reference	134
Figure 3-21: Histogram of lab-measured α and n distributions .	135
Figure 3-22: Comparison of average water storage from numerical simulations with optimum input VG parameters versus TDR measured field data	136
Figure 3-23: Comparison of average soil water storage from numerical simulations with optimum input VG parameters versus TDR measured field data	137
Figure 3-24: Contour maps of sum of square errors (SSE) of average water storage and the corresponding variance.	138
Figure 3-25: Indication of the transect corresponding to the hydraulic properties measurement and transect of the 2D infiltration experiment.	139
Figure 3-26: Classed post maps of lab-measured θ_s and the optimized θ_s along the line source transect	140
Figure 3-27: Classed post maps of lab-measured α and the optimized α along the line source transect.....	141
Figure 3-28: Classed post maps of lab-measured n and the optimized n along the line source transect.....	142
Figure 3-29: Classed post maps of lab-measured n and the optimized Ks along the line source transect	143
Figure 3-30: Comparison of the parametric variogram models and the corresponding empirical variograms of the simulated VG parameter θ_s.....	144
Figure 3-31: Comparison of the parametric variogram models and the corresponding empirical variograms of the simulated VG parameter α.....	145
Figure 3-32: Comparison of the parametric variogram models and the corresponding empirical variograms of the simulated VG parameter n.....	146
Figure 3-33: Comparison of the parametric variogram models and the corresponding empirical variograms of the simulated VG parameter Ks.....	147

Figure 3-34: Spatial-scale dependent variance of average water storage of both 25 cm and 60 cm depth of both field measurement and numerical model simulation148

List of Symbols and Abbreviations

VG	van Genuchten
2D	two-dimensional
3D	three-dimensional
q	water flux density
K	soil water hydraulic conductivity
H	total hydraulic potential
h	soil water matric potential
z	vertical direction coordinate
x	horizontal directions coordinate (perpendicular to the source)
y	horizontal directions coordinate (along the source)
θ	volumetric water content
t	time
K_s	saturated hydraulic conductivity
α	van Genuchten or Gardner's hydraulic parameter related to air entry potential
n	van Genuchten hydraulic parameter related to the slope of water retention curve
θ_s	saturated soil water content
θ_r	residue soil water content
S_e	effective saturation
ϕ	matric flux potential
q_z	vertical flux density

q_x	horizontal flux density
v	vertical velocity
Q_L	line source strength
T	conservative ionic tracer travel time
Y	$\ln(K_s)$
$\langle \cdot \rangle$	expectation value operator
$Var\langle \cdot \rangle$	variance operator
$Cov\langle \cdot \rangle$	covariance operator
\mathbf{u}	location vector
λ_h	soil water matric potential scaling factor
λ_K	soil water matric hydraulic conductivity scaling factor
h^*	field average soil water matric potential
K^*	field average soil water hydraulic conductivity
γ	semivariogram
c_0	nugget effect
c	variance contribution
a	actual range
l	lag distance
A_{ave}	mean of λ_h in the A horizon
B_{ave}	mean of λ_h in the B horizon
A	number of scaling factors corresponding locations or number of finite element nodes in the A horizon

B	number of scaling factors corresponding locations or number of finite element nodes in the B horizon
T_w	conservative solute travel time
CV	coefficient of variation
W_L	soil water storage beneath surface line sources
L	length of soil water storage measurement
$E[\cdot]$	mean operator
$CV[\cdot]$	coefficient of variation operator
G_i	field measurement
$\hat{G}_i(t)$	model prediction
ε_i	error term associated with the field measurement and the model prediction
SSE	sum of squared errors function
X	spatial series

1. General Introduction

1.1 Background

The human health and environmental risks associated with the aqueous transport of contaminants released into the soil profile are major public concerns. Onsite wastewater treatment systems are designed to facilitate the treatment of wastewater from small communities where it may be impractical to have services from large centralized treatment systems (Tyler and Mokma, 2004). How to design, manage and maintain well performed, cost effective, environmental safety onsite wastewater treatment systems for small communities across Canada is one of the four priority Environmental issues identified by the Canadian Council of Ministers of Environment (Joy et al., 2003).

Most wastewater treatment systems in Canada are subsoil, septic tank systems. However, newer onsite pressurized at-grade wastewater treatment systems are potentially a better choice than the subsoil systems when septic tank installation is not feasible, practical, cost-effective or desirable such as in forested regions, shallow water table areas, and tight clay soils. Onsite, pressurized, at-grade wastewater

system are composed of pressurized, piping with equally spaced orifices placed on the soil surface, which delivers wastewater evenly to the soil surface along a transect (Juma et. al, 2007; Juma et. al, 2010). There is a great potential for the onsite pressurized at-grade wastewater treatment system to be widely used in Alberta (Juma et. al, 2010).

The purification process of wastewater delivered to the soil is achieved by extensive and lengthy contact between the effluents with the soil matrix in the vadose zone (Van Cuyk, 2000). Effective treatment in soil is an aerobic process, so treatment depends on the travel time through the vadose zone, and by corollary depth of the vadose zone. Therefore, it is very important to understand and to accurately model the hydraulic processes of the system, especially the solute travel time to assess the environmental risk associated with the system.

Water flow and solute transport in the vadose zone at the field scale is much more complex than a homogeneous laboratory column soil. The complexity of the process is due to the spatial variability of soil hydraulic properties (Tuli et al, 2001). Quantification of the environmental risks associated with the design of on-site wastewater

treatment system requires the application and development of models that describe water flow and solute transport processes in soils and predict the magnitude of water and contaminant fluxes in the vadose zone.

Variability in soil hydraulic properties is a result of variability inherent in the soil parent material (i.e. texture, mineralogy and mode of parent material deposition) and soil horizons developed during pedogenesis. Pedogenic processes acting on soil parent material have resulted in the formation of distinct soil horizons separated by horizon interfaces. The process of soil genesis is primarily hydraulically based. Therefore, it is reasonable to expect that the spatial patterns of soil horizon properties above and below a horizon interface are statistically dependent on each other. Field experiments have shown that the hydraulic variability of soil is spatially scale-dependent and cross-correlated across the horizon interface. However, how to best incorporate the influence of the spatial correlation into soil hydrological models has not been thoroughly investigated.

In the following, a brief review of literature of both the analytical models and the numerical models of water flow and solute transport in soils relevant to onsite at-grade wastewater treatment

system, and a description of the onsite waste water treatment systems is given. The relevant literature has been grouped into the following categories: 1) analytical solutions of steady state infiltration from surface line source; 2) tracer travel time as a function of average water content and Gardner's parameter α ; 3) analytical solution for two dimensional (2-D) infiltration in heterogeneous soil; 4) numerical model for predicting infiltration process in heterogeneous model; and 5) onsite pressurized At-grade Waste Water Treatment System. The literature review is followed up by an overview of the research content and organization of the thesis. At the end of this chapter, a statement of the focus and objective of this thesis is outlined.

1.2. Analytical Models of water flow and solute transport in soils

1.2.1. Analytical solutions of steady state infiltration from a surface line source

Water flow and solute transport through soil is dependent on the initial and boundary conditions and by the nature of hydraulic properties of the soil system. In this study, we are particularly interested in two-dimensional (2D) infiltration from a surface line source through heterogeneous layered (horizonated) soil because these

conditions are most similar to onsite pressurized at-grade wastewater treatment systems.

The analytical solution for the infiltration process from an infinite surface line source through homogeneous soil developed by Philip (1971) is two-dimensional, symmetric and also assumes the soil is isotropic. In a field soil, the process under the same boundary condition is three-dimensional and asymmetric due to the hydraulic heterogeneity of the soil. Field soils may also be anisotropic. Regardless, the 2D homogeneous solution of Philip (1971) is useful for understanding which soil hydraulic properties are most influential over the hydraulic behavior of these systems.

In unsaturated soils, soil water flux density q ($\frac{cm^3}{cm^2}$), is described by the Buckingham-Darcy flux law (Jury et al., 1991):

$$q = -K(h)\nabla H \quad [1-1]$$

where $K(h)$ is the soil hydraulic conductivity ($\frac{cm^3}{cm^2 day}$) as a function of matric potential h in head units (cm), $H = h + z$ (cm), H is total hydraulic potential in head units (cm), which is the sum of the matric

potential h and gravitational potential z , ∇ is the gradient operator, with

$$\nabla H = \frac{\partial H}{\partial x} + \frac{\partial H}{\partial y} + \frac{\partial H}{\partial z} \quad [1-2]$$

where x , y and z are the spatial coordinates (cm). Water flows from high H to low H .

Recall the equation of continuity,

$$\frac{\partial \theta}{\partial t} = \nabla \cdot \mathbf{q} \quad [1-3]$$

where θ ($\frac{m^3}{m^3}$) is the volumetric soil water content, and t (day) is the time. Richards (1931) combined the continuity equation with the Buckingham-Darcy flux law into what is now known as the Richard's equation:

$$\frac{\partial \theta}{\partial t} = -\nabla[K(h)\nabla H] \quad [1-4]$$

A quasilinear solution for steady state infiltration from a surface line source through a homogeneous, infinite soil system with unrestricted drainage was developed by Philip (1971) using the Kirchoff transform. The Kirchoff transform defines the matric flux

potential $\phi(h)$ ($\frac{m^2}{s}$), as the area under the soil hydraulic conductivity versus matric potential curve

$$\phi(h) = \int_{-\infty}^h K(h)dh \quad [1-5]$$

The non-linear relationship between k and h can be approximated by an exponential function (Gardner, 1958). Specifically,

$$K(h) = K_s e^{\alpha h} \quad [1-6]$$

Where $h \leq 0$, and α ($\frac{1}{cm}$) is the slope of $\ln(K)$ versus $\ln(h)$ curve.

For steady-state 2D flow, the left hand side of Eq. [1-4] equals zero. Substituting Eqs. [1-5] and [1-6] into Eq. [1-4], Philip (1966) derived an equation called the quasilinearized steady flow equation:

$$\alpha \left(\frac{\partial \phi}{\partial z} \right) = \nabla^2 \phi \quad [1-7]$$

Where ∇^2 is the Laplacian operator in Cartesian rectangular coordinates x and z with z representing the vertical direction (positive downward), and x is in the horizontal direction perpendicular to the surface line source (along the y direction). Eq. [1-5] can be reformulated as (Philips, 1971)

$$2 \left(\frac{\partial \Theta}{\partial Z} \right) = \nabla^2 \Theta \quad [1-8]$$

where Θ and Z are dimensionless variables given by,

$$X = \frac{\alpha x}{2} \quad Z = \frac{\alpha z}{2} \quad R = \frac{\alpha r}{2} \quad [1-9]$$

and for a surface infinite line source with a source strength Q ($\frac{m^3}{m \text{ day}}$),

the dimensionless variables Θ , V , U are given by

$$\Theta = \frac{2\pi\phi}{Q} \quad [1-10]$$

$$V = \frac{2\pi q_z}{aQ} = \Theta - \frac{1}{2} \frac{\partial \Theta}{\partial Z} \quad U = \frac{2\pi q_x}{aQ} = -\frac{1}{2} \frac{\partial \Theta}{\partial X} \quad [1-11]$$

Where q_z and q_x ($\frac{m^3}{m^2 s}$) are the soil water flux density from the surface line source in the vertical direction and horizontal direction respectively. In particular,

$$q_z = \alpha\phi - \partial\phi / \partial z \quad q_x = -\partial\phi / \partial x \quad [1-12]$$

The solution of the surface line source is defined in the range $-\infty \leq X \leq \infty, 0 \leq Z \leq \infty$. The appropriate boundary conditions are (Philip, 1971);

$$\lim_{S \rightarrow \infty} \Theta = 0, \text{ and } \lim_{S \rightarrow \infty} V = 0 \quad [1-13]$$

$$Z = 0, X \neq 0, V = 0 \quad [1-14]$$

where $S = (X^2 + Z^2)$.

Thus the analytical solution for predicting infiltration process below a surface line source is:

$$V = \frac{Z}{S} e^Z K_1(S) \quad [1-15]$$

and

$$\Theta = 2e^Z [K_0(S) - e^Z \int_Z^\infty e^{-Z} K_0(S) dZ] \quad [1-16]$$

The dimensionless matrix flux along the vertical axis is found to be

$$\Theta(0, Z) = 2e^Z [(1 + Z)K_0(Z) - ZK_1(Z)] \quad [1-17]$$

and the vertical soil water flux density

$$V(0, Z) = e^Z [K_1(Z)] \quad [1-18]$$

where K_0 and K_1 are the zeroth order and the first order modified Bessel function of the second kind.

1.2.2 Solute travel time as a function of average water content and Gardner's parameter α

By utilizing Philip's (1971) solution for two dimensional surface infiltrations from a line source under steady state conditions, Zhang (2000) derived a solution for travel time of an ionic tracer along a vertical streamline. Expansion of the solution of Philip (1971) gives

$$q_z(x, z) = \frac{\alpha Q_L}{2\pi} \frac{z}{\sqrt{z^2 + x^2}} e^{\frac{\alpha z}{2}} K_1\left(\frac{\alpha}{2} \sqrt{z^2 + x^2}\right) \quad [1-19]$$

where Q_L is the line source strength.

When $x = 0$, the flow is directly below the line source and is vertical and Eq. [1-19] becomes

$$q_z(z) = \frac{\alpha Q_L}{2\pi} e^{\frac{\alpha z}{2}} K_1\left(\frac{\alpha}{2} z\right) \quad [1-20]$$

The velocity of the pore water $v\left(\frac{m}{s}\right)$, in the vertical direction is given by

$$v(z) = \frac{dz}{dt} = \frac{q_z(z)}{\theta(z)} \quad [1-21]$$

Combine Eq. [1-20] and Eq. [1-21], the travel time $T(z^*)$ of a conservative ionic tracer under vertical flow is (Zhang, 2000)

$$T(z^*) = \frac{2\pi}{\alpha Q_L} \int_0^{z^*} \frac{\theta(0,z)}{e^{\frac{\alpha z}{2}} K_1\left(\frac{\alpha}{2}z\right)} dz \quad [1-22]$$

1.2.3 Analytical solution for infiltration in heterogeneous soil

In heterogeneous soils, the mean, variance and covariance of hydraulic properties of the soil influence significantly water flow and solute transport.

Small perturbation theory

Zhang (2002) presented an analytical solution that incorporated the influence of the variance of soil matric potential (h), soil water content (θ), and water storage (W) for two dimensional infiltration from an infinite surface line source through heterogeneous soil. In his approach, he assumed that the variability of Gardner's α and Y are small, where

$$Y = \ln(K_s) \quad [1-23]$$

In the solution, each hydraulic parameter are represented as a mean expectation value $\langle \cdot \rangle$ and a random space fluctuation (Zhang 1999)

$$\begin{aligned} \alpha &= \bar{\alpha} + \alpha' & \langle \alpha \rangle &= \bar{\alpha} & \langle \alpha' \rangle &= 0 \\ Y &= \bar{Y} + Y' & \langle Y \rangle &= \bar{Y} & \langle Y' \rangle &= 0 \end{aligned} \quad [1-24]$$

In addition, the variance operator is defined as $\text{Var}(\cdot)$, and the covariane operator is defined as $\text{Cov}(\cdot)$.

From Eq. [1-5] and [1-6],

$$h(x, z) = \frac{1}{\alpha} \ln \left[\frac{\alpha}{K_s} \phi(x, z) \right] \quad [1-25]$$

Substituting Eq. [1-24] into Eq. [1-25] , and expanding Eq.[1-25] about $\bar{\alpha}$ and \bar{Y} into a first order Taylor series approximation for h,

$$h(x, z) = \langle h(x, z) \rangle + h'(x, z) \quad [1-26]$$

The expectation value $\langle h \rangle$ and the random fluctuation of h given by $h'(x, z)$ are

$$\langle h(x, z) \rangle = \frac{1}{\alpha} \ln \left(\frac{\bar{\alpha} \langle \phi(x, z) \rangle}{e^{\bar{Y}}} \right) \quad [1-27]$$

$$h'(x, z) = A_\alpha(x, z) \alpha' + A_Y Y' \quad [1-28]$$

Zhang (2000) claimed that sufficient field data supported that K_s follows a lognormal distribution, and $A_Y = \langle \frac{\partial h(x, z)}{\partial Y} \rangle = -\frac{1}{\alpha}$. However, there was not enough information for determining the natural distribution of α , and the expression of $A_\alpha(x, z) = \langle$

$\partial h(x, z)/\partial \alpha >$ depends on the shape of the probability density function (Zhang 2002).

From Eq. [1-28], the analytical solution for variance of h, Var_h is given by

$$Var_h(x, z) = A_\alpha^2(x, z)Var_\alpha + A_Y^2Var_Y + 2A_\alpha(x, z)A_YCov_{\alpha Y} \quad [1-29]$$

Zhang (1999) applied a similar procedure to estimate the variance of θ , $Var_\theta(x, z)$. The expected value for soil water content was

$$\langle \theta(x, z) \rangle = \theta_r + (\bar{\theta}_s - \theta_r) [e^{0.5\bar{\alpha}\langle h(x, z) \rangle} (1 - 0.5\bar{\alpha}\langle h(x, z) \rangle)]^{\frac{2}{2+m}} \quad [1-30]$$

In this equation, θ_r is the residual water content and was assumed constant. The variance of θ , Var_θ was obtained as

$$\begin{aligned} Var_\theta(x, z) = & B_{\theta_s}^2(x, z)Var_{\theta_s} + B_\alpha^2(x, z)Var_\alpha + B_Y^2(x, z)Var_Y + \\ & 2B_\alpha(x, z)B_YCov_{\alpha Y} + 2B_{\theta_s}(x, z)B_\alpha Cov_{\theta_s \alpha} + \\ & 2B_{\theta_s}(x, z)B_Y(x, z)Cov_{\theta_s Y} \end{aligned} \quad [1-31]$$

And where $B_{\theta_s}(x, z) = \langle \frac{\partial \theta(x, z)}{\partial \theta_s} \rangle$,

$$B_\alpha(x, z) = \langle \frac{\partial \theta(x, z)}{\partial \alpha} \rangle, B_Y(x, z) = \langle \frac{\partial \theta(x, z)}{\partial Y} \rangle$$

For the case of water storage $w(x, L)$, integrate Eq. [1-31] from soil surface to depth L, the variance Var_w is given by

$$\begin{aligned}
Var_w(x, L) = & \left[\int_0^L B_{\theta_s}(x, z) dz \right]^2 Var_{\theta_s} + \left[\int_0^L B_{\alpha}(x, z) dz \right]^2 Var_{\alpha} + \\
& \left[\int_0^L B_Y(x, z) dz \right]^2 Var_Y + 2 \left[\int_0^L B_{\alpha}(x, z) dz \right] \left[\int_0^L B_Y(x, z) dz \right] Cov_{\alpha Y} + \\
& 2 \left[\int_0^L B_{\theta_s}(x, z) dz \right] \left[\int_0^L B_{\alpha}(x, z) dz \right] Cov_{\theta_s \alpha} + \\
& 2 \left[\int_0^L B_{\theta_s}(x, z) dz \right] \left[\int_0^L B_Y(x, z) dz \right] Cov_{\theta_s Y} \quad [1-32]
\end{aligned}$$

In the small perturbation model, it was assumed there was no cross-correlation between α and K_s , and the model is of first order precision.

1.3. Numerical models for predicting infiltration in heterogeneous model

Field soils are usually composed of at least two horizons. Soil properties in each horizon are spatially variable. Different than independent geological layers, the soil properties of soil horizons are spatially-dependent on each other as they were formed under pedogenic process acting on the same parent material. Dyck (2008) tested the influence of soil horizons on the hydraulic behavior of the entire soil profile and found that the influence is scale dependent, different for transient and steady infiltration, and is dependent on the covariance of the shape of the interface and soil hydraulic properties.

Numerical models for simulating water flow and heat and solute transport processes have become more popular than analytical models over the last 20 years because of the development of cost-effective, powerful computing. The hydraulic property models used in analytical solutions for predicting infiltration process in heterogeneous soil are not always very representative of natural soils (Yeh et al., 1985a, Yeh et al., 1985b, Yeh et al., 1985c, Zhang, 1999). There are lots of assumptions that have to be made in the analytical approaches. For example, the small perturbation theory (Zhang, 1999) has assumed the variability of Gardner's α and the Y value are small, and there is no cross-correlation between α and K_s . The Numerical models (e.g. HYDRUS 3D) on the other hand, allow prediction of infiltration with a larger degree of complexity and dimensionality in both saturated and unsaturated media (Šimůnek and van Genuchten, 2007; Šimůnek and van Genuchten, 2008). Numerical model can also utilize more realistic hydraulic models such as van Genuchten's (VG) hydraulic model (van Genuchten, 1980).

van Genuchten (1980) derived a model for the soil water retention curve and the corresponding expression of the relative hydraulic conductivity $K_r(S_e)$ (cm/day) as a function of effective

water saturation S_e . The van Genuchten (VG) parameters α, n, θ_r and θ_s may be obtained from curve fitting of the theoretical water retention model to experimental data of specific soils. The VG model is given by

$$S_e(h) = (1 + (\alpha h)^n)^{\frac{1}{n}-1} \quad [1-33]$$

$$K(S_e) = K_S(S_e)^{0.5} \left\{ 1 - \left(1 - (S_e)^{\frac{n}{n-1}} \right)^{1-\frac{1}{n}} \right\}^2 \quad [1-34]$$

and the effective saturation S_e is determined as

$$S_e = \frac{\theta - \theta_r}{\theta_s - \theta_r} \quad [1-35]$$

where h is the soil water matric potential (cm), α (cm^{-1}) is related to the air entry value, n (dimensionless) is an indicator of the variance of pore size distribution, θ is the volumetric water content ($cm^3 cm^{-3}$), θ_r is the residual volumetric water content ($cm^3 cm^{-3}$), and θ_s is the saturated soil water content or porosity ($cm^3 cm^{-3}$).

The hydraulic variability of a soil in a numerical model can be incorporated in various ways. For example, in a linear scaling scheme, the soil hydraulic properties ($\theta(h)$, $K(h)$, K_s) at a given location are related to the field average soil hydraulic properties of the soil domain

considered by using spatially variable, linear scaling factors (Miller and Miller, 1956, Miller, 1980):

$$h(S_e, \mathbf{u}) = \lambda_h(\mathbf{u}) \cdot h^*(S_e) \quad [1-36]$$

$$K(S_e, \mathbf{u}) = \lambda_K(\mathbf{u}) \cdot K^*(\Theta S_e) \quad [1-37]$$

where $h(S_e, \mathbf{u})$ is the soil water matric potential (cm) at location (node) \mathbf{u} as a function of effective water saturation S_e , $\lambda_h(\mathbf{u})$ is the soil water matric potential scaling factor as a function of \mathbf{u} , h^* is the field average soil water matric potential (cm) as a function of S_e , $K(S_e, \mathbf{u})$ is the soil water hydraulic conductivity (cm/day) at location \mathbf{u} as a function of S_e , $\lambda_K(\mathbf{u})$ is the soil water hydraulic conductivity scaling factor at location \mathbf{u} , and K^* is the field average hydraulic conductivity (cm/day) as a function of effective saturation S_e . In a Miller-similar media (Miller and Miller, 1956, Miller, 1980), $\lambda_K(\mathbf{u}) = (1/\lambda_h(\mathbf{u}))^2$. All linear scaling schemes, including Miller similarity, assume only the mean of the pore size distribution varies from location to location while the variance of the pore size distribution stays constant (Jury and Sposito, 1990). Therefore, by assigning an appropriate single set of spatially variable, linear scaling factors, soil hydraulic property variability is modeled as a soil with a spatially variable mean pore size.

Another way to model the heterogeneity of a soil is to assign a different set of hydraulic parameters (i.e. VG hydraulic parameters) to each location considered in a soil domain. The hydraulic parameters at each location can be spatially correlated or spatially independent. Unlike the linear scaling schemes, the variance of the pore size distribution may vary from location to location.

Hydraulic properties of soils are usually randomly distributed (van Wesenbeeck and Kachanoski, 1991, 1994; Dyck and Kachanoski, 2009a, 2009b, 2011). The variogram is a function that describes the degree of spatial correlation of a random field (Deutsch and Journé, 1998), which could be used to model the spatial variability of the scaling factors in a linear scaling scheme or the spatial variability of the VG hydraulic parameters. There are several components in a variogram model that influence the nature of the spatial dependence of a random field: The nugget effect of a variogram model which is the value of discontinuity of the variogram at the origin; c , the variance contribution; and a , the actual range which is the distance from the origin to where the variogram started to reach the sill.

The influence of spatial dependence on water flow and soil transport in a field soil can be explained in the concept of stochastic stream tube models. Thus, field soils can be visualized as a composition of infinitesimally small layers of vertical parallel stream tubes with some degree of spatial dependence (Jury and Roth, 1990; Vereecken et al, 2007; Jury and Uttermann, 1992; Sec 1.2.1). In the case of perfect independent stream tubes (hydraulic property of the soil is spatially independent), water leaving a fast flow stream tube at a layer has an equal probability to enter a stream tube at any speed, which implies water flow discontinuity at the stream tubes layer interfaces (Jury and Uttermann, 1992; Sec 1.2.1). In the other case where there are perfect correlations between the layered stream tubes (hydraulic property of the soil is spatially perfectly correlated), water flow has a perfect continuity at the layer interfaces. Water and solute travel time in the bottom layer can be described as a function of the travel time in the top layer (Jury and Uttermann, 1992; Sec 1.2.1). A field soil usually falls in between the two extreme cases. van Wesenbeeck and Kachanoski (1991) had derived that water flow and solute travel time at the field scale is a function of the sum of the travel time in smaller scales. Dyck (2008) had given a detailed

literature review on the scale dependence of water flow and solute travel time in the concept of stochastic stream tube models.

1.4. Onsite pressurized At-grade Waste Water Treatment

System

Onsite wastewater treatment systems are designed for small communities. These systems can be divided into two types of systems: 1) the septic tank system (Bouma 1975, Siegrist 1987, Tyler 2001); 2) the pressurized at-grade system (Juma et al., 2007; Juma et al., 2011). In both systems, the waste water has been treated to an acceptable quality to an acceptable concentration prior to being delivered to the soil system (Tyler and Mokma, 2004). In the septic tank wastewater treatment system, the treated waste water is delivered through an underground septic tank. There is a thin, fine-texture organic biomat on the bottom and side surface of the tank which significantly reduces the flow rate of the effluent into the soil system and has an important role for purifying the sewage (Van Cuyk et.al, 2000). The at-grade pressurized waste water treatment system delivers treated waste water to the soil surface instead of under the ground. As described by Juma et al. (2007), the system is composed of an arrangement of at-grade

pressurized distribution piping with equally spaced orifices which delivers waste water evenly to the surface of the soil. Compared to the traditional septic tank waste water treatment system, the new onsite pressurized at-grade waste water treatment system does not contain an organic biomat. However, the length of contact time between the sewage and the soil matrix is maximized since the sewage is delivered to the soil surface instead of underground. In addition, the organic matter in the top A horizon of the soil is very chemically reactive, adsorbs many substances and provides energy for soil microorganisms that can degrade the organic contaminants in the wastewater.

For the pressurized at-grade system, human and environmental safety concerns require a system design that minimizes the risk for human and wild life contact with the effluent. Therefore, the distribution piping is often covered by an open bottom chamber or a half-pipe to providing a shielding housing and is further covered by shredded tree branched and wood chips.

There are five main processes in soil that lead to the treatment of waste water (Tyler and Mokma, 2004):

- 1) Filtration: constriction of flow due to the nature of varied pore size distribution which works on the suspended particles.
- 2) Ion exchange: most of the clay mineral in soil contains negative charges, therefore, cations such as sodium, ammonium, and calcium in the wastewater are attracted to the clay mineral surface.
- 3) Chemisorption: substance removed from the sewage by chemical sorption.
- 4) Oxidation-Reduction: these reactions change the form of the compounds and are mainly controlled by microbial activity.
- 5) Soil microorganisms: break down organic matter, enhance chemical reactions (i.e. nitrogen, iron, carbon and sulfur), and remove bacteria and viruses from waste water.

The thickness of the vadose zone and thus the water table depth significantly affects the purification process of sewage in the vadose zone (soil water content, aeration status, and media surface area) and the hydraulic retention time (Van Cuyk et al., 2000). In this study, we assume the water table is very deep and does not affect the process.

The time required for adequate treatment of the water to occur is different for various components of the sewage. For example, the reaction time of nitrogen and phosphorus is very short compared to some fecal coliforms which may take several days to weeks (Tyler and Mokma, 2004). Therefore the sewage travel time in the vadose zone with respect to the soil hydraulic conditions, purification efficiency of the soil, and delivered sewage quality and quantity, is very important to the purification process.

1.5. Modeling of heterogeneous layered soil

In the following two chapters, two different approaches for modeling the heterogeneity and layers for the soil under boundary conditions similar to on-site waste water treatment systems are given. In Chapter 2, the soil domain is assumed to be Miller-similar media. The linear scaling factors at each nodal point in the domain are simulated continuously and layers are introduced by assigning different averages/expected values to the scaling factors for different soil horizons. The spatial variabilities of the scaling factors are modeled using variograms. In Chapter 3, a numerical model is used to predict the hydraulic output of a simulated field soil at the site

investigated by Dyck (2008). The generated VG hydraulic parameters are based on hydraulic properties estimated from laboratory measurements on undisturbed soil cores of the two soil horizons taken from the field site. The spatial correlation of the each hydraulic property was estimated by variograms.

1.6. Objective of the Study

The overall objective of the research is to increase our understanding of, and develop methods to predict, the infiltration of water and chemicals into field soils for boundary conditions typical of surface at-grade (on-site) waste water treatment systems. Specific objectives include:

1. To quantify the influence of heterogeneity of the soil properties of layered soil in a miller similar media on vertical flux, vertical pore water velocity, volumetric water content, and conservative solute travel time for water flow directly underneath a surface line source at steady state.
2. Quantify the influence of spatial correlation (within a layer/horizon and between layers/horizons) on predicted (modelled) infiltration and solute travel time.

3. To develop a method to construct and calibrate a numerical model to predict the hydraulic behaviour of at-grade line source systems in layered heterogeneous field soils. Observed spatial patterns of hydraulic properties of a field soil will be utilized and to get a better understanding of how is the heterogeneity of the hydraulic properties affects the hydraulic behaviour of the at-grade line source systems. In addition, the accuracy or validity of the model will be assessed by comparing the predicted values of a number of state variables (average of the soil water storages, variance of the soil water content) to measured values from a field study (Dyck and Kachanoski, 2009a, Dyck and Kachanoski 2009b).

Since the conservative solutes represent the most mobile form of contaminants, their simulations represent the most risk-conservative scenarios. The transport of organic contaminants and microbes is very complex (these processes are a field study within themselves), thus the simulations in this thesis will only use output from the hydrological model to calculate conservative solute travel times.

1.7. References

- Bouma, J. 1975. Unsaturated flow during soil treatment to septic tank effluent. *J. Am. Soc. Civ. Eng.* 01 (EE6): 967-983.
- Deutsch, C. V. and A. G. Journel, 1998. *GSLIB: Geostatistical software library and user's Guide*, Second Edition.
- Dyck, M. F. 2008. *Physics of water flow and solute transport across a horizon interface*. Ph.D. Univ. of Alberta, Edmonton, AB, Canada.
- Dyck, M. F. and R. G. Kachanoski, 2009a. Measurement of transient soil water flux across a soil horizon interface. *Soil Sci. Soc. Am. J.* 73:1604-1613.
- Dyck, M. F. and R. G. Kachanoski, 2009b. Measurement of steady-state soil water flux across a soil horizon Interface. *Soil Sci. Soc. Am. J.* 73: 1786-1795.
- Dyck, M. F. and R. G. Kachanoski, 2011. Scale-dependent covariance of soil physical properties above and below a soil horizon interface: Pedogenic versus anthropogenic influences on total porosity. *Can. J. Soil Sci.* (2011) 91.
- Evelt, S. R. 2000. The TACQ computer program for automatic time domain reflectometry measurement: I. Design and operating characteristics. *Trans. ASAE* 43: 1939-1946.
- Gardner, W. R. 1958. Some steady-state solutions of the unsaturated moisture flow equation with application to evaporation from a water-table. *Soil Sci.* 85: 228-232.
- Joy, D., C. Kinsley, K. Schaefer, V. Pileggi, S. Skog and S. Kok. 2003. *Link water source to science: Wastewater Treatment for Small Communities*. CCME, Winnipeg, Manitoba. CCME Linking Water Science to Policy Workshop. Series. Report No. 4. 16 p.
- Juma, N. G., I. Bitterlich, and M. H. Rahman, 2007. *Scientific investigation of pressurized, at-grade, private sewage treatment systems*. Department of Ren. R., Univ. of Alberta. Final Report

submitted to the Safety Codes Council, Edmonton, Alberta.
65pp.

Juma, N. G., B. S. Chhabra, S. Khan, S. Singh, A. Durnie and A. Chu. 2010. Comparison of performance of four, pressurized, soil-based dispersal systems at an at-grade installation in Leduc County, Alberta. Department of Renewable Resources, Univ. of Alberta, Edmonton, AB, Canada. Final report submitted to Canada Mortgage and Housing Corp., Ottawa, ON; Alberta Municipal Affairs, Edmonton, AB; Leduc County, AB. 50 pp.

Jury, W.A. and J. Utermann. 1992. Solute transport through layered soil profiles: Aero and perfect travel time correlation models. *Trans. Porous Media*: 8:277-297.

Jury, W. A. and K. Roth. 1991. *Transfer Functions and Solute Movement through Soil. - Theory and Applications -*. Birkhäuser Verlag, Basel, Boston, Berlin 1990; 226 Seiten, DM 65,-. ISBN 3-7643-2509-7.

Miller, E. E., 1980, Similitude and scaling of soil water phenomena. In *Applications of soil Physics*, ed. D. Hillel, 300-318. New York: Academic Press.

Miller, E. E., and R.D. Miller. 1956. Physics theory for capillary flow phenomena. *J. Appl. Phys.* 27:324-32.

Philip, J. R. 1966. Discussion to session IIa. P.523. In *Water in the unsaturated zone. Proc. Wageningen Symposium. IASH/Unesco. Vol. I.*

Philip, J. R. 1971. General theorem on steady infiltration from surface sources, with application to Point and Line Sources. *Proc. Soil sci. Soc.* 35.

Philip, J. R. 1989. Multidimensional steady infiltration to a water table. *Water Resour. Res.*, 25: 109-116.

- Radcliffe, D. E., and L. T. West. 2009. Design hydraulic loading rates for onsite wastewater system. *Vadose Zone J.* 8:64-74.
- Richards, L. A., 1931. Capillary conduction of liquids through porous mediums. *Phys.* 1 (5): 318–333.
- Siegrist, R. L. 1987. Hydraulic loading rates for soil absorption systems based on wastewater quality. In: *On-site wastewater treatment. Proc. Of the 6th National Symposium Individual and Small Community Sewage Systems.* ASAE, St. Joseph, MI. p. 232-241.
- Šimůnek, J., M. Šejna and M. Th. van Genuchten, 2007. The HYDRUS software package for simulating the two- and three-dimensional movement of water, heat and multiple solutes in variably-saturated media. *User Manual, Version 1.02.* PC Progress, Prague, Czech Republic.
- Šimůnek, J. and M. Th. van Genuchten, 2008. Modeling nonequilibrium flow and transport processes using HYDRUS *Vadose Zone J.* 7(2) pp782-797.
- Tuli, A., K. Kosugi, and J. W. Hopmans. 2001. Simultaneous scaling of soil water retention and unsaturated hydraulic conductivity functions assuming lognormal pore-size distribution. *Advanced on Water Resour.* 24 (2001) 677-688.
- Tyler, E. J. 2001. Hydraulic wastewater loading rates to soils. In: K. Macncel (ed.) *Onsite wastewater treatment. Proc. of the 9th International Symposium on Individual and Small Community Sewage Systems.* ASAE. St. Joseph, MI. p.80-86.
- Tyler, E. J. and L. D. Mokma. 2004. *Onsite wastewater treatment performance codes- A review of selected state and model code performance provisions and implementation strategies.* NOWRA, Edgewater, Maryland.
- Van Cuyk, S., R. Siegrist, A. Logan, S. Masson, E. Fischer and L. Figueroa, 2000. Hydraulic and purification behaviors and their

- interactions during wastewater treatment in soil infiltration systems. *Wat. Res.* Vol. 35, No. 4, pp. 953-964, 2001.
- van Genuchten, M. Th. (1980). A closed-form equation for predicting the hydraulic conductivity of unsaturated soils. *Soil sci. Am.J.*, 44 (5): 892–898.
- van Wesenbeeck, I. J. and R. G. Kachanoski. 1991. Spatial scale dependence of in situ solute transport. *Soil Sci. Soc. Am. J.* 55:3-7.
- van Wesenbeeck, I. J. and R. G. Kachanoski. 1994. Effect of variable horizon thickness on solute transport. *Soil Sci. Soc. Am. J.* 58:1307-1316.
- Vereecken R., J. Kasteel, J. Vanderbricht, and T. Harter. 2007. Upscaling hydraulic properties and soil water flow processes in heterogeneous soils: A review. *Vadose Zone J.* 6:1-28.
- Yeh, T.-C. L. W. Gelhar, and A. L. Gutjahr, 1985a. Stochastic analysis of unsaturated flow in heterogeneous soils, 1, Statistically isotropic media, *Water Resour. Res.*, 21(4), 447-456.
- Yeh, T.-C., L. W. Gelhar, and A. L. Gutjahr, 1985b. Stochastic analysis of unsaturated flow in-heterogeneous soils, 2, Statistically anisotropic media with variable α , *Water Resour. Res.*, 21(4), 457-464.
- Yeh, T.-C., L. W. Gelhar, and A. L. Gutjahr, 1985c. Stochastic analysis of unsaturated flow in heterogeneous soils, 3, Observations and applications, *Water Resour. Res.*, 21(4), 465-471.
- Zhang, Z. F., R. G. Kachanoski, G. W. Parkin, and B. Si, 2000. Measuring Hydraulic Properties Using a Line Source: I. Analytical Expressions. *Soil. Sci. Soc. Am. J.* 64:1554-1562.
- Zhang, Z. F., G. W. Parkin, R. G. Kachanoski, and J. E. Smith, 2002, Effects of soil heterogeneity on steady state soil water pressure

head under a surface line source, *Water Resour. Res.*, 38(7), 1112, doi:10.1029/2000WR000019.

2. Sensitivity of vertical flux, volumetric water content, velocity and conservative solute travel time directly underneath surface line source at steady state

2.1 Introduction

Decentralized, onsite wastewater treatment systems have become more popular for sparsely populated areas because of their low capital costs, but human health and environmental risks associated with the aqueous transport of contaminants released into the soil profile from these systems are major public concerns. Therefore, it is very important to understand and to accurately model the hydraulic processes of the system, especially solute travel times, to assess the environmental risks associated with the system.

Soil water flow and solute transport processes can be simulated with the aid of analytical or numerical solutions to the Richard's equation (Richards, 1931). Water flow processes in unsaturated soils at the field scale are much more complex than a homogeneous laboratory soil column because of the spatial variability of soil hydraulic properties (Tuli et al., 2001). Therefore, to accurately

simulate flow and transport in wastewater systems, models must include the variability in soil hydraulic properties.

The heterogeneity of soil hydraulic properties was inherited from the heterogeneity of the parent material (i.e. texture and mode of parent material deposition) and as a result of the soil horizon development during pedogenesis. Most soil profiles were formed from the same parent material as a result of pedogenic process. These processes have contributed to the heterogeneity of soil hydraulic properties. Therefore, the spatial patterns of soil horizon properties above and below the horizon interface are expected to be statistically dependent on each other, but are often assumed to be independent. Studies of field experiments have indicated that hydraulic heterogeneity of soil is spatially scale-dependent and cross-correlated across the horizon interface. The shape of the horizon interface also influences soil water flow and solute transport processes in the soil (Dyck and Kachanoski, 2009a, 2009b, 2011).

The minimum travel time required for sewage water to achieve environmentally safe quality prior to recharge to the water table is dependent on the soil morphology and initial sewage water quality (Van Cuyk et al, 2000). Thus, the design of the hydraulic loading rate

of an onsite waste water treatment system requires an understanding of the influence of heterogeneity of soil hydraulic property and soil layers on the sewage water travel time (Tyler, 2001; Radcliffe and West, 2009; Tyler and Mokma, 2004).

In this study, a numerical model was constructed to examine the effects of soil heterogeneity on two-dimensional infiltration in Miller-similar media (Miller & Miller, 1956; Miller, 1980). Specifically, the objectives of this chapter are:

4. To quantify the influence of heterogeneity of soil properties in a layered Miller-similar soil on vertical flux, vertical pore water velocity, volumetric water content, and conservative solute travel time for water flow directly underneath a surface line source at steady state.
5. Quantify the influence of spatial correlation (within a layer/horizon and between layers/horizons) on predicted (model) infiltration and solute travel time.

2.2. Theory

In this chapter, linear scaling factors will be used to define spatial variability of hydraulic properties in the numerical models. In

linear scaling schemes, the heterogeneity of field soil properties at each location \mathbf{u} is characterized by a single scaling factor for the node.

Specifically,

$$h(S_e, \mathbf{u}) = \lambda_h(\mathbf{u}) \cdot h^*(S_e) \quad [2-1]$$

$$K(S_e, \mathbf{u}) = \lambda_K(\mathbf{u}) \cdot K^*(S_e) \quad [2-2]$$

and S_e is the effective saturation which is determined as

$$S_e = \frac{\theta - \theta_r}{\theta_s - \theta_r} \quad [2-3]$$

where $h(S_e, \mathbf{u})$ is the soil water matric potential in head units (cm) at location \mathbf{u} as a function of effective saturation S_e , $\lambda_h(\mathbf{u})$ is the soil water matric potential scaling factor at location \mathbf{u} , h^* is the field average soil water matric potential (cm) as a function of S_e , $K(S_e, \mathbf{u})$ is the soil water hydraulic conductivity (cm/day) at location \mathbf{u} as a function of S_e , $\lambda_K(\mathbf{u})$ is the soil water hydraulic conductivity scaling factor at location \mathbf{u} , and K^* is the field average hydraulic conductivity (cm/day) as a function of S_e . θ is the volumetric water content ($cm^3 cm^{-3}$), θ_r is the residual volumetric water content ($cm^3 cm^{-3}$), and θ_s is the saturated soil water content ($cm^3 cm^{-3}$).

If $\lambda_K(\mathbf{u}) = (1/\lambda_h(\mathbf{u}))^2$, the media is said to be Miller-similar (Miller&Miller, 1956; Miller, 1980). All linear scaling schemes including Miller similarity assume only the mean of the pore size distribution varies from location to location while the variance of the pore size distribution stays constant (Sposito,1998).

For this study, the scaling factors were assumed to be log normally distributed. Tuli et al. (2011) has shown this linear scaling approach successfully predicted the heterogeneity of soil hydraulic properties of the soil samples collected at their field sites.

The spatial heterogeneity of soil hydraulic properties was included in the numerical model through sequential Gaussian Simulation with specification of the variance and semi-variogram (Deutsch and Journel, 1998; details in section 2.3).

2.3. Methods

2.3.1. Model construction

The numerical model for predicting two-dimensional (2D) surface infiltration in a Miller-similar layered soil was built in HYDRUS 2D. The two-dimensional domain (Fig. 2-1) can be viewed as the cross section of a three dimensional soil, and the line source is

represented as a point source in two dimensional space. The horizontal direction was defined as the x-direction, and the vertical direction was defined as the z-direction. The dimension of the soil domain was 1000cm×200cm (horizontal and vertical respectively). The domain of the model was split into two surfaces (Fig.2-1(a)). One is an arc inscribed around the surface line source (labeled as area 1) with target finite element size of 3cm, and the rest (labeled as area 2) was considered to be a second surface with target size of 13cm. The average hydraulic properties of the domain were assigned to be the same as the default loam-textured soil in HYDRUS (hydraulic property parameters will be defined in 2.3.2). The initial time was set to 0 days and the model was run for 1000 days with an initial time step of 0.0001 days, a minimum time step of 1×10^{-5} day, and a maximum time step of 10 days. Initially, the matric potential at the bottom of the domain was -1000 cm, and decreased linearly from the bottom to the top of the domain. A water flow magnitude of 10 cm²/day was assigned to the center node at the top of the domain and the domain was set to free drainage at the bottom boundary and the side wall boundaries (Fig 2-1(b)).

2.3.2. Miller-Miller scaling factors

The soil domain was assumed to be Miller-similar. Multiple field tests showed that scaling factors of both matric potential and hydraulic conductivity usually follow a lognormal distribution (Hopmans, 1987, Tuli, Kosugi, Hopmans, 2001). The mean of the matric potential scaling factors of the entire domain was constrained to 1. Layers were introduced to the domain by assigning different means to the matric potential scaling factors for different horizons while still keeping the mean of the entire domain at 1 (Eq. [2-5]). The horizon interface was set to a depth of 40 cm below the surface on average, but varied slightly because of the irregular element size. The scaling factors (λ_h and λ_K) were obtained from isotropic, autocorrelated random field generation with a sequential Gaussian simulation (sGs) algorithm in GSlib 90 (Deutsch and Journal, 1998).

The spatial variability of the scaling factors was modeled using the semivariogram. The semivariogram $\gamma(l)$ is a function that describes the autocorrelation function of a random field (Deutsch and Journal, 1998). Semivariogram models generally consist of an isotropic nugget effect in all directions and combinations of standard semivariogram models (e.g. spherical, exponential, Gaussian; GSlib,

1997). The nugget effect c_0 (cm^2), of a semivariogram model, represents the portion of variance that is spatially random. The following spherical variogram model was utilized in this study,

$$\gamma(l) = c_0 + c \cdot Sph\left(\frac{l}{a}\right) = \begin{cases} c_0 + c \cdot \left[1.5 \frac{l}{a} - 0.5 \left(\frac{l}{a}\right)^3\right], & \text{if } l \leq a \\ c_0 + c, & \text{if } l \geq a \end{cases} \quad [2-4]$$

where $\gamma(l)$ is the semivariogram (cm^2) as a function of the lag distance l (cm), c (cm^2) is the variance contribution (total variance minus the nugget effect), and a is the actual range (cm) which is the distance from the origin to where the semivariogram starts to reach a sill (i.e. the autocorrelation range). The sill of the semivariogram model is the variance of the random field which is normalized to 1.

The output from sGs follows a standard normal distribution. For the A and B horizon locations, this output was back-transformed to lognormal distributions with predetermined means and variances (Table. 2-1). For the non-layered scenarios, the mean of the scaling factors was equal to 1. For layered scenarios, the lognormal distributions of the scaling factors λ_h for the A and B horizons had equal variances, but different means under the constraint that the mean of the entire domain was equal to 1:

$$A_{\text{ave}} \frac{A}{A+B} + B_{\text{ave}} \frac{B}{A+B} = 1 \quad [2-5]$$

where A_{ave} is the mean of λ_h of the A horizon, and B_{ave} is the mean of λ_h of the B horizon. A and B are the number of scaling factors corresponding locations or the number of finite element nodes in the numerical model in the A horizon and B horizon respectively. In this way, the horizon-specific average scaling factors were weighted according to the dimensions of the horizons. The mean of the hydraulic properties of each horizon may be different but the hydraulic properties are still cross correlated to each other as one might expect from a soil profile derived from a single parent material (Dyck and Kachanoski, 2010), and since the average of the domain scaling factor was constrained to be 1, the average soil water hydraulic conductivity of the domain is known and equal to the specified values.

The average hydraulic properties of the domain were specified using one set of van Genuchten parameters. van Genuchten (1980) derived a model for the soil water retention curve and the corresponding expression of the relative hydraulic conductivity $K_r(S_e)$ (cm/day) as a function of effective water saturation S_e . The

van Genuchten (VG) parameters α, n, θ_r and θ_s describe the functions describing the moisture retention curve and the hydraulic conductivity curve as part of the following functions:

$$S_e(h) = (1 + (\alpha h)^n)^{\frac{1}{n}-1} \quad [2-6]$$

$$K(S_e) = K_s(S_e)^{0.5} \left\{ 1 - \left(1 - (S_e)^{\frac{n}{n-1}} \right)^{1-\frac{1}{n}} \right\}^2 \quad [2-7]$$

Where h is the soil water matric potential (cm), α (cm^{-1}) is related to the air entry value, and n (dimensionless) is an indicator of the variance of pore size distribution. Specifically, the parameters for this study were: θ_r $0.078 \text{ cm}^3 \text{ cm}^{-3}$, θ_s $0.43 \text{ cm}^3 \text{ cm}^{-3}$, α 0.036 cm^{-1} , n was 1.56, and K_s 24.96 cm/day .

As mentioned above, GSlib 90 was utilized to simulate sets of standard normal random field numbers from the Gaussian model (Deutsch and Journel, 1998) with a nugget effect of 0.5 and a spherical structure with a unique range for each simulation (Table 2-1). The range of the semivariogram is an indicator of the range of spatial correlation of the property considered. Any two nodes that are separated further than the semivariogram range are not spatially correlated. For the sGs random field generation, the size of grid

spacing was 12.0 cm in the x-direction and 5.0 cm in the z-direction. The soil was assumed to be isotropic thereby the ranges of correlation in both x and z directions were identical. The scaling factors were simulated with varied correlation ranges, coefficient of variation (CV), A_{ave} and B_{ave} as presented in Table 2-1. In the table, the term uniform stands for homogeneous loam soil. $A_{ave}=1$, $B_{ave}=1$ refers to heterogeneous soil without layers.

Since the finite element mesh of the numerical model in HYDRUS 2D was irregularly spaced, and the simulated results from SGSIM were on a regular grid, the simulated results of the scaling factors were matched to the finite element coordinates through the lspline function in Mathcad. Specifically, the lspline function created a piecewise continuous linear function through linear interpolation (lspline function in Mathcad). In addition, another set of random number was generated for a simulation with correlation range equaling 0 cm in Mathcad (completely random hydraulic properties).

2.3.3. Calculations

Observation nodes were selected directly underneath the line source at depths of 0cm (at the line source), 4.75cm, 10.97cm, 14.59cm, 21.41cm, 26.87cm, 31.8cm, 36.64cm, 45.39cm, 52.69cm,

58.43cm, and 65.41cm. Since the size of the elements in the domain was not regular, the distance between the observation nodes were not regular. Each observation node was about 4.75 cm to 9 cm apart from the adjacent neighbors. The vertical flux directly underneath the line source at each observation point at steady state and the corresponding water content was obtained from the simulation results.

$$v(z) = \frac{q_z(z)}{\theta(z)} \quad [2-8]$$

where $q_z(z)$ is the water flux density (cm/day) directly under the line source along the vertical steam line. Thus, the conservative solute travel time, T_w to depth z^* (cm), is obtained as

$$T_w(z^*) = \int_0^{z^*} \frac{1}{v(z^*)} dz = \int_0^{z^*} \frac{\theta(z^*)}{q(z^*)} dz \quad [2-9]$$

2.4. Results and Discussion

The influence of soil layering on the water flux density in the vertical direction (q_z) directly underneath the surface line source and the corresponding water content (θ), water pore velocity (V_w), and travel time $T_w(z^*)$ simulated from the numerical model from 0 cm to 65 cm depth are analyzed in this section.

Three examples of soil water content output of the numerical model simulation are presented in Fig. 2-2, Fig. 2-3, and Fig. 2-4. Fig. 2-2 shows the simulated water content corresponding to a uniform loam soil. Fig. 2-3 shows the simulated water content corresponding to a layered soil profile with a mean scaling factor for the horizon of 0.75 and 1.318 for the B horizon (i.e. relatively fine over relatively coarse), 0 cm correlation range, 10% coefficient of variation (CV). Fig. 2-4 show the simulated water content corresponding to a layered soil profile with a mean layer scaling factor for the A horizon of 1.236 and 0.7 for the B horizon (i.e., relatively coarse over relatively fine texture), 15 cm correlation range, 100% CV. The corresponding soil water matric potential are given in Fig. 2-5, Fig. 2-6, Fig. 2-7. Soil water matric potentials for the three simulations were much more similar than the soil water contents. More variability of the water content output can be observed as heterogeneity was introduced. The boundary between the two horizons became more obvious in the soil water distribution figures as the variability was introduced (Fig. 2-3 and Fig. 2-4). These simulated water content figures is used as references in the following results comparisons and discussions.

Fig. 2-8 and Fig. 2-9 show the field average water retention curve (θ versus h) and hydraulic conductivity curve respectively corresponding to various mean-scaling factors (λ_h) assigning to each horizon. The magnitude of the scaling factor is proportional to mean pore size, thus larger λ_h is similar to a coarsening trend in soil texture, and smaller λ_h is similar to a fining trend in soil texture. Larger λ_h is corresponding to more negative value of soil water matric potential. As shown in Fig. 2-8, at the same soil water matric potential, soil water content increased as the mean of the matric potential scaling factor λ_h decreased. The soil water hydraulic conductivity λ_k is negatively correlated to the matric potential scaling factor λ_h since $\lambda_k = \frac{1}{\lambda_h^2}$. Therefore, with the same soil water hydraulic conductivity, soil water content increased as the mean of soil water hydraulic conductivity decreased (Fig. 2-9).

The volumetric water content directly below the line source was very sensitive to soil heterogeneity and differences in soil layers as shown in Figure 2-11 (a-i). The plot corresponding to the uniform loam (homogeneous) soil in each figure was very smooth and decreased as depth increased. With the introduction of variability in

soil hydraulic properties, the water content oscillated up and down over the observed depth. When the CV was increased and the other two parameters (correlation length, mean of scaling factors) held constant, the amplitudes of the water content variations increased. Fig. 2-10 gives an example of the matric potential scaling factor distribution versus depth directly below the line source for various CVs with range=5, and $A_{ave}=B_{ave}=1$. Comparing the distribution of the scaling factors (Fig. 2-10) to the corresponding water content distributions (d, e and f of Fig. 2-11), the spatial pattern of the scaling factor was very similar to the spatial pattern of the volumetric water storage as the CV changed. The increased variability in the scaling factors increases the variability in the soil moisture retention curves and therefore increased the variability in the soil water content (Fig.2-8).

The fluctuation of the water content distribution decreased as the range of correlation increased from 0cm to 5cm with the same CV, but less significant changes were observed as the correlation range increased from 5 cm to 15 cm. This suggests the distribution of water content is very different from 0 correlation range to a finite correlation range, but less different from a finite correlation range to a longer

correlation range. As discussed above, the matric potential scaling λ_h is positively related to the water content. Fig 2-10 gives examples of λ_h distributions for Range equals 5 cm and mean of the matric potential scaling factor equals 1 for both horizons and CV varied from 10% to 100%. Compare the distribution of matric potential scaling factor in Fig. 2-10 to the corresponding distributions of water content (middle column of Fig. 2-11), their patterns were very similar. Therefore, the distribution of water content (Fig. 2-11) is consistent with the linear scaling theory. For all the simulations, a larger A_{ave} corresponded to a smaller B_{ave} and vice versa, and it caused a transition from relatively low to relatively high water content (When $A_{ave} > B_{ave}$) or from relatively high to relatively low water content ($A_{ave} < B_{ave}$) at about 40 cm depth (horizon interface). This illustrates the effect of a horizon boundary if the soil was Miller-similar media and the only difference between A and B horizon was the mean of the scaling factor. The transition from the A horizon to the B horizon with different mean hydraulic properties is also smooth, not abrupt, as one might expect in a natural soil.

The vertical flux density directly underneath the surface line source did not change much with a change in the CV, range of the

scaling factors or introduction of layers with varying mean scaling factors (Fig. 2-12). All the fluxes were less than two of their surface magnitudes within 10 cm below the surface. After this depth, the flux density asymptotically approach a minimum as depth increased. Small fluctuations of the fluxes were observed as the variability was introduced. The vertical flux density was re-plotted to emphasize the small variability in the distribution (Fig. 2-13). In the log scale, differences in steady state flux as a function of depth for the different scenarios are more apparent, especially below 10 cm. Below 10 cm, the fluctuation of the flux density increased as CV increased, and decreased as the range of the correlation increased from 0 cm to 5cm. The fluctuation of the vertical flux density did not change significantly as the range of correlation changed from 5 to 15 cm. The vertical flux densities corresponding to different layer mean scaling factor at the same CV and range of correlation were very similar indicating continuity of mass flux across the horizon interface.

The soil pore water velocity was calculated using Eq. [2-8]. Since the variability of the distribution of vertical flux density for the different scenarios was small, the variability of the velocity is mainly determined by the variability of the soil water content which was

shown to be highly influenced by the variability of the hydraulic property scaling factors. With the same vertical flux density, the corresponding velocity is expected to be inversely proportional to the soil water content.

The soil pore water velocity corresponding to the vertical flux directly underneath the surface line source versus depth is plotted in Fig. 2-14. In each sub-figure (i.e. a, b, etc.), the velocity of the homogeneous soil was plotted to compare with the heterogeneous soils. For depths greater than about 10cm, the differences of the vertical velocity between the heterogeneous soils and the uniform loam soil appear minor. Increasing the CV for this range of depth only introduces more fluctuations to the curves. For depths less than about 10 cm, the differences between the heterogeneous soils and the homogeneous soil are more significant. To exam more closely the differences, the velocity within the top 10 cm depth are re-plotted in Fig. 2-15. Generally, the vertical velocity was only different within 5 cm to 7.5 cm of the surface as the heterogeneity of the soil changed. With the same autocorrelation range, an increase in CV would influence the magnitude of the velocity which is a reflection of the variability of the volumetric water content. Significant increases in the

velocity are observed as the range increased from 0cm to 5cm (with constant CV); very little change of the velocity occurred when the range increased further to 15cm. With the same correlation range and CV, the vertical velocity increased as the mean of the hydraulic scaling factor, A_{ave} increased.

When the steady state vertical soil pore water velocity was plotted in a log scale (Fig. 2-16), the differences in velocity at depths greater than 10cm became more apparent. The fluctuation of the vertical velocity increased as the CV increased and decreased when the range increased from 0 cm to 5 cm. Similar to the vertical flux and the corresponding soil water content, the differences between the vertical soil pore velocity was less significant as the range increased from 5 cm to 15 cm. The effect of layering on the distribution of velocity attributed to the fact that within the top layer (top 40 cm), the magnitude of the vertical soil pore velocity increased as A_{ave} increased (relatively coarse A horizon). Within the B horizons, however, the differences in velocities as a function of the scaling factors (B_{ave}) became less apparent. In the B horizon, the magnitude of the flux was very small; changes in the texture (different B_{ave}) in this range did not affect the velocity significantly.

In summary, the vertical flux density q_z was not very sensitive to hydraulic heterogeneity or layers. The velocity was determined by the vertical flux density divided by the corresponding volumetric water content. The magnitude of the vertical flux densities were very low after 5 to 7 cm depths, and when the magnitude of the vertical flux was low, changes in the water content only affect the velocity a little. Thus the variability of the soil water content due to heterogeneity of soil hydraulic property within the top 5cm to 7.5 cm was the primary cause of the differences between the velocities. The variability of both of the soil water flux density and the soil water content below 7.5 cm still caused fluctuations in the velocities however only in very small magnitudes.

The vertical travel time was negatively correlated to the corresponding velocity (Eq. [2-9]). Since the velocity was significantly affected by the variability of the volumetric water content close to the source (0 cm to 7.5 cm in this case), the solute travel time was also significantly affected by the change of soil water content close to the source. Since the soil water content was positively correlated to the mean of the matric potential scaling factors λ_h , and the scaling factors of the soil water hydraulic conductivity was determined as $\lambda_K(u) =$

$(1/\lambda_h(u))^2$), the travel time was also expected to be positively correlated to λ_h , and negatively correlated to λ_K close to the source. In other words, if the mean of λ_h is very high or the mean of λ_K is very low close to the source, the corresponding travel time tends to be low and vice versa.

The vertical travel time (Eq. [2-9]) directly underneath the surface line source (source strength $10 \text{ cm}^2/\text{day}$) from 0 cm to 65 cm in depth at steady state is presented in Table 2-1 and Fig. 2-17. The vertical travel time versus correlation range for different CVs are given in Fig. 2-17, and the travel time corresponding to a uniform loam soil (42.10 days) is also given as a reference. The maximum vertical travel time to 65.41 cm depth was 44.51 days corresponding to a 0 cm correlation range (random), 10% CV, and $A_{ave} = 0.75$ $B_{ave} = 1.318$. The minimum observed travel time was 33.62 days corresponding to a 15 cm correlation range, 100% CV, and $A_{ave} = 1.236$, $B_{ave} = 0.7$. The mean of all the travel times was 39.80 days. The difference between the maximum and minimum observed travel times was 10.89 days.

From the above observations and discussions, for the situation with similar boundary condition, the vertical flux density directly underneath surface line source in variable or layered soil were not very sensitive to soil variability. The soil variability close to the surface line source is most important to assess in order to estimate the conservative solute travel time and vertical velocity. Layers only significantly affect water content. Change of Range of correlation only affects the hydraulic outputs within 5cm of soil.

Fig. 2-17 shows that the layered scenario with $A_{ave} > B_{ave}$ (relatively coarse versus relatively fine) always had a shorter travel time than the scenarios with $A_{ave} < B_{ave}$ (relatively fine over relatively coarse). This observation suggested that the average hydraulic properties in each layer and the orientation of the layers also had a significant influence on the water flow process. As discussed above, coarse textures were corresponding to relatively low water content, and the variability of the velocity and travel time was mainly determined by the variability of the water content close to the surface line source. Therefore, the layered scenario with $A_{ave} > B_{ave}$ (relatively coarse versus relatively fine) always had a greater travel

time than the scenarios with $A_{ave} < B_{ave}$ (relatively fine over relatively coarse).

Pathogens contained in human wastes from the onsite wastewater treatment system are the major sources of waterborne disease (Reneau et al., 1989). The pathogenic viruses and bacteria in the wastewater are more a concern to health than the protozoans and parasitic worms, since the size of protozoans and parasitic worms are much larger than the viruses and bacteria and therefore are more efficiently remediated in the soil (Yavuz Corapcioglu and Haridas, 1984). Soil temperatures, moisture content, soil textures, soil total organic carbon, soil pH, water table depth, hydraulic loading rate of the onsite wastewater treatment systems all affect the remediation of pathogens in the wastewater (Reneau et al., 1989). There are various types of pathogenic viruses and bacteria with wide ranges of half-life contained in the effluent. Life times of viruses and bacteria in soil range from a few weeks to a few months or longer depending on the soil environment (Corapcioglu and Haridas, 1984). Studies indicated most pathogenic viruses and bacteria die off in the soil within 2 to 3 months although some bacteria may live as long as 5 years under certain environmental conditions (Bitton, 1975; Gerba et

al., 1975). In this study, the longest travel time from the simulations for 0cm to 65 cm in depth (44.51 days) was 10.89 days longer than the shortest travel time (33.62 days). The 10.89 days difference is expected to have significant impact on the remediation of the pathogenic viruses and bacteria contained in the wastewater.

2.5. Conclusion

A two-dimensional numerical model with variable soil hydraulic properties and soil layers was developed in HYDRUS 2D to investigate surface line source infiltration process at steady state. The soil domain was assumed to be Miller similar. Variable ranges of correlation, CV and mean of Miller-Miller scaling factors corresponding to the A horizon and B horizon were selected to generate the linear scaling factors of the hydraulic potential and hydraulic conductivity. The sensitivity of the simulated results of the vertical flux densities directly beneath the surface line source from 0 cm to 65 cm in depth, the corresponding soil water content, and the travel time was analyzed. The results showed the vertical flux density was not very sensitive to the changes in variability or the presence of soil layers; the vertical velocity and conservative solute travel time

were more sensitive to changes in the variability of soil close to the surface line source than at greater depths; the volumetric water content was very sensitive to changes in variability and horizon interface. The range of correlation only significantly affected the hydraulic outputs (volumetric water content, vertical velocity and conservative travel time) from 0cm range to 5cm range. Measurement of the variability of the top layers of soil is necessary to determine vertical velocity and solute travel time. The hydraulic output of the water flow process was also influenced by the average hydraulic properties in each layer and the layers orientation. Generally, a relative coarse layer over a relatively fine layer corresponds to a relatively high water content over relatively low water content, and a relatively low velocity and high travel time over the soil profile, vice versa.

2.6. References

- Bitton, G. 1975. Adsorption of viruses onto surfaces in soil and water. *Water Res.* 9:473-484.
- Deutsch, C. V. and A. G. Journel, 1998. *GSLIB: Geostatistical software library and User's Guide*, Second Edition.

- Dyck, M. F. and R. G. Kachanoski, 2009a. Measurement of transient soil water flux across a soil horizon interface. *Soil Sci. Soc. Am.J.* 73:1604-1613.
- Dyck, M. F. and R. G. Kachanoski, 2009b. Measurement of steady-state soil water flux across a soil horizon Interface. *Soil Sci. Soc. Am.J.* 73: 1786-1795.
- Dyck, M. F. and R. G. Kachanoski, 2011. Scale-dependent covariance of soil physical properties above and below a soil horizon interface: Pedogenic versus anthropogenic influences on total porosity. *Can. J. Soil Sci.* (2011) 91.
- Gerba, C. P., C. Wallis, and J. L. Melnick, 1975. Fate of wastewater bacteria and viruses in soil. *J/Irr/ Drain. Div. Am. Soc. Civ. Eng.* 101:157-174.
- Hopmans, J. W. 1987. A comparison of various methods to scale soil hydraulic properties. *J. Hydrol.*, 93: 241-256.
- Miller, E. E., 1980, Similitude and scaling of soil water phenomena. In *Applications of soil Physics*, ed. D. Hillel, 300-318. New York: Academic Press.
- Miller, E. E., and R. D. Miller. 1956. Physics theory for capillary flow phenomena. *J. Appl. Phys.* 27:324-32.
- Radcliffe, D. E., and L. T. West. 2009. Design hydraulic loading rates for onsite wastewater system. *Vadose Zone J.* 8:64-74.
- Reneau, R. B., Jr., C. Hagedorn, and M.J. Degen. 1989. Fate and transport of biological and inorganic contaminants from on-site disposal of domestic wastewater. *J. Environ. Qual.* 18:135–144.
- Richards, L. A., 1931. Capillary conduction of liquids through porous mediums. *Phys.* 1 (5): 318–333.
- Sposito, G. 1998. Scale dependent and scale invariance in hydrology. ISBN 0-521-57125-1.

- Tuli, A., K. Kosugi, and J. W. Hopmans. 2001. Simultaneous scaling of soil water retention and unsaturated hydraulic conductivity functions assuming lognormal pore-size distribution. *Advanced on Water Resour.* 24 (2001) 677-688.
- Tyler, E. J. 2001. Hydraulic wastewater loading rates to soils. In: K. Macncel (ed.) *Onsite wastewater treatment. Proc. Of the 9th International Symposium on Individual and Small Community Sewage Systems.* ASAE. St. Joseph, MI. p.80-86.
- Tyler, E. J. and L. D. Mokma, 2004. *Onsite wastewater treatment performance codes- A review of selected state and model code performance provisions and implementation strategies.* NOWRA., Edgewater, Maryland.
- Van Cuyk, S., R. Siegrist, A. Logan, S. Masson, E. Fischer and L. Figueroa, 2000. Hydraulic and purification behaviors and their interactions during wastewater treatment in soil infiltration systems. *Wat. Res.* Vol. 35, No. 4, pp. 953-964.
- van Genuchten, M.Th. (1980). A closed-form equation for predicting the hydraulic conductivity of unsaturated soils. *Soil Science Society of America Journal* 44 (5): 892–898.
- Vereecken, 2007, *Modelling pesticide leaching in virtual realities: progress, opportunities, and threats. Environmental fate and ecological effects of pesticides: 13th Symposium Pesticide Chemistry, P.: 426-435.* Editors: del Re, A. A. M., E. Capri, G. Fragoulis, M. Trevisan. Piacenza., Italy.
- Yavuz Corapcioglu, M. and Haridas, A., 1984. Transport and fate of microorganisms in porous media: a theoretical investigation. *J. Hydro.*, 72: 149-169.

Table 2-1: Scaling factors and related parameters and corresponding conservative travel time

Scaling Parameters				Travel time (days)
Range	A horizon average	B horizon average	CV	
homo	homo	homo	homo	42.10
0	1	1	10	42.16
0	1	1	50	41.86
0	1	1	100	40.39
0	0.75	1.318	10	44.51
0	0.75	1.318	50	43.38
0	0.75	1.318	100	40.49
0	0.9	1.127	10	43.21
0	0.9	1.127	50	42.01
0	0.9	1.127	100	39.15
0	1.236	0.7	10	39.33
0	1.236	0.7	50	38.31
0	1.236	0.7	100	35.54
15	1	1	10	41.91
15	1	1	50	39.32
15	1	1	100	35.63
15	0.75	1.318	10	43.75
15	0.75	1.318	50	41.02
15	0.75	1.318	100	41.72
15	0.9	1.127	10	42.58
15	0.9	1.127	50	40.00
15	0.9	1.127	100	36.21
15	1.236	0.7	10	38.97
15	1.236	0.7	50	36.88
15	1.236	0.7	100	33.87
50	1	1	10	41.76
50	1	1	50	39.11
50	1	1	100	35.61
50	0.75	1.318	10	43.71
50	0.75	1.318	50	42.98
50	0.75	1.318	100	37.08
50	0.9	1.127	10	42.58
50	0.9	1.127	50	39.66
50	0.9	1.127	100	36.39
50	1.236	0.7	10	38.96
50	1.236	0.7	50	36.68
50	1.236	0.7	100	33.62

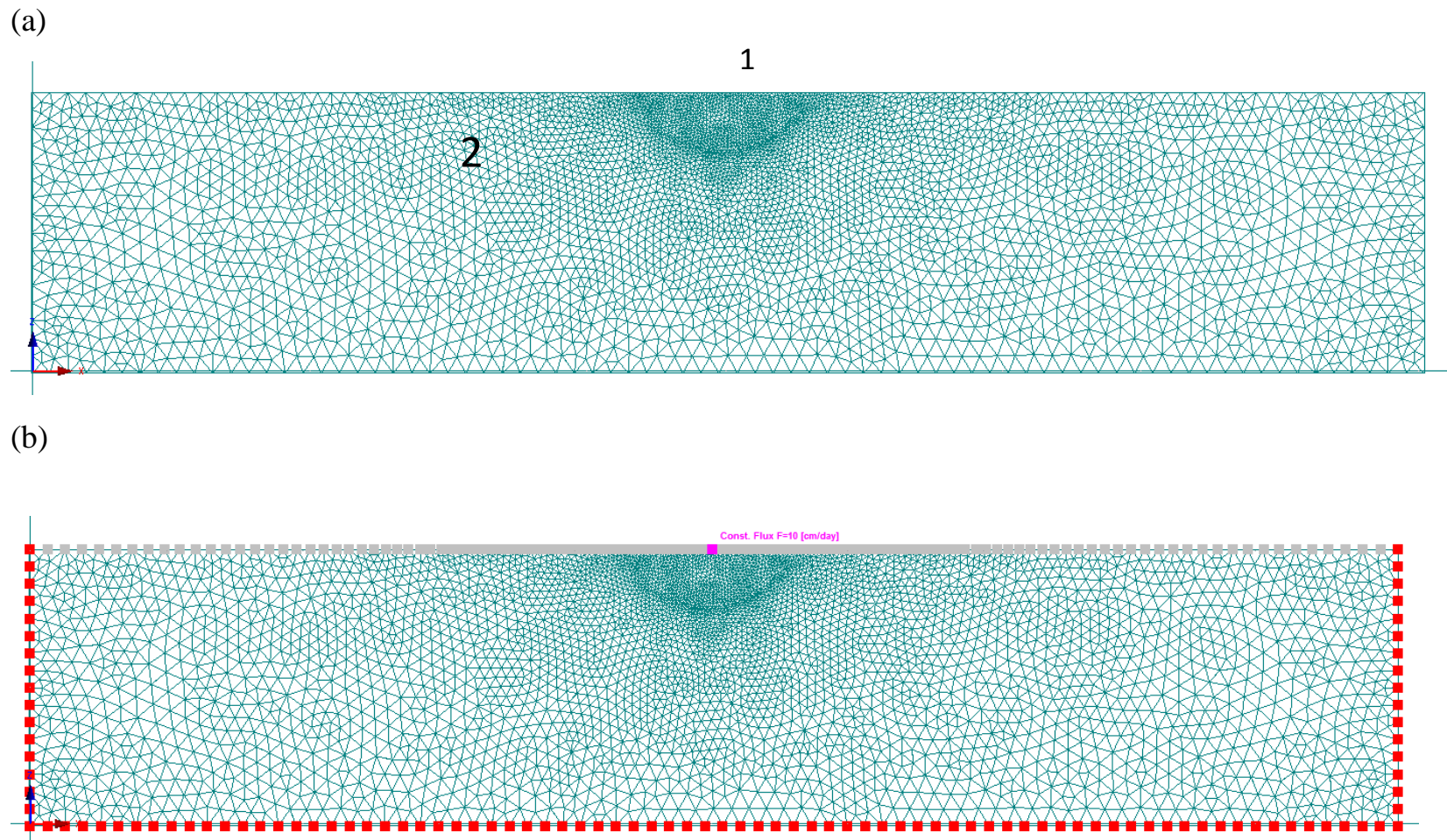


Figure 2-1: (a) Illustration of finite element size distribution and (b) Boundary conditions of two dimensional numerical model in HYDRUS 2D

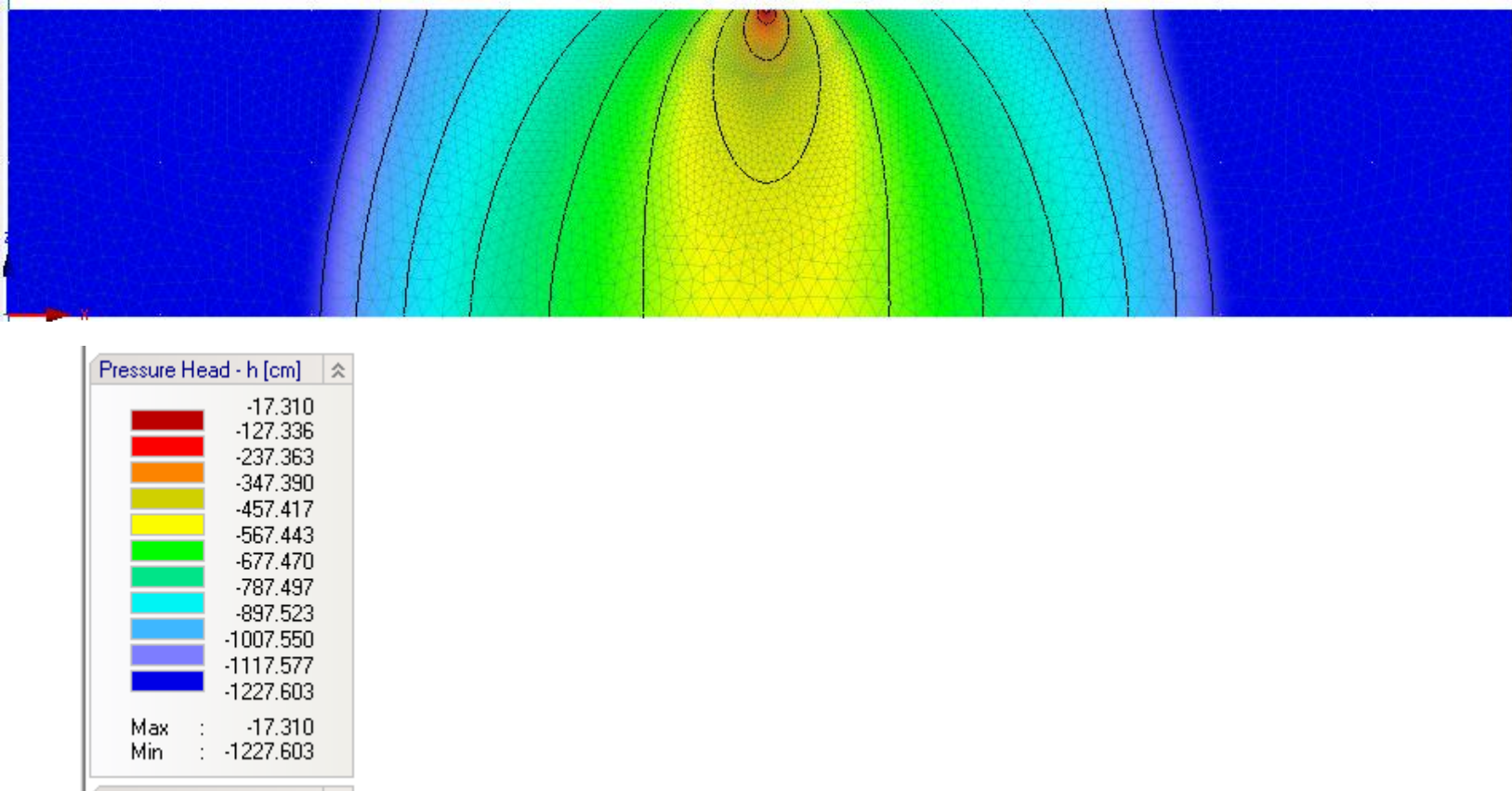


Figure 2-2 : HYDRUS model output of soil water content at steady state (1000 days) corresponding to uniform loam soil

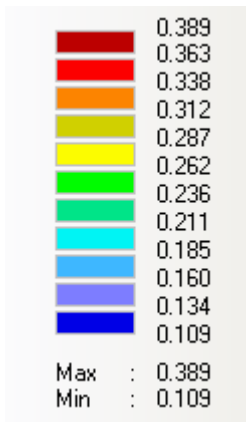
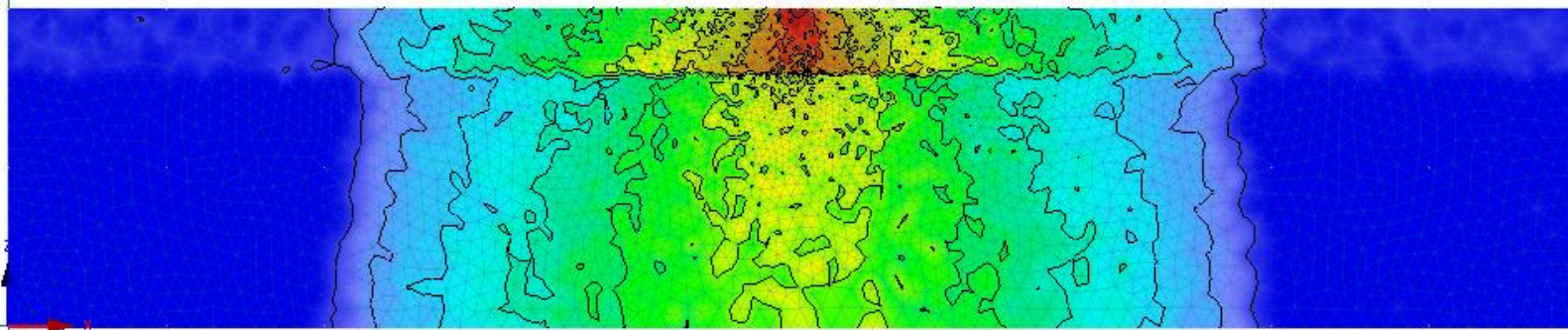


Figure 2-3: HYDRUS model output of soil water content at steady state (1000 days) corresponding to 0 cm correlation range, 10% CV, and $A_{ave}=0.75$ $B_{ave}=1.318$ (maximum travel time)

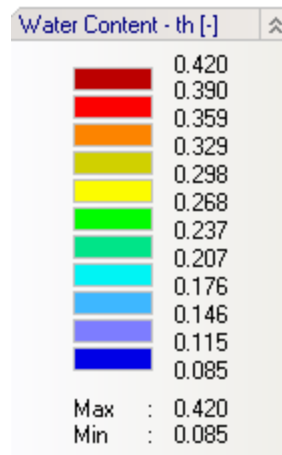
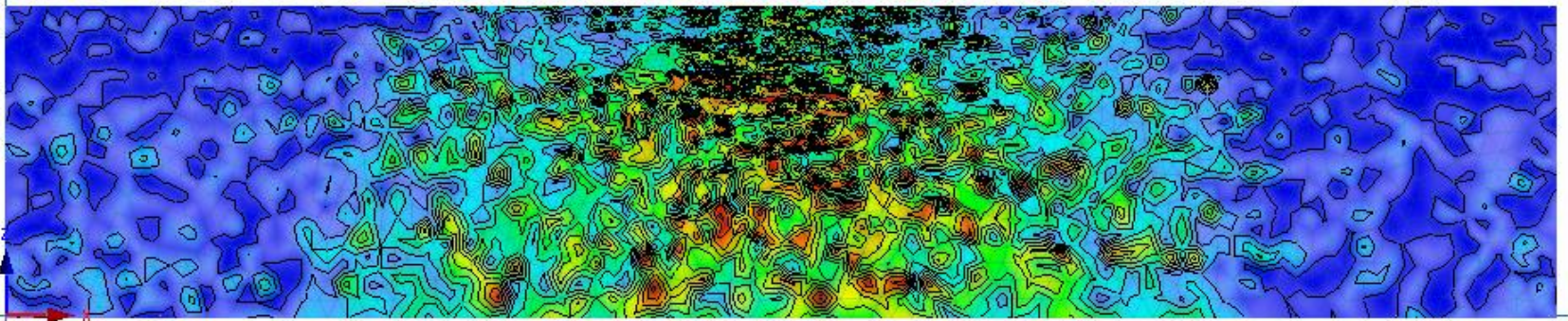


Figure 2-4: : HYDRUS model output of soil water content at steady state corresponding to 15 cm correlation range, 100% CV, and $A_{ave}=1.236$ $B_{ave}=0.7$ (minimum travel time)

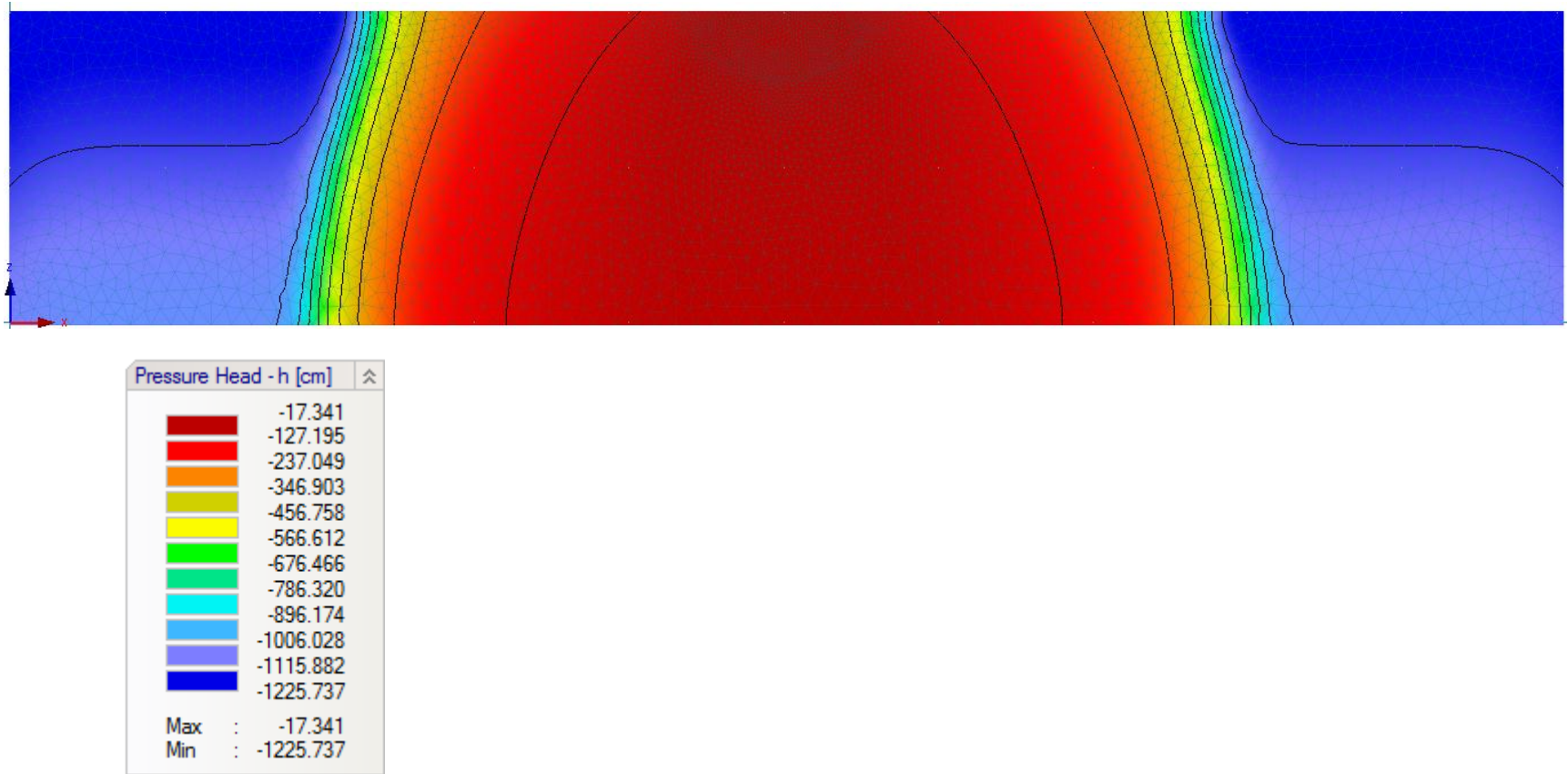


Figure 2-5: HYDRUS model output of soil water matric potential at steady state (1000 days) corresponding to uniform loam soil

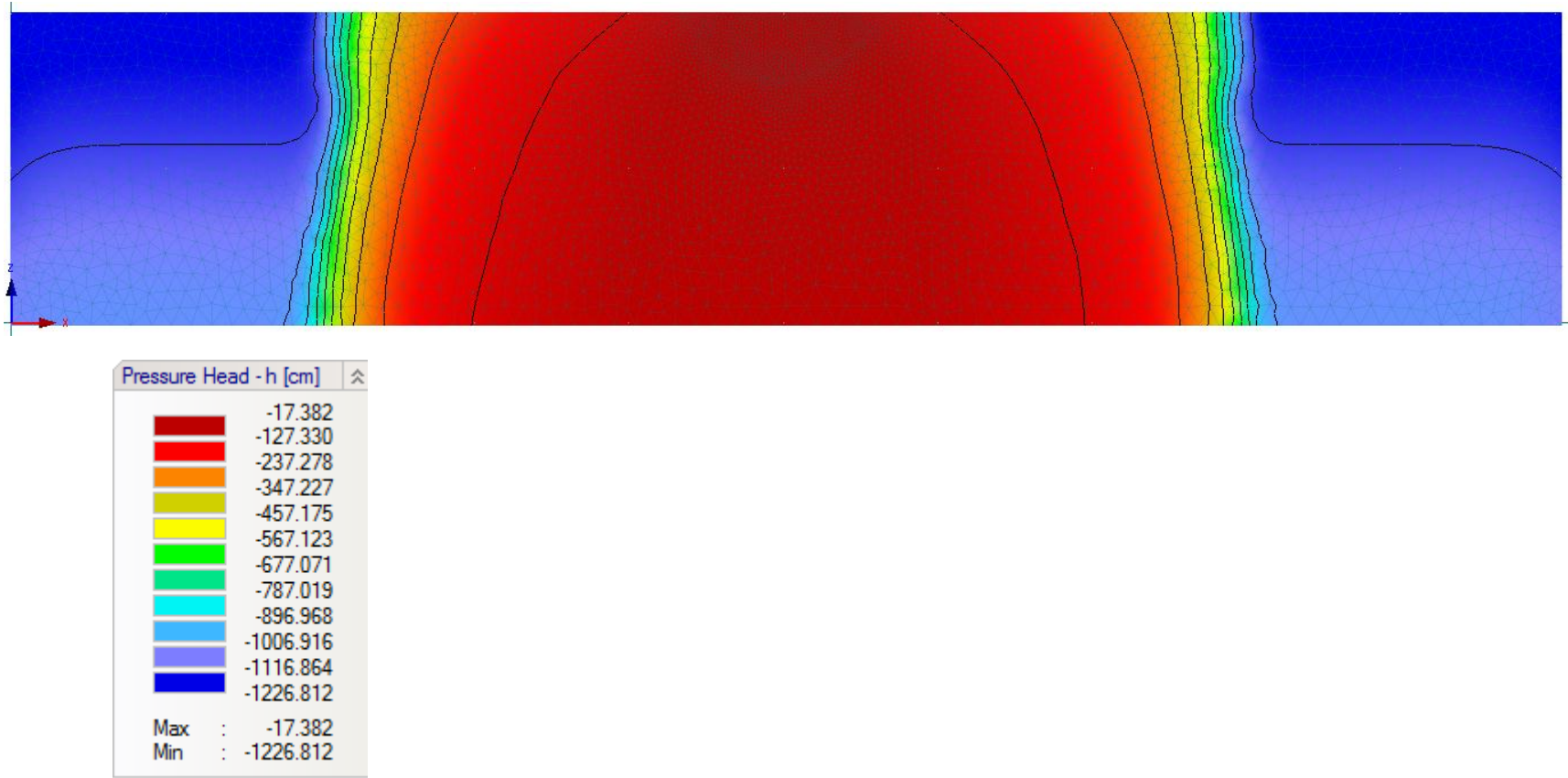


Figure 2-6: HYDRUS model output of soil water matric potential at steady state (1000 days) corresponding to 0 cm correlation range, 10% CV, and $A_{ave}=0.75$ $B_{ave}=1.318$ (maximum travel time)

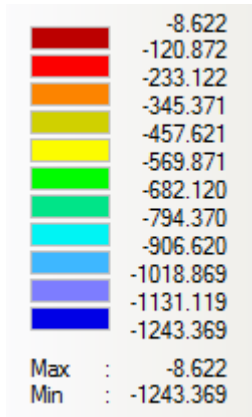
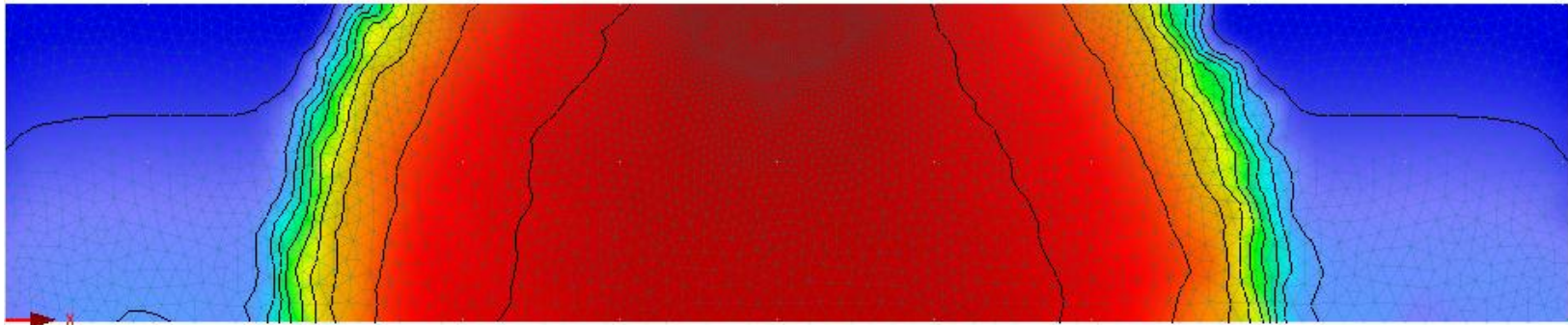


Figure 2-7: HYDRUS model output of soil water matric pressure head at steady state (1000days) corresponding to 15 cm correlation range, 100% CV, and $A_{ave}=1.236$ $B_{ave}=0.7$ (minimum travel time)

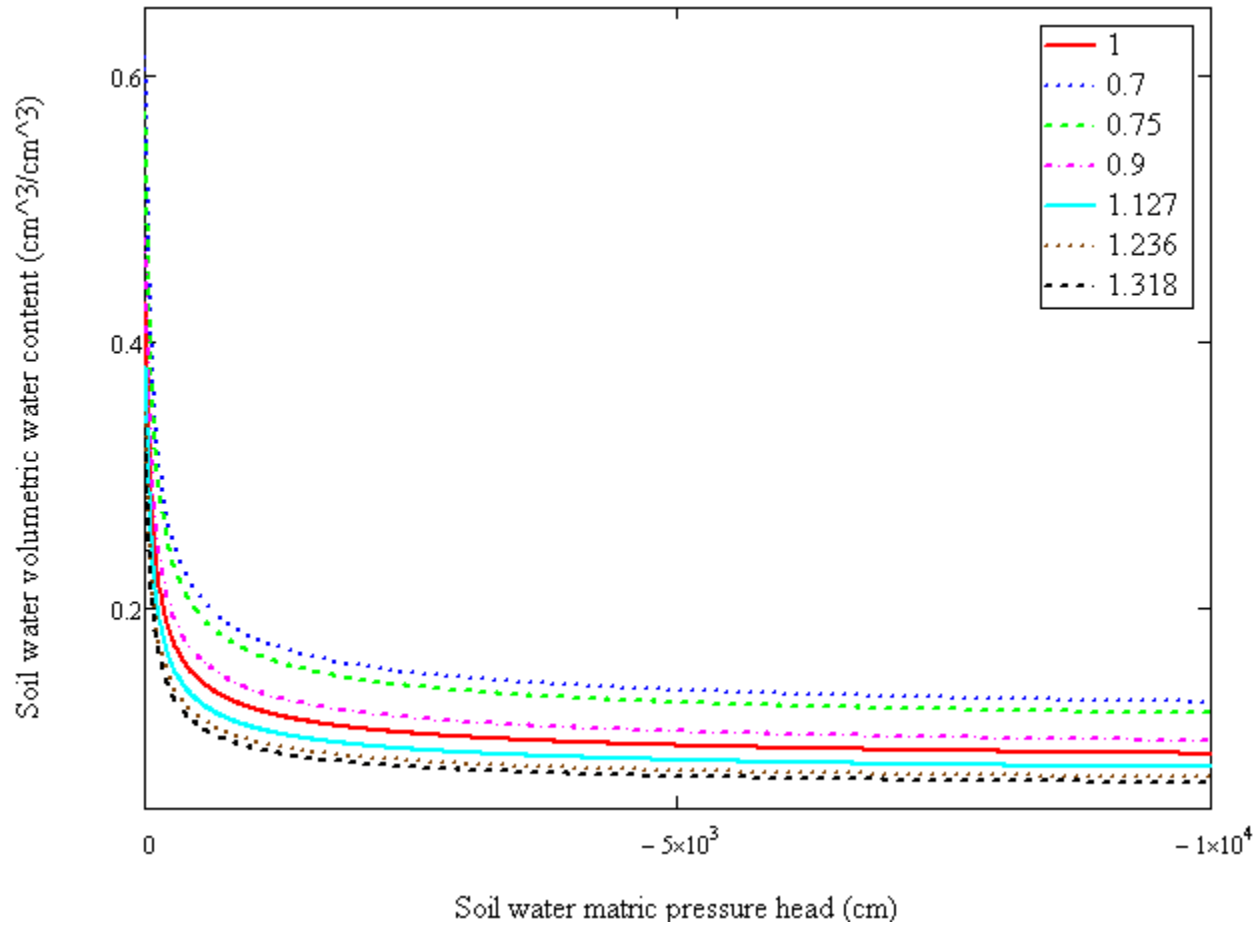


Figure 2-8: Soil water retention curve (θ versus h) with average of matric potential scaling factors equals 1, 0.7, 0.75, 0.9, 1.127, 1.236, 1.318

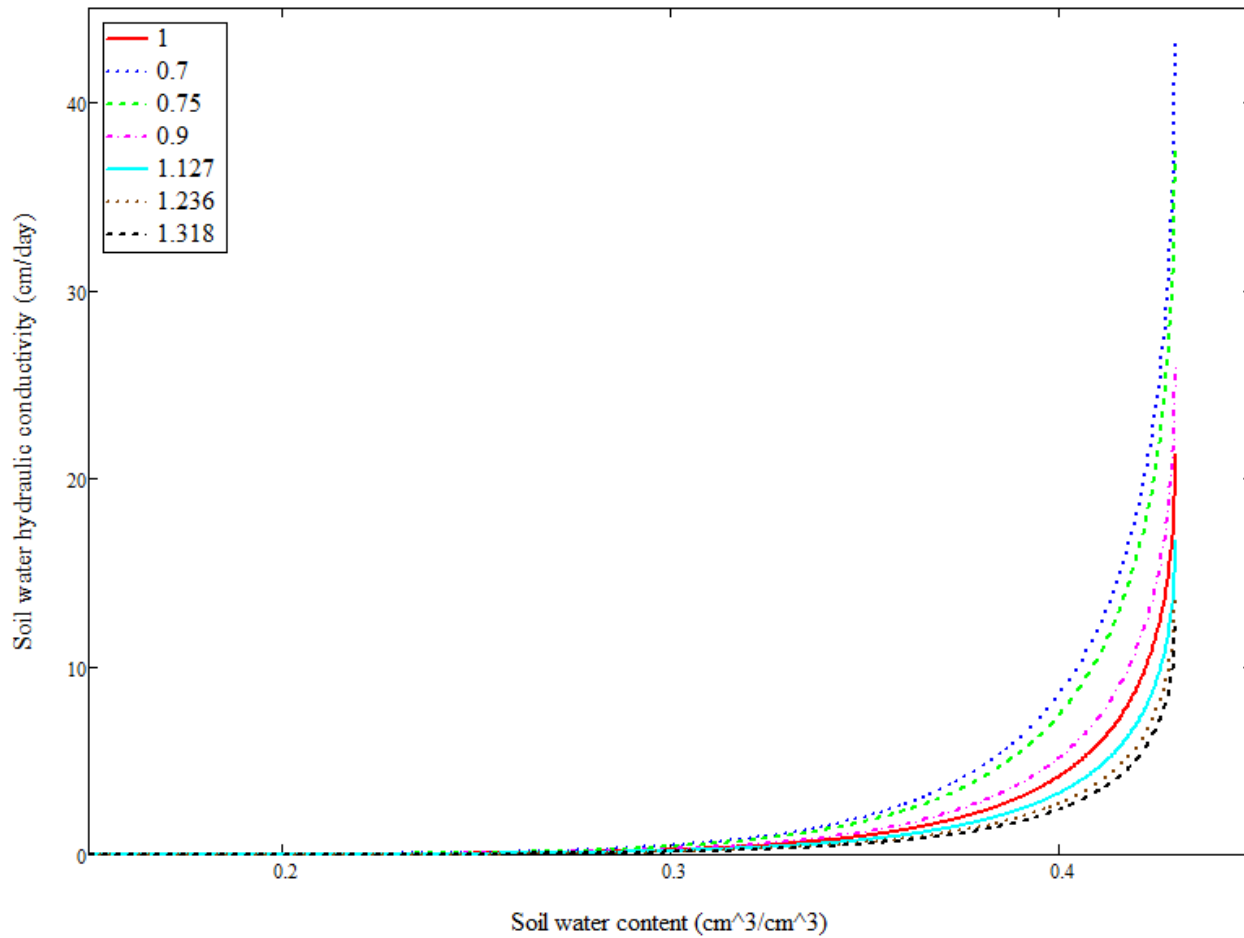
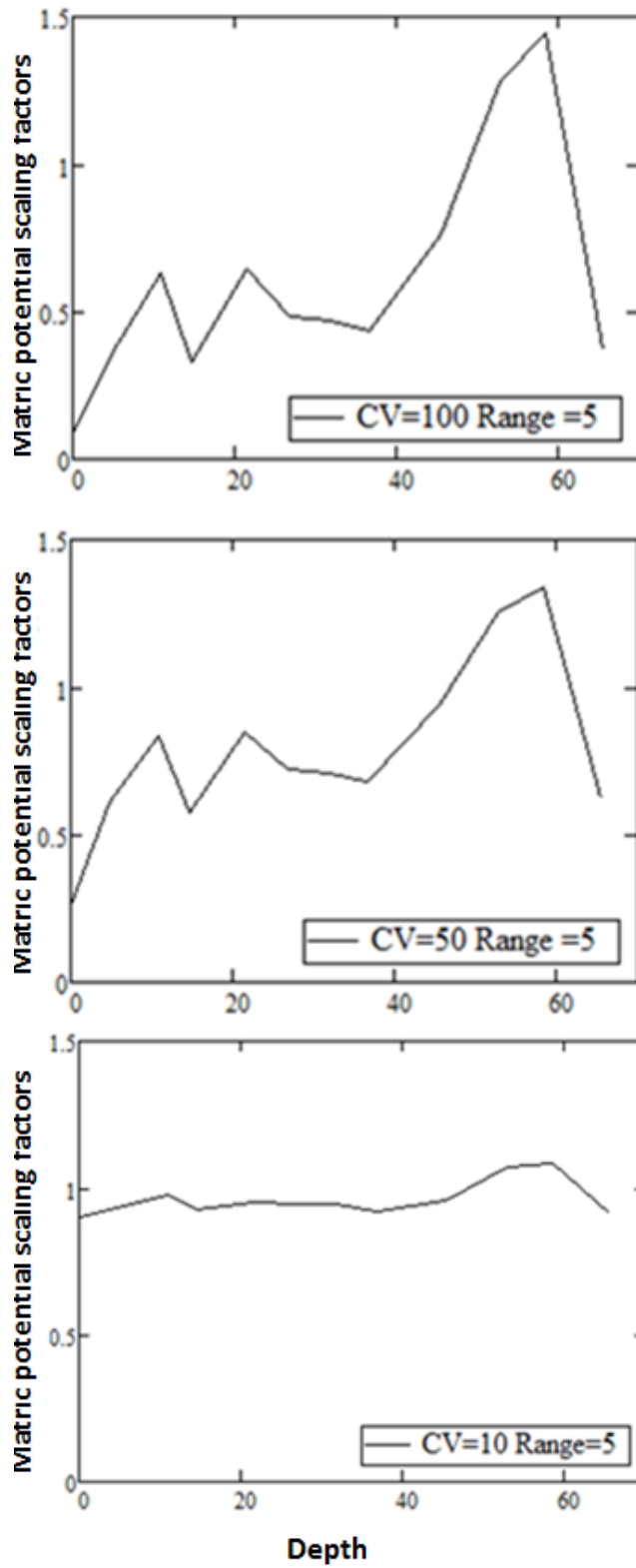


Figure 2-9: Soil water hydraulic conductivity (K_s) versus soil water content (θ) average of matric potential scaling factors equals 1, 0.7, 0.75, 0.9, 1.127, 1.236, 1.318



**Figure 2-10: Soil water matric potential scaling factor
($A_{ave}=B_{ave}=1$)**

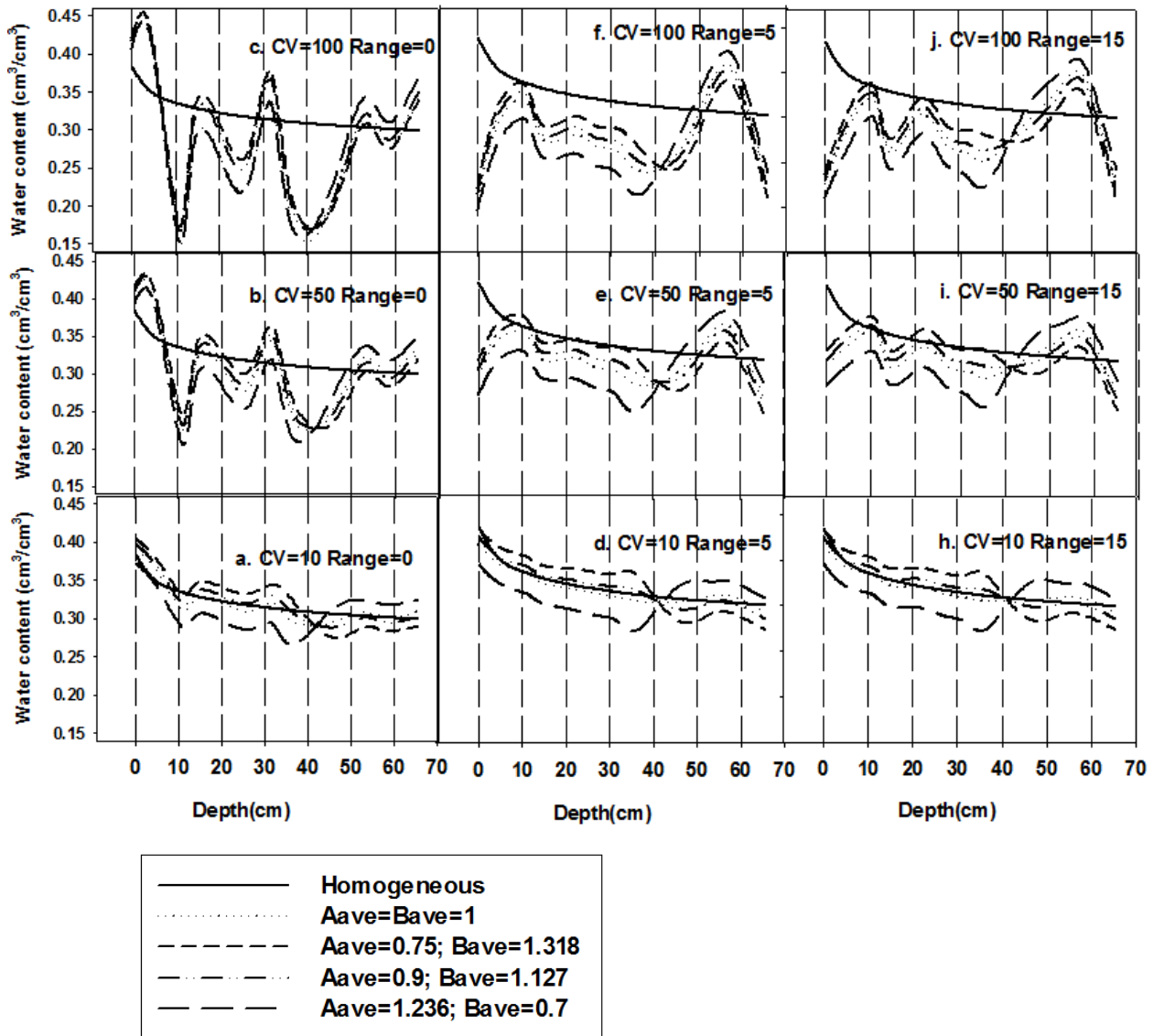


Figure 2-11: Volumetric water content directly beneath the surface line source at steady state

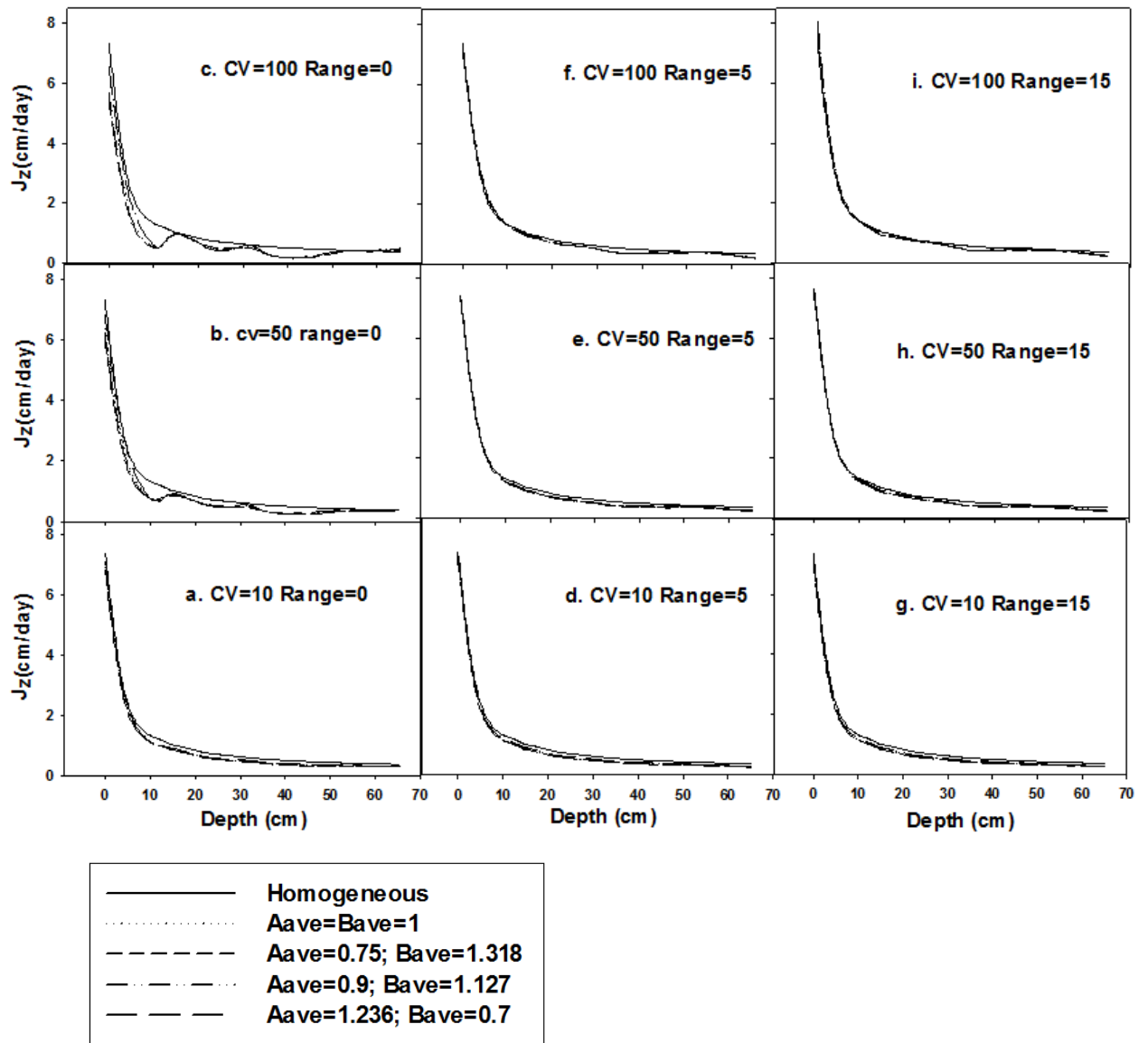


Figure 2-12: Vertical flux density directly beneath the surface line source at steady state

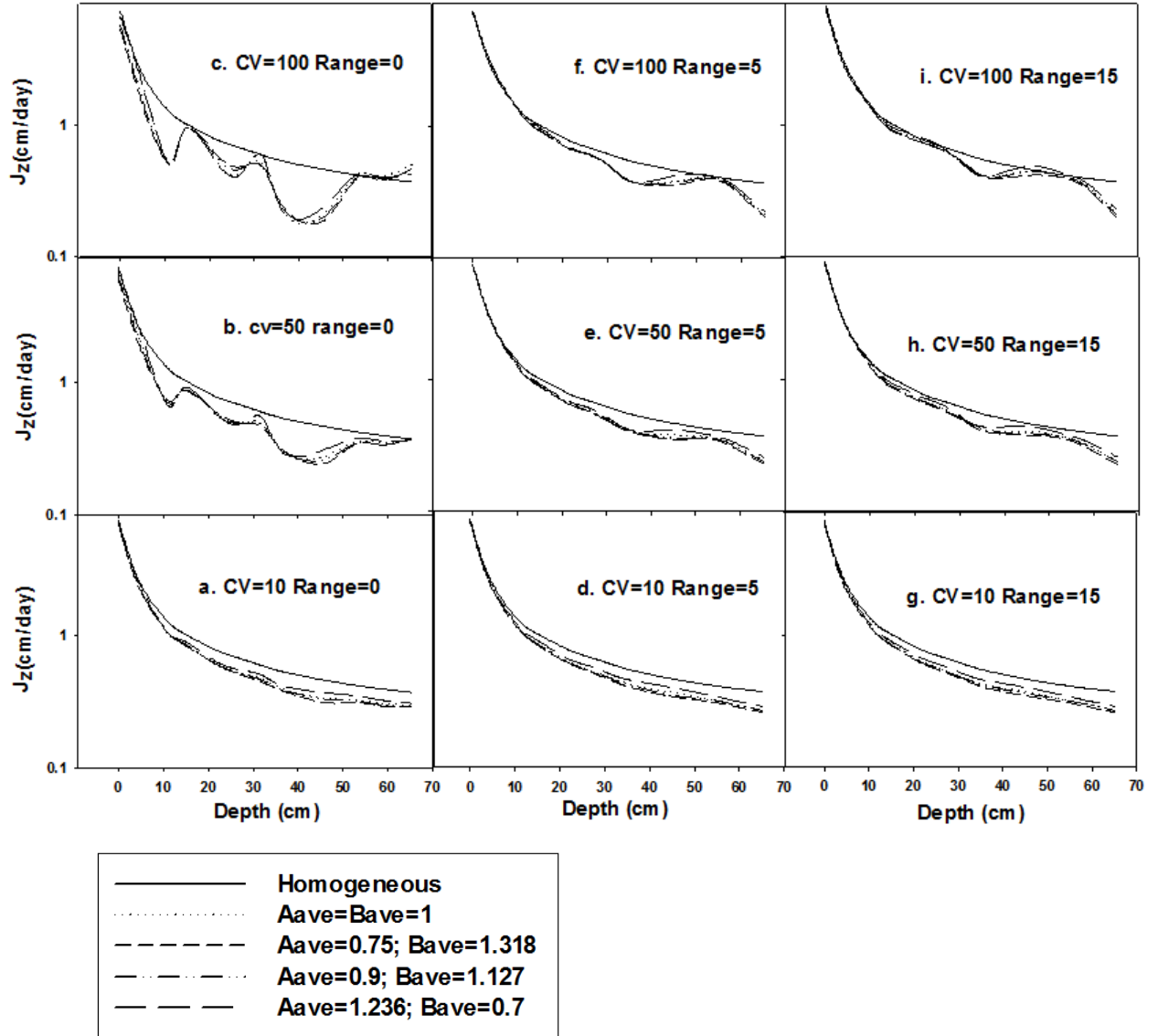


Figure 2-13: Vertical flux density (log scale) directly beneath the surface line source at steady state

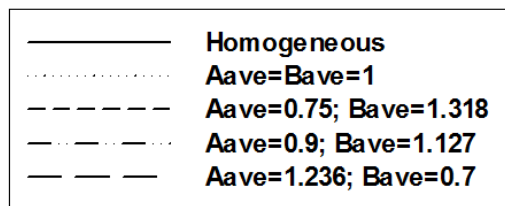
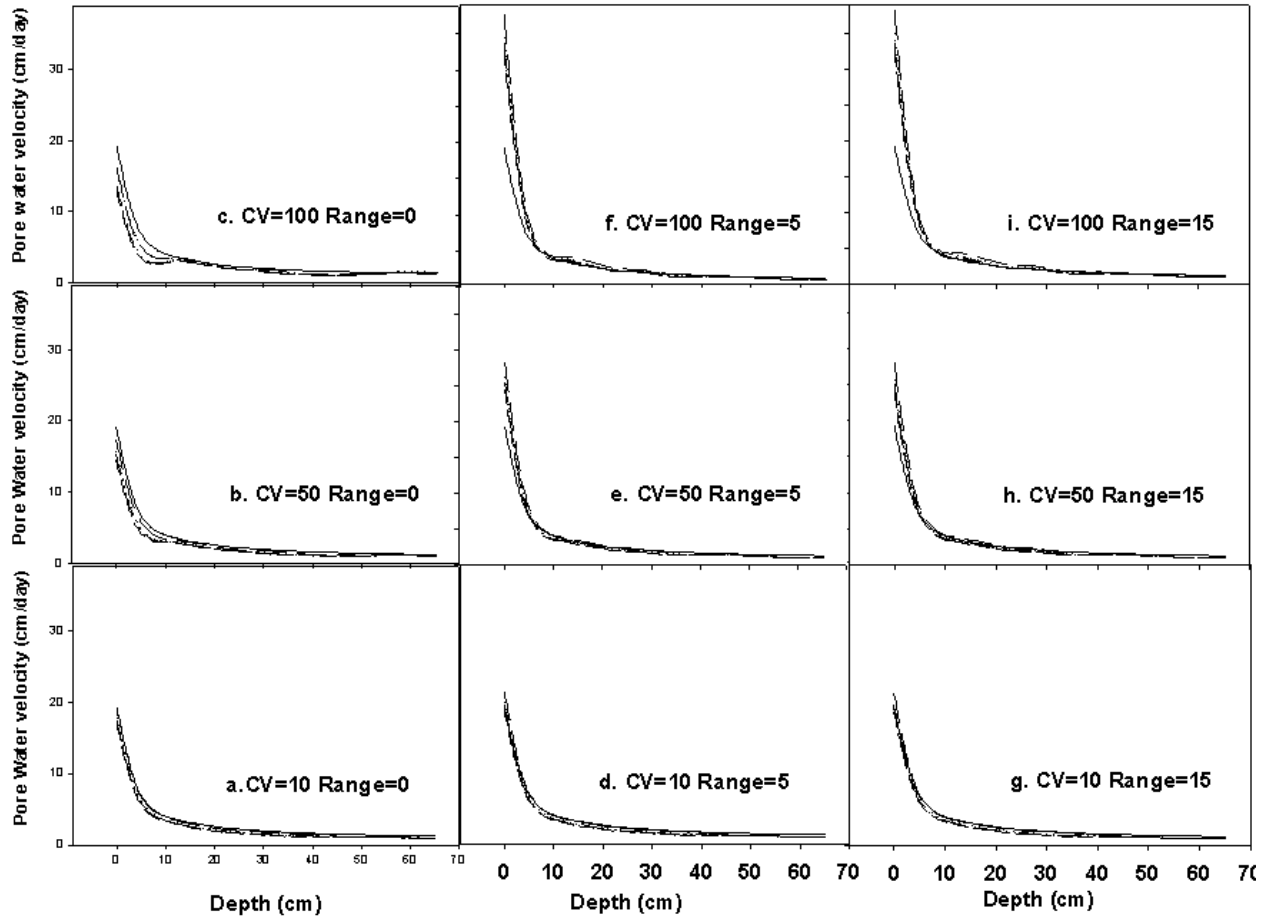


Figure 2-14: Vertical velocity directly beneath the surface line source at steady state

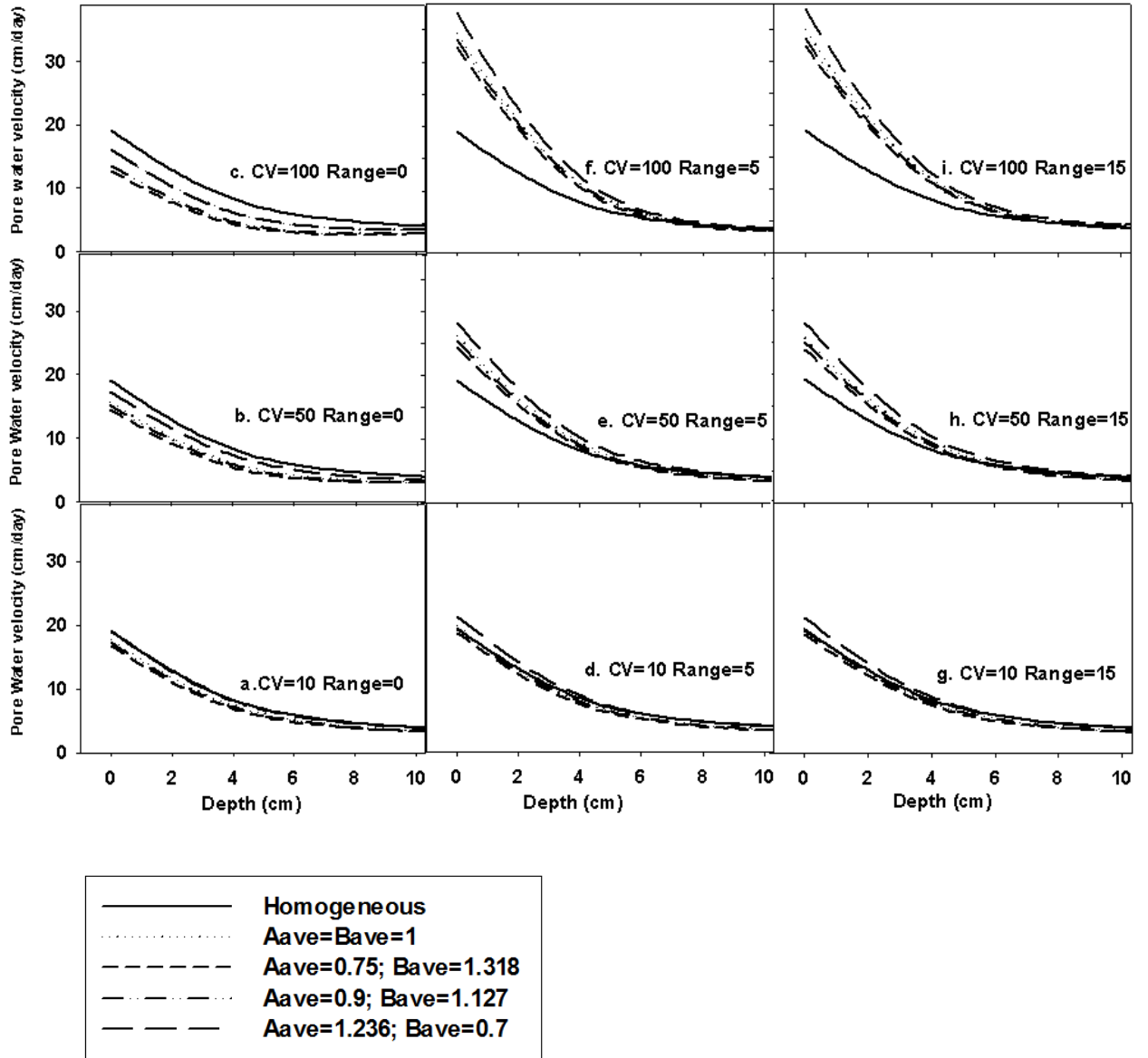


Figure 2-15: Vertical velocity directly beneath the surface line source within top 10 cm at steady state

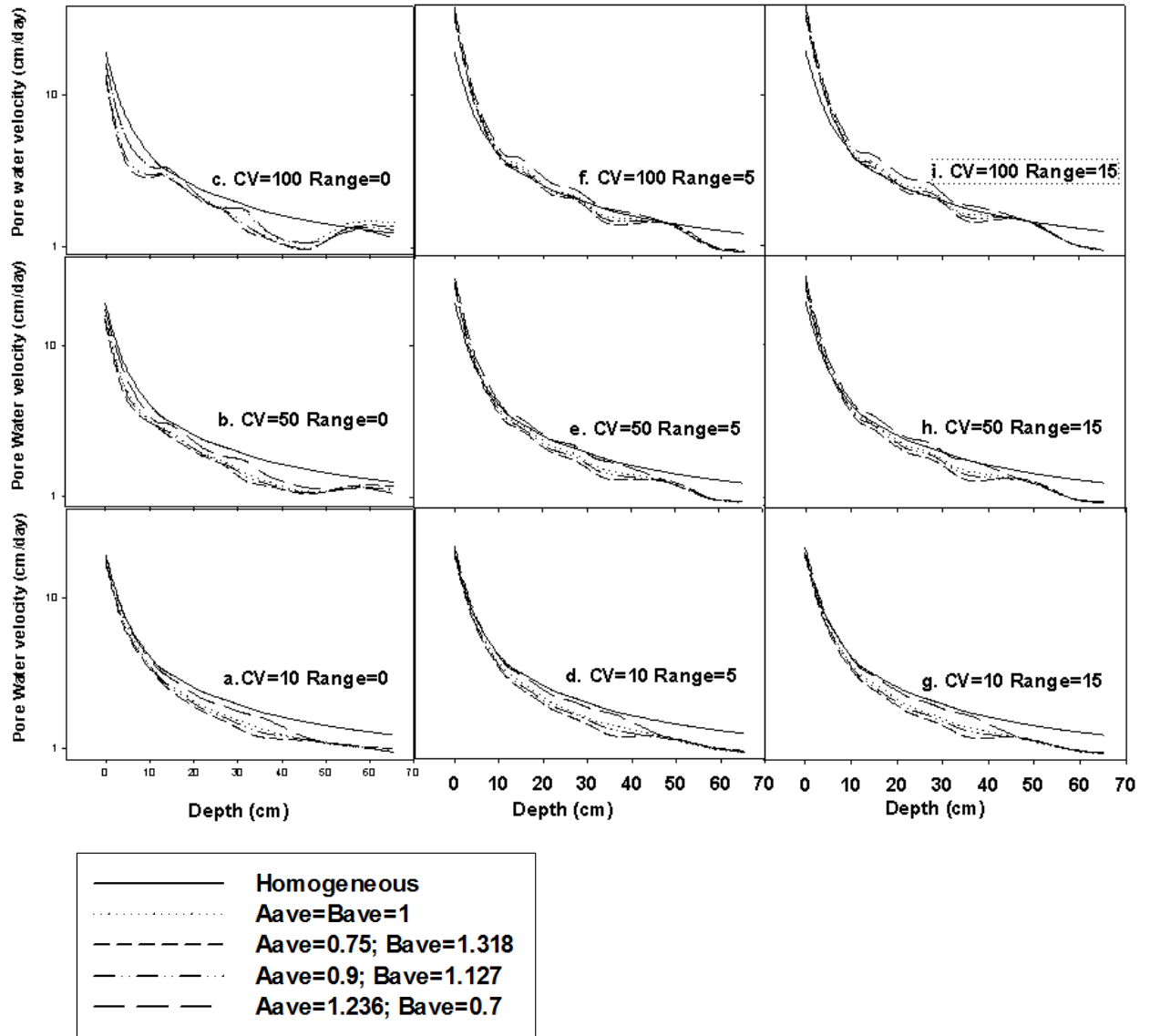


Figure 2-16: Vertical velocity (log scale) directly beneath the surface line source at steady state

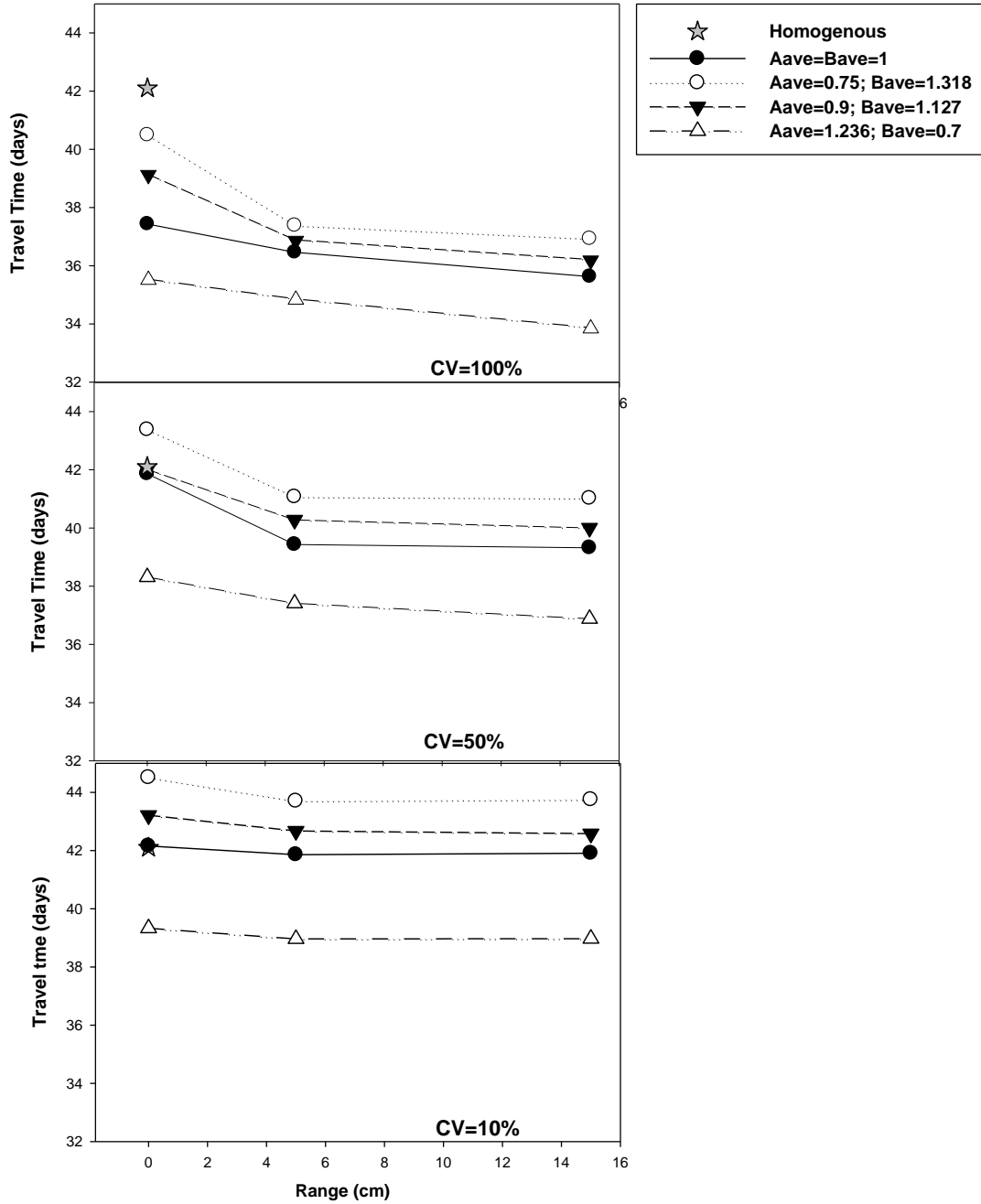


Figure 2-17: Conservative travel time versus Range of correlation in vertical direction directly beneath the surface line source at steady state

3. Simulation of three-dimensional flow under surface line sources: sensitivity analysis and model calibration

3.1. Introduction

Soil horizons originated from the same parent material and were differentiated by hydrological-based pedogenic process. The variability of the hydraulic properties of the soil profile was inherited from the parent material (i.e. texture and mode of parent material deposition). The pedogenic processes were scale-dependent; thus, the hydraulic properties of the overlying horizons are expected to be spatially-correlated. Field experiments have shown that the soil water fluxes within and across the visually distinct soil horizons interfaces are significantly spatially-correlated to each other (Dyck and Kachanoski, 2009a, 2009b, 2011).

Many onsite, pressurized, at-grade wastewater treatment systems can be modeled as an infiltration and percolation process through layered heterogeneous field soil under a surface line source boundary condition. The soil profile plays an important role for purifying sewage water prior to recharge to the ground water. (Tyler, 2001; Radcliffe and L. T. West, 2008; Tyler and Mokma, 2004). The

complex interactions of hydraulic and purification processes potentially remediate the sewage so it has acceptable recharging water quality (Van Cuyk et al, 2000). Therefore, it is essential to understand how the hydrological variability and soil layers affect the hydraulic behaviour of the soil at the field scale and design a numerical model to predict the process.

As indicated in Chapter 2, the linear scaling schemes to describe or represent heterogeneous field soils assume the variance of the soil pore size stays constant while the mean varies from location to location (Miller and Miller 1956; Sposito, 1998). However, when this assumption is not valid an alternative way of representing and modeling the hydraulic heterogeneity of the soil is required.

One approach to characterize the heterogeneous hydraulic properties of the soil is to allow the van Genuchten (VG) hydraulic parameters (van Genuchten 1980) to vary in space that can be simulated with random field methods which preserve observed or assumed spatial patterns (Deutsch and Journel, 1998).

The objective of this chapter is to test the sensitivity of the hydraulic behaviour of at-grade line source systems to the VG soil

hydraulic parameters, and identify the VG hydraulic parameters that best describe the field measurements of transient infiltration of water from a surface line source (Dyck and Kachanoski, 2007; unpublished data).

3.2. Methods

3.2.1. Data from 2-D surface infiltration on layered field soil

In this chapter, a three-dimensional (3-D) numerical model was constructed in HYDRUS 3D (detailed description of the software is given in Appendix I) and calibrated to predict the field-measured hydraulic behaviour of a two-dimensional (2-D) infiltration experiment in a layered, field soil carried out by Dyck and Kachanoski (2007, unpublished data). The hydraulic properties of the soil were measured from undisturbed soil cores taken from the site, and were used to obtain initial estimates of the input hydraulic parameters for the model.

The field site was located 75 km north of Edmonton, and had not been cultivated for at least 15 years. Soils at the site consist of 80% orthic Gray Luvisols (Bright bank series) and 20% Orthic Dark Gray Chernozem developed on sandy aerolian parent material. The

Chernozemic soil was observed to be composed of distinct Ah and Bm horizons and the average depth of A/B horizon interface was measured to be 27cm with a coefficient of variation (CV) of =21%. The site is part of the Aspen Parkland Natural region of Alberta. The mean annual precipitation of the site is approximately 400mm and with 2°C mean annual temperature and 95 mean annual frost-free days.

A 2D quasi-steady surface infiltration condition was set up in a greenhouse with dimensions 10m x 5m. The 2-D quasi-steady flux boundary condition at the soil surface was achieved by applying water with an Andpro Spray Rite Watering system (Dyck and Kachanoski, 2009a). The system consists of a nozzle spray boom attached to an electronic drive-train moving back and forth along a rail suspended from the roof of the green house. The spray boom was oriented such that it sprayed a 0.1-m x 8.0-m strip on the soil surface (approximate to a line source). The average water application rate was 10cm/day. The spatial variability of the surface water application rate was low with a coefficient of variation (CV) equaling 5%.

Time domain reflectometry (TDR) probes, 25-cm and 60-cm long with 5-cm inter-rod spacing were deployed to measure the water

content in the soil directly beneath the line source. The 25-cm probes were assumed to span the A horizon and the 60 -cm probes were assumed to span both the A and B horizons. There were 46 pairs of 25-cm and 60-cm probes that were installed in a cross pattern with 15-cm spacing along a 6.75 m transect. In addition, 45 60-cm probes were installed between each pair of the crossed pattern probes. The TDR probes were switched manually, and the waveform was collected and analyzed with TACQ BETA software (Evet, 2000). It was found that the manual switching was fast enough to log the waveform accurately (Dyck and Kachanoski, 2009a and 2009b).

The hydraulic properties of A horizon and B horizon were measured from 128 aluminum cores with dimensions 5cm i.d, 50cm to 60cm length taken from a transect close to the west wall of the green house. Each core sample was divided vertically into approximately 10, 5-cm thick subsamples (5 for A horizon and 5 for B horizon). Each core was split at the soil horizon interface and each horizon above and below the interface was subsequently subsampled. The saturated hydraulic conductivity (K_s) was measured from selected subsamples (N=677) under constant head boundary conditions. The four moisture retention curve points for each subsample was measured by applying

standard pressure plate methods and tension table method (Renold and Topp, 2008). The van Genuchten (1980) soil hydraulic characteristic parameters were estimated by fitting van Genuchten equations to the measured data using a least-squares Levenberg-Marquardt algorithm with Mathcad.

3.2.2. Hydraulic Property Model and Parameterization of Flow

Model

The van Genuchten (VG) expressions of volumetric water content as a function of matric potential and relative hydraulic conductivity as a function of water content are as following (van Genuchten, 1980)

$$\theta(h) = \theta_r + (\theta_s - \theta_r)(1 + (\alpha h)^n)^{\frac{1}{n}-1} \quad [3-1]$$

$$K(\theta) = K_S \left(\frac{\theta - \theta_r}{\theta_s - \theta_r} \right)^{0.5} \left\{ 1 - \left(1 - \left(\frac{\theta - \theta_r}{\theta_s - \theta_r} \right)^{\frac{n}{n-1}} \right)^{1 - \frac{1}{n}} \right\}^2 \quad [3-2]$$

where θ is the volumetric water content ($cm^3 cm^{-3}$), θ_r is the residue volumetric water content ($cm^3 cm^{-3}$), θ_s is the saturated water content. h is the matric potential in head units (cm), α (cm^{-1}) is related to the air entry value, and n is an indicator of the variance of

the pore size distribution. The van Genuchten parameters α, n, θ_r and θ_s were estimated for the samples by fitting Eq. [3-1] to the measured moisture retention data. The saturated water content θ_s was assumed to be equal to the measured volumetric water content at zero matric potential, and θ_r was assumed to be equal to the permanent wilting point which was estimated with the pedotransfer function (PTF) of Rawl et al. (1982). The Rawls et al. (1982) PTF uses soil texture to estimate soil water content at various matric potentials. It was observed that the soil texture for this soil was quite uniform so θ_r was assumed to be a constant equal to $0.03 \text{ cm}^3/\text{cm}^3$.

3.2.3. Three-dimensional random field generation hydraulic properties for the numerical model

The hydraulic properties of the soil were measured on a 2-D transect, but the hydraulic model was 3-D. Therefore, the input VG parameters for the numerical model in HYDRUS 3D were generated from a geostatistical random field simulation with modeled 2-D spatial pattern from the measurement of the soil samples taken from the field. The spatial variability of the measured VG hydraulic parameters was estimated using variograms. Variogram is a function

that describes the degree of spatial dependent of a random field (Deutsch and Journal, 1998):

$$2\gamma(l) = E\{[Z(u) - Z(u + l)]^2\} \quad [3-3]$$

where $\gamma(l)$ (unit dependent on the specific variable) is the semivariogram as a function of the lag distance l (cm), $E\{\}$ is the expectation value operator, and $Z(u)$ is the random field variable as a function of location vector u . The sill of a variogram is defined as where the variogram appears to flatten off (Deutsch, 2002). The range of a variogram is the distance from the origin to where the variogram reached the sill.

The input VG parameters were generated using geostatistical random field simulations. Geostatistical random field simulations required positive-definite, parametric variogram models in standard Gaussian space instead of empirical variograms (Deutsch and Journal, 1998). An acceptable variogram model consists of an isotropic nugget effect in all directions and any combinations of the standard variogram models (Deutsch and Journal, 1998). In addition to the nugget effect, the following two models were utilized in this study, Spherical:

$$\gamma(l) = c \cdot Sph\left(\frac{l}{a}\right) = \begin{cases} c \cdot \left[1.5 \frac{l}{a} - 0.5 \left(\frac{l}{a}\right)^3\right], & \text{if } l \leq a \\ c, & \text{if } l \geq a \end{cases} \quad [3-3]$$

Exponential:

$$\gamma(l) = c \cdot Exp\left(\frac{l}{a}\right) = c \cdot \left[1 - \exp\left(-\frac{3l}{a}\right)\right] \quad [3-4]$$

where $\gamma(l)$ (unit depends on the specific variable) is the semivariogram as a function of the lag distance, c is the variance contribution (unit depends on the specific variable) (the sum of the nugget effect and variance contribution of each variogram is equal to the variance of the random field), and a (cm) is the actual range which is the distance from the origin to where the semivariogram reached the sill. The sill of the semivariogram model is the variance of the random field which is 1 by definition in standard Gaussian space.

The cumulative probability density function of each hydraulic parameter was transformed to a standard Gaussian distribution prior to variogram calculations (Eq. [3-3]) since the estimated variograms were modeled in standard Gaussian space. There are two questions need to be answered before the variogram modeling and geostatistical simulations: 1) Whether the hydraulic variables of the two horizons

can be modeled simultaneously; 2) the decision of stationarity (which data to pool together for the subsequent analysis (Deutsch, 2002)).

The variograms of each hydraulic parameter for each horizon separately and both horizons simultaneously were estimated by Eq. [3-3] in Gaussian space using the GAMV program in GSLIB 90 (Deutsch and Journel, 1998). The calculated variograms are presented in Fig. 3-1, Fig. 3-2, Fig. 3-3, and Fig. 3-4. The variograms of each hydraulic parameter was estimated for up to 15 cm total lag distance in the vertical direction. Deutsch (2002) suggested for a reasonable variogram estimation, the total lag distance should be about half of the domain being considered (in the interested direction). The depth of each A or B horizon measured was about 20 cm to 35 cm, so 15 cm was about half of the average depth of each horizon.

The comparisons of the variograms of each hydraulic parameter for each horizon separately and both horizons simultaneously (Fig. 3-1., Fig. 3-2., Fig. 3-3., Fig. 3-4) suggested the spatial patterns and ranges of the variograms of each parameter in the A horizon and B horizon separately and in both horizons simultaneously in both vertical and horizontal directions were similar although the amplitude

of some of the variograms were different and some variograms in the vertical directions show different trends. As discussed above, the sill of an accepted variograms have to be constrained to 1, so the amplitudes of the variogram models have to be scaled according to the theoretical sill. Therefore, the differences in the variogram amplitudes do not affect the variogram modeling. An increasing trend of a variogram indicates the differences between the data pairs systematically increase as the lag distance increases. It was not expected that the mean of a variable is independent of the location if a significant trend is present in the variogram. In a geostatistical modeling or simulation, it is essential to make sure the variable being modeling is stationary (mean of the variable is independent of the location) over the domain of study (Deutsch, 2002). Therefore, the trend of the variograms must be removed before variogram modeling and geostatistical simulations. From the above discussion, it was reasonable to model variograms of the two horizons simultaneously as long as the shapes and the ranges of the variograms of each VG parameter for the two horizons are similar.

The calculated variograms of each hydraulic parameter with two horizons simulated simultaneously were sequentially fitted by

variogram models as shown in Table. 3-2. 3-1., Fig. 3-5., Fig. 3-6., Fig.3-7., and Fig. 3-8. Some of the variogram distributions of the measured hydraulic parameters show periodic patterns (Fig. 3-5, Fig. 3-6, Fig.3-7., and Fig. 3-8). To model these cyclical patterns, periodic geometric functions are required. However, the sum of the variance contributions for each parameter in each direction has to be equal to 1, and the sine and cosine function oscillate around 1, the inclusion of geometric functions to model cyclical (“hole effect”) variograms violates the constraints of the geostatistical simulation algorithm (sgsim) in GSLib. However, a kriging estimate (numerical algorithm used to estimate simulated variables in sgsim) of a parameter at a given location is not likely to use values of the parameter beyond the range of the variogram. Therefore the cyclicity of the measured data (which is only apparent at distances beyond the range of the variogram) for variogram fitting was ignored.

The estimated variograms for each of the VG hydraulic parameters were used to generate a three-dimensional random field of the hydraulic parameters by extending the 2-D variogram to three dimensions assuming variogram isotropy in the east-west, north-south horizontal directions.

Using the calculated 2-D variograms for each hydraulic parameter for the 3-D model domain, the hydraulic parameters were simulated as standard Gaussian variables with the sequential Gaussian simulation (sgsim) program in GSLIB (Deutch and Journel, 1998). The sgsim algorithm simulates spatial variables in Gaussian space with a combination of kriging and Monte Carlo simulation. The cumulative probability density function of each hydraulic parameter (measured data) was transformed to a standard Gaussian distribution prior to the geostatistical simulation. Each hydraulic parameter was simulated in standard Gaussian space and then back-transformed to its original distribution.

The dimensions of the random field simulation domain were 500 cm (x-direction, east-west), 1000 cm (y-direction, north-south), and 150 cm (z-direction, vertical) with discretization of 10 cm in all the three directions. It was assumed 1) the spatial dependence of the hydraulic properties was isotropic in both x and y directions; 2) the hydraulic properties of the soil measured from the samples taken approximate 2.5-m away from the line source, are representative of the soil underneath the surface line source; and 3) the normalized

variograms of all the hydraulic parameters are continuous across the horizon interface.

3.2.4. Model selection and description

The numerical model for predicting the surface line source infiltration process in layered variable soil was built in HYDRUS 3D (detailed description of the software is given in Appendix I). The dimensions and discretization of the domain were the same as those of the random field simulation, $500\text{cm} \times 1000\text{cm} \times 150\text{cm}$ with 10-cm discretization in all directions. The x direction in the domain was defined from left to right (east-west), the y direction points into the page (north-south), and the z-direction is from the bottom to the top. The soil was assumed to have two soil horizons. The horizon interface is set at 25 cm. Every node in the domain was defined as a single hydraulic material, so a unique set of hydraulic parameters (random field simulation results) was given to each node. A boundary condition of 10cm/day was set at each node at the midpoint on the surface along a 1000cm transect in the y direction as shown in Fig. 3-9. The total volume of water applied to each node (cm^2/day) with the constant flux is calculated by 10cm/day times the dimension of the discretization in X and Y directions, $10\text{cm}/\text{day} \times 10\text{cm} \times 10\text{cm}$

(same rate as the field boundary condition). The bottom boundary of the domain was treated as free drainage while the vertical side boundaries were set to zero flux. The simulation was run for 10 days and an example of output water content after 10 days is shown in Fig. 3-10.

The hydraulic parameters were measured on small-scale core samples and from a transect different from the actual flow experiment, it was unreasonable to expect simulated and measured hydraulic behaviour to match without adjustment of the hydraulic parameters.

3.2.5. Calibration of the numerical model

The VG hydraulic parameters simulated from SGSIM were incorporated into the 3D numerical model with a fixed residual volumetric water content θ_r equals to $0.030 \text{ cm}^3/\text{cm}^3$. The running time was 10 days, and the hydraulic output of every node in the domain at observation times of 0, 0.3, 0.6, 1, 1.5, 2, 3, 4, 6, 8, 10 days was recorded. Observation points at 69 locations along the line source (10 cm apart) with 10cm apart at depth of 0 cm (on the surface at the line source) to 60 cm depth in 10 cm increment were chosen. The calibration goal was for the model to match the field-measured

average water storage as a function of time and the variance of the field measured water storage as a function of time.

The vertical TDR probes in the field measured average water content (or storage) over the length of the probe rods, which was easily converted to soil water storage by multiplying by the length of the TDR probe. In order to compare the field measurements and the model output, the HYDRUS water content output for the observation nodes directly under the line source were converted to soil water storage. Water content at each of the 69 observation node profile locations at each observation time was estimated by linear interpolation (linterp function in Mathcad). Water storage in the top 25cm and 60 cm soil directly beneath the line source was calculated by

$$W_L = \int_0^L \theta(l)dl \quad [3-5]$$

where L is the length of measurement, θ is the water content (cm^3/cm^3) and W_L is the soil water storage over the distance 0 to L.

For determining the optimal hydraulic parameters, it was assumed that the autocorrelation range of each hydraulic parameter

was essentially correct and in order to minimize difference between the spatial pattern of the optimized and measured hydraulic properties, VG parameters were adjusted in two ways: multiply the VG parameter considered at each of the 76 locations by a constant number and keep the coefficient of variation constant; and adjust the variance or standard deviation without changing the mean of the parameter.

To adjust the mean of the parameter without changing the coefficient of variation (CV), the parameter at each location is multiplied by a constant, $X \rightarrow aX$, and the mean and variance become

$$E[aX] = aE[X] \quad [3-8]$$

$$VAR[aX] = a^2VAR[X] \quad [3-9]$$

$$CV[aX] = \frac{\sqrt{a^2VAR[X]}}{aE[X]} = CV[X] \quad [3-10]$$

To adjust the variance of the parameter without changing its mean, the following transformation is used: if $X \rightarrow aX + (1 - a)E[X]$, then the variance will become

$$VAR[ax + (1 - a)E[x]] = a^2VAR[x] \quad [3-11]$$

while the mean remains the same,

$$E[aX + (1 - a)E[X]] = E[X] \quad [3-12]$$

and the standard deviation or CV of the variable is increased by

$(a-1)*100\%$.

3.2.6. Initial condition

In the field, the water application experiment was started following 10 days of drainage. It was observed that the daily change in the water content at this time was around 1% which indicated very low-flux or zero flux conditions. The initial condition in the model was obtained by setting the domain at almost saturation and then letting it drain until the output water storage matched the field measured initial average water storage (Table 3-2).

3.2.7. Error Analysis-Least Square Method

The simulation outputs of the numerical model were analyzed against the field measurement. For each field measurement, $G_i(t)$, as function of time, t (days),

$$G_i(t) = \hat{G}_i(t) + \varepsilon_i; \quad i = 1, 2, \dots, N \quad [3-13]$$

Where $\hat{G}_i(t)$ is the model prediction, ε_i is the error term associated with the field measurement and the model prediction.

There were four types of field measurements: TDR measured average soil water storage in the top 25 cm soil along the line source transect and the corresponding variance (G1 and G2 in Eq. [3-14], respectively); TDR measured average soil water storage in the top 60 cm soil and the corresponding variance (G3 and G4 in Eq. [3-14], respectively). In order to find the optimum input VG parameters for the prediction, a sum of squared errors function, SSE (dimensionless) was introduced:

$$SSE = \frac{1}{4} \sum_{i=1}^4 \sum_t \left(\frac{\hat{G}_i(t) - G_i(t)}{G_i(t)} \right)^2$$

[3-14]

where $\frac{\hat{G}_i(t) - G_i(t)}{G_i(t)}$ is the discrepancy of model prediction with respect to the field measurement at each time.

3.2.8. Scale-dependent variance

The variance of a spatial scale-autocorrelated variable is dependent on the spatial scale. Therefore, in order to determine the stationary variance for such a variable it is necessary to estimate the variance at a length scale greater than its autocorrelation scale length (Dyck and Kachanoski, 2011). The scale-dependent variance as

outlined by van Wesenbeeck and Kachanoski (1991) considers spatial series X of N total observations. The variance of the series within an i sampling interval is given by:

$$Var_i(X) = E[V_i] \quad i = 1 \dots N - 1 \quad [3-15]$$

where $Var_i(X)$ is the variance of the series X at the spatial scale $i \cdot \Delta x$, and V_i is:

$$V_i = E[(X_j - E[X_j])^2] \quad j = k \dots k + i \quad k = 1 \dots N - i \quad [3-16]$$

and

$$\bar{X}_i = E[X_j] \quad [3-17]$$

Similar to the variogram the scale dependent variogram also estimates the spatial correlation of the spatial-autocorrelated variable. The spatial auto-correlation length of a variable can be calculated as the spatial length requires for the scale dependent variance to reach a stationary value.

3.2.9. Sensitivity Analysis for VG parameters

In order to decide which VG parameters to adjust in order to calibrate the model, the sensitivity of the model output with respect to

all of the VG parameters was assessed. There were two parts in the sensitivity analysis. The first part was to adjust each parameter without changing the CV of the parameter. The second part was to change the variance of each VG parameter while keeping the mean of the parameter constant. For both parts, only one parameter was adjusted at each time while the other parameters were remaining unchanged from the sgsim simulated values.

In the first part of the sensitivity analysis, each parameter at each location simulated from the SGSIM was multiplied by +20% or -20%. Thus, the CV of the parameter considered stayed constant, and the simulated water storage was compared to the measured values while the other parameters were held constant at the original simulated values.

Similar to the first part, for the second part, only one parameter was adjusted for each sensitivity comparison. The CV of each input VG parameter was increased or decreased by 10% to simulate the water storage. When the CV of K_s was increased by 10%, some of the K_s were to negative values which are not reasonable. Therefore, the sensitivity analysis of K_s was only tested with the CV decreased by 10%. According to Eq. [3-8] and Eq. [3-9], to change the CV by 10%

while keep the mean of each parameter constant, each value, x was modified to $x \rightarrow ax + (1 - a)E[x]$, $a = 1 \pm 0.1$.

3.3. Results and Discussion

3.3.1. Calibration

The average TDR measurement of the initial water storage of the field soil for the transient water infiltration experiment was 3.483 cm for the 25-cm probes and 8.273 cm for the 60-cm probes. The initial condition of the model was calibrated by setting the soil domain at $h = -20$ cm (i.e. near saturation) everywhere and then simulating drainage for 20 days. The output results (Table. 3-2.) showed that the simulated results of 14 days best matched the initial condition of the field measurements with the model output water storage for the 25 cm depth equaling 3.506 cm and 1.96% daily water storage change, and for the 60 cm depth equaling 7.935 cm and 2.42 % daily water storage change. Therefore the model output matric potential corresponding to 14 days of drainage was imported to the numerical model as the initial condition.

Prior to adjusting any hydraulic properties, the simulated and measured soil water storage was compared. At each observation time,

the water storage was averaged over all locations and compared with the average field data measured by TDR as shown in Fig. 3-11. For all measurement, thus, the simulated output average water storage in both the top 25 cm and 60 cm depths was higher than the measured field average. The corresponding variance was compared in Fig. 3-12. The simulated output variance of the water storage in the top 25 cm depth was lower than the measured field output while the simulated output variance in the top 60 cm depth was higher than the measured field output. To calibrate the model, the results of the sensitivity analysis to the changes in the mean and variance of the VG parameters were analyzed.

3.3.2. Sensitivity Analysis

The simulated output of first part of the sensitivity analysis where each input VG parameter at each location simulated from SGSIM was multiplied by +20% or -20% are presented in Fig. 3-13, Fig. 3-14, Fig. 3-15, and Fig. 3-16. The simulated output with unchanged estimated field average input parameters was plotted in each figure as a reference. The average soil water storage was positively related to θ_s , negatively related to K_s and n . The time for the soil water storage to reach steady state was positively correlated to α .

The magnitude of the average soil water storage was not sensitive to α . The variance of the soil water storage was not sensitive to any of the VG parameters, which was consistent with keeping the CV of each parameter constant.

In the second part of the sensitivity analysis, the CV of each input VG parameter was increased or decreased by 10% to simulate the water storage and the results were compared in Fig. 3-17, Fig. 3-18, Fig. 3-19, and Fig. 3-20. A change in the CV of each parameter did not affect the average distribution of the water storage. A decrease in the CV of K_s or α by 10% resulted in a slight decrease of the variance of the water storage (Fig. 3-13). The variance of the soil water storage was positively affected by the CVs of K_s , n and α , and negatively affected by the CV of θ_s , and it was most sensitive to the change of the CV in the n parameter compared to other parameters. A change in the CV of K_s did not affect the initial storage since initially the total potential was the same everywhere over the domain and there was not any flow until time was greater than zero. The initial variance of the soil water storage appeared to be most sensitive to n .

3.3.3. Mean and variance of transient soil water storage

There are a number of reasons why the simulated model output may not match the field measurements. The soil samples taken from the field were from a near but different transect than where the field infiltration process was carried out. Thus we would not expect the VG parameters from the soil samples to be a perfect match to the parameters of the infiltration transect. The measurement of the applied water flux rate in the field experiment also indicated some spatial variance in the application rate. The variograms of K_s and θ_s (Fig. 3-5. and Fig.3-8.) did not approach constant sills which indicate spatial trends in the mean of these parameters in the vertical direction for both the A horizon and B horizon. Similarly, the variograms of α and n (Fig. 3-6. and Fig.3-7.) indicate a spatial trend in the mean of these parameters in the vertical direction for the A horizon. These patterns indicate that the modeled variables did have a stationary mean (i.e. the mean of the variable varies from location to location). Thus it is likely that the variability of the VG parameters is higher than what we have modeled.

From the above considerations, it is reasonable to modify the VG parameter to calibrate the model to predict the hydraulic output of

the field soil. The measured hydraulic properties of the field soil showed a very narrow distribution of the α parameter compared to the n parameter (Fig. 3-21.). This suggests the soil had a more spatially-variable pore size variance and a fairly consistent mean pore size. Laboratory measurement of the saturated hydraulic conductivity K_s is very sensitive to the sample size (Reynolds and Topp, 2008). It was observed that the laboratory measurement of K_s from small soil cores most likely to be smaller than the actual values (Fodor et al., 2011). The size of the soil cores for the hydraulic property measurement in this study was very small (5-cm radius and 10 cm height). Therefore it was expected that the actual values of K_s are higher than the laboratory measurement. Therefore it was reasonable to adjust K_s and n to obtain the optimum input VG parameters instead of adjusting α and θ_s .

The simulated water storage and measured field data were very similar when: 1) the K_s at each node was modified by 1.5 times its originally simulated value for both A and B horizons; 2) the standard deviation of the n parameter was increased by 25% from 0.335 to 0.418 for A horizon and decreased by 25% from 0.354 to 0.2875 for B horizon; and 3) all of the originally simulated n parameter values in

the A horizon were multiplied by 1.1, and all of the originally simulated n parameter values in the B horizon were multiplied by 1.22. The simulated results for these “optimized” VG parameters are shown in Fig. 3-22 and Fig. 3-23.

3.3.4. Least Square Error Contour Map

To test the uniqueness of the “optimized” VG parameters, the SSE was calculated for a number of different K_s and n parameter combinations. A contour map of the sum of squared errors as calculated using Eq. [3-14] were represented in Fig. 3-24. In the figure, $K_s = 1$, and $n = 1$ represent the normalized “optimized” parameters. The ratio of each parameter in the A horizon to the B horizon was assumed constant. For example, $K_s = 1.1$ means the “optimized” K_s parameter in each horizon was multiplied by 1.1.

The distribution of the contour lines of the sum of least square error map in Fig. 3-24 shows that the simulated water storage was less sensitive to K_s than n , and less sensitive to n in the increasing magnitude direction than the decreasing magnitude direction. The major contribution of the error source was from the variance of the 60-cm probes water storage. Fig. 3-23 shows that the variance of

TDR-measured soil water storage of the 60-cm probes had more fluctuations than the other measurements. The measured variance of the 25-cm probes decreased as time increased which had the same pattern as the simulated results while the measured variance of the 60-cm probes increased as time increased.

The soil horizon interface affects the transient local flux differently than the steady state since the physics governing the two processes is different. It was shown by Dyck and Kachanoski (2009a and 2009b) that the correlation of the transient flux above and below the horizon interface was positive while the correlation of the steady state flux was negative. This fact explains why the measured water storage variance of the 60-cm TDR probes was lower in the early time period (transient state).

3.3.5. Limitations of the numerical model

3.3.5.1. Classified post maps of the optimized VG parameters

The classified post maps, Fig. 3-26, Fig. 3-27, Fig. 3-28, and Fig. 3-29, were plotted to compare the VG parameter distributions of the lab measurements to a 2D slice of the optimized parameters for the numerical model. For each parameter, the lab measurement was

plotted from -3.5 cm to -56.5 cm in depth and 0 to 967.5cm (the coordinates of the data were selected from the mid-point of the soil cores); the optimized parameters were plotted from $x=250$ cm, y from 0 cm to 60 cm, z from 0 cm -60 cm, the cross section along the line source (the coordinates of the data were the same as the finite element coordinates).

The classed post maps of lab measurement of θ_s , K_s and (Fig. 3-26., Fig. 3-27, Fig. 3-28, Fig. 3-29.) show a local feature at the bottom right which did not show up in the simulated parameter distributions. Fig. 3-25 shows the transect of where the soil cores for measuring the hydraulic properties were taken from and where the transect of the infiltration experiment took place. The dimensions of the transect for taking the soil samples were $970\text{cm} \times 60\text{cm}$ ($y \times z$), and the dimensions of the entire simulated domain were $500\text{cm} \times 1000\text{cm} \times 60\text{cm}$ ($y \times z$). Since the hydraulic properties of a two dimensional transect was used to simulate hydraulic properties of a three dimensional field, and the transect of where the hydraulic properties measured was far away from the transect where the field experiment took place. The variograms used for the simulation represent the average spatial variation of the domain not local

anomalies. Therefore, it was not expected that the simulated model would represent the local features in the measured hydraulic properties.

3.3.5.2. Variogram of the optimized VG parameters

Parametric variogram models were used to fit the estimated variograms of the lab-measured VG parameters, and sequentially used to simulate the input VG parameters for the numerical model as mentioned in the methodology part. Fig. variograms (fitting versus simulation) compared the parameter variogram fitting models to the variogram of the sgsim generated VG parameters of the entire domain (direct simulation) (Fig. 3-30., Fig. 3-31., Fig. 3-32., and Fig. 3-33) In addition, the variogram of the “optimized” K_s and n were also plotted to compare the changes of the spatial pattern of the parameters after modification.

The range of a variogram of a variable is an indication of the spatial correlation length of the variable, which can be estimated as the distance from the origin to the sill (as mentioned in the methodology part). Table. 3-3. Shows the ranges of the parametric variogram models and the variograms of the sgsim simulated results for each VG parameter. For all the VG parameters, the range of the variograms

from the sgsim simulated results (direct dimulation) were longer than the the parametric variogram models in the vertical direction. The variogram of the simulated θ_s (Fig. 3-30.) showed an increasing trend in the vertical direction. The range of both the variograms of the K_s and α was about 2 times the range of the parametric variogram models. The range of both the variograms of the simulated results of the n and θ_s was much shorter than the range of the parametric models.

The observations of the discrepancies of the variogram comparisons indicate that the predetermined spatial patterns (VG parameters) were disrupted during the simulation process. Since the simulation process also used the kriging algorithm to simulate the missing data in the domain from the measured data, the discrepancies can be analyzed as the fact the parametric variogram models did not 100% corroborate the empirical variograms of the kriged data.

The variograms of the sgsim simulated K_s did not change after modified the simulated K_s by mutipling 1.1 at every loation to obtain the “optimized” K_s (Fig. 3-33). This observation was expected since the spatial correlation of K_s was not disrupted after the modification. On the other hand, the variograms of the “optimized” n (Fig. 3-32) did not overlap with the variograms of the sgsim simulated n since the CV

of the n parameter of the two horizons were modified differently and also the n parameter at each location in the A horizon was multiplied by a different number than the B horizon. However, the shape of the variograms and the range of the variogram corresponding to the “optimized” n still matched with the variogram of the sgsim simulated n, which indicate the spatial correlation of the variogram did not change after the modification.

3.3.5.3. Scale dependent variance

The spatial-scale dependent variance (Dyck and Kachanoski, 2011) of the water storage from the field measurement to the model output was compared (Fig. 3-34). Unlike the variogram, spatial-scale dependent variance is not sensitive to outliers. The variance of the field measurement and the numerical output matched fairly well for the 0 cm to 25 cm water storage, while it did not match in the mid-range for 0 – 60 cm. The variance of the field measurement reached the equilibrium much slower than the model output. There were a few measured water storage data at some locations at the field showed much lower values than the mean.

3.4. Conclusion

A numerical model was constructed to predict the hydraulic output, specifically water storage, of a field soil. Random field generated VG parameters were obtained for the model under a constant line source by using the measured spatial pattern of laboratory measured hydraulic properties on undisturbed cores. Sensitivity analysis was carried out to quantify the influence of the variation of the VG parameters on the simulated water storage. The numerical model was calibrated by modifying the VG parameters n and K_s to match the field measurements of water storage. The least square error maps showed that the simulated outputs were more sensitive to n than K_s , and more sensitive to n in the increasing magnitude direction. The spatial pattern of the VG parameter distributions indicated that the local features in the field soil did not show up in the numerical model. The range and shape of the variograms of the random field generated VG parameters were found to be different from the parametric variogram model used to govern the generation. The scale dependent variance of the simulated water storage was also compared against the field measurements. The scale dependent variance corresponding to 25 cm of simulated water storage matched well with the field data. However, the 60 cm

simulated water storage reached equilibrium at a greater spatial scale than the field measurement.

There are five types of error for the numerical model: 1) The water application rate of the field condition had a CV of 5%. 2) The laboratory measurement of the hydraulic property of the soil cores can be different than the field scale measurement due to the limited size of the soil sample and the type of applied methods(Hillel, 1998). For example, the soil texture is directly associated with the pore size distribution and significantly affects the hydraulic conductivity. A measurement of the texture content of the field soil showed that B horizon has a higher sand content than the A horizon. Thus different n and K_s values was expected for the two horizons. However, the laboratory measurements of n and K_s are very similar for the two horizons. 3) The error of the TDR measurement is 1%. 4) The discrepancy between the fitted variogram model and the calculated variogram 5) only one variogram was estimated for both A horizon and B horizons, however, the spatial auto correlation of the two horizons might be different, and the spatial cross correlation between the two horizons can be different from the auto correlation of each horizon. Again, the different structures of the two horizons can cause

the difference of spatial correlation. 5) There were some field measured data of water storage much lower than the average value, which may suggest some local features of the soil which was not considered in the model.

3.5. References

- Deutsch, V. Clayton and Andre G. Journel, 1998, GSLIB: geostatistical software library and user's guide, Second Edition. ISBN 978-0-19-510015-0.
- Deutsch, V. Clayton, 2002, Geostatistical reservoir modeling p. cm.- (Applied geostatistics series). ISBN 0-19-513806-6.
- Dyck, M. F. and R. G. Kachanoski. 2009a. Measurement of transient soil water flux across a soil horizon interface. *Soil Sci. Soc. Am.J.* 73:1604-1613.
- Dyck, M. F. and R. G. Kachanoski. 2009b. Measurement of steady-state soil water flux across a Soil Horizon Interface. *Soil Sci. Soc. Am.J.* 73: 1786-1795.
- Dyck, M. F. and R. G. Kachanoski. 2011. Scale-dependent covariance of soil physical properties above and below a soil horizon interface: Pedogenic versus anthropogenic influences on total porosity. *Can. J. Soil Sci.* (2011) 91.
- Fodor, N., R. Sandor, T. Orfanus, L. Lichner, K. and Rajkai 2011. Evaluation method dependency of measured saturated hydraulic conductivity. *Geoderma* 165 (2011) 60-68.
- Miller, E. E., and R.D. Miller. 1956. Physics theory for capillary flow phenomena. *J. Appl. Phys.* 27:324-32.

- Radcliffe, D. E., and L. T. West. 2009. Design hydraulic loading rates for onsite wastewater system. *Vadose Zone J.* 8:64-74.
- Rawls, W. J., D. L. Brakensiek, K. E. Saxton, 1982. Estimation of soil water properties. *Trans. ASAE*, 25, pp. 1316-1320.
- Reynolds, W. D. and G. C. Topp, 2008. Soil water desorption and imbibition: tension and pressure techniques. In Carter, M.R. and Gregorich, E.G. (eds.) - *Soil Sampling and Methods of Analysis*. 2nd Edition, CRC Press Taylor & Francis, Boca Raton, FL, USA, Chapter 72.
- Sposito, G. 1998. Scale dependent and scale invariance in hydrology. ISBN 0-521-57125-1.
- Tyler, E. J. 2001. Hydraulic wastewater loading rates to soils. In: K. Macncel (ed.) *Onsite wastewater treatment. Proc. of the 9th International Symposium on Individual and Small Community Sewage Systems*. ASAE. St. Joseph, MI. p.80-86.
- Tyler, E. J. and L. D. Mokma, 2004. *Onsite wastewater treatment performance codes- A review of selected state and model code performance provisions and implementation strategies*. NOWRA., Edgewater, Maryland.
- Van Cuyk, S., R. Siegrist, A. Logan, S. Masson, E. Fischer and L. Figueroa, 2000. Hydraulic and purification behaviors and their interactions during wastewater treatment in soil infiltration systems. *Wat. Res.* Vol. 35, No. 4, pp. 953-964.
- van Genuchten, M.Th, 1980. A closed-form equation for predicting the hydraulic conductivity of unsaturated soils. *Soil sci. Am.J.*, 44 (5): 892-898.
- van Wesenbeeck, I. J. and R. G. Kachanoski. 1991. Spatial scale dependence of in situ solute transport. *Soil Sci. Soc. Am. J.* 55:3-7.

Table 3-1: Parametric variogram model parameters

parameter	Nugget effect	Type of Variogram	Variance Contribution	Horizontal range, cm	Vertical range, cm	Total range, cm	
						horizontal	vertical
K_s	0.2	Gaussian	0.8	45	20	36	16
α	0.32	Gaussian	0.68	47	40	32	27
n	0.2	Gaussian	0.63	38	48	364	32
		Gaussian	0.17	2000	10		
θ_s	0.45	Gaussian	0.43	85	50	277	25
		Spherical	0.12	2000	25		

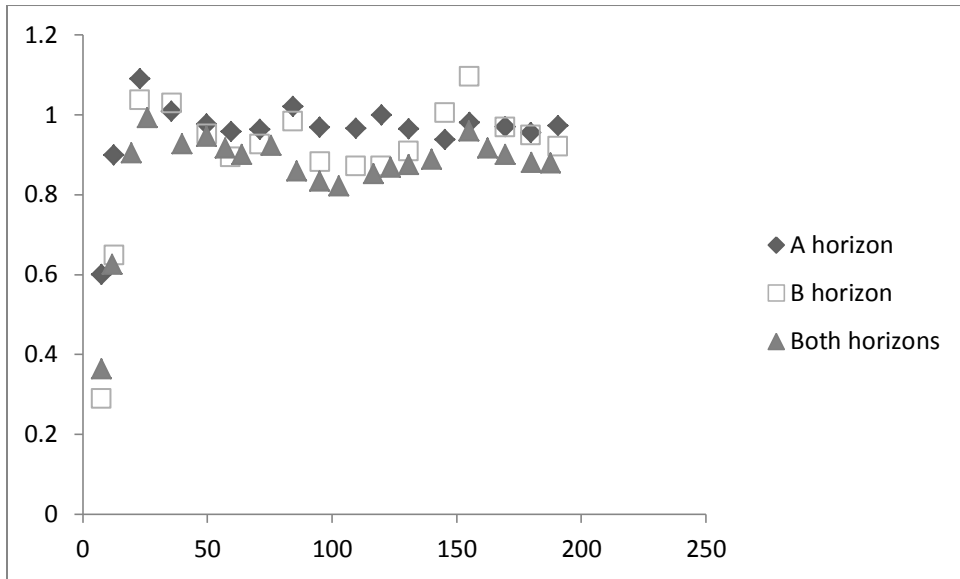
Table 3-2: Simulated average water storage with initial condition
 $h=-20$ cm and followed by 20 days drainage

Time	water storage (cm)			
	25-cm	% change	60-cm	% change
0	8.187	0	19.79	0
2	4.484	45.23	10.82	45.33
4	4.102	8.52	9.673	10.6
6	3.898	4.97	9.067	6.26
8	3.759	3.57	8.661	4.48
10	3.658	2.69	8.368	3.38
12	3.576	2.24	8.132	2.82
14	3.506	1.96	7.935	2.42
16	3.448	1.65	7.772	2.05
18	3.399	1.42	7.636	1.75
20	3.357	1.24	7.516	1.57

Table 3-3: Ranges of the parametric variogram models and the corresponding empirical variogram of the each simulated van Genuchten parameter

Parameter	Range (cm)			
	fitting model		direct simulation	
	horizontal	vertical	horizontal	vertical
K_s	36	16	65	20
α	32	27	60	45
n	364	32	120	45
θ_s	277	25	150	trend

a) horizontal



b) vertical

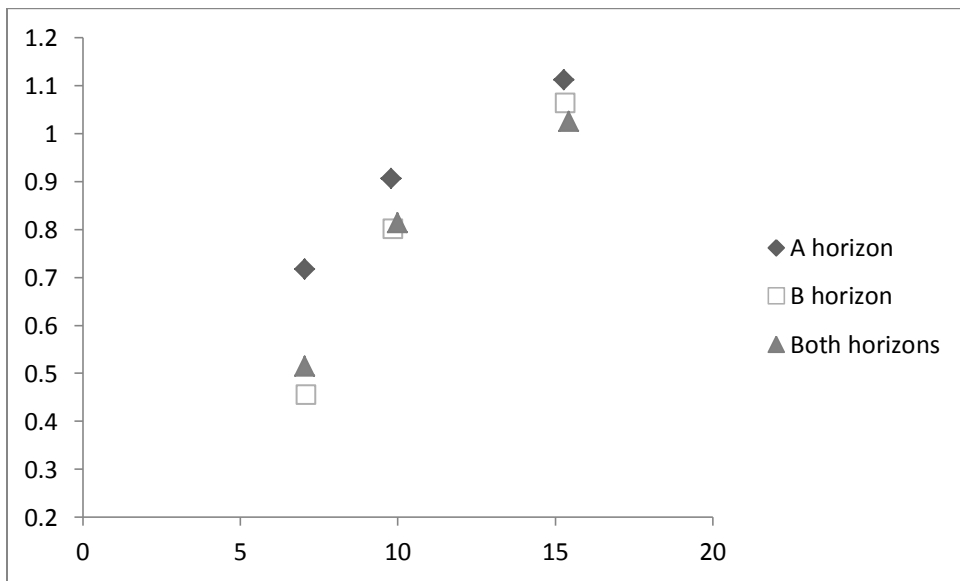
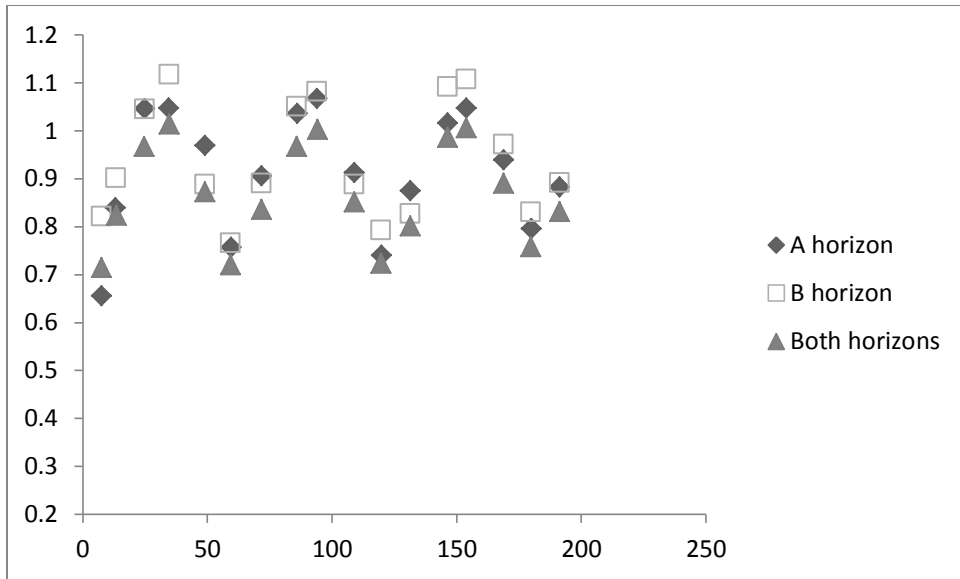


Figure 3-1: Estimated empirical variogram for Ks

a) horizontal



b) vertical

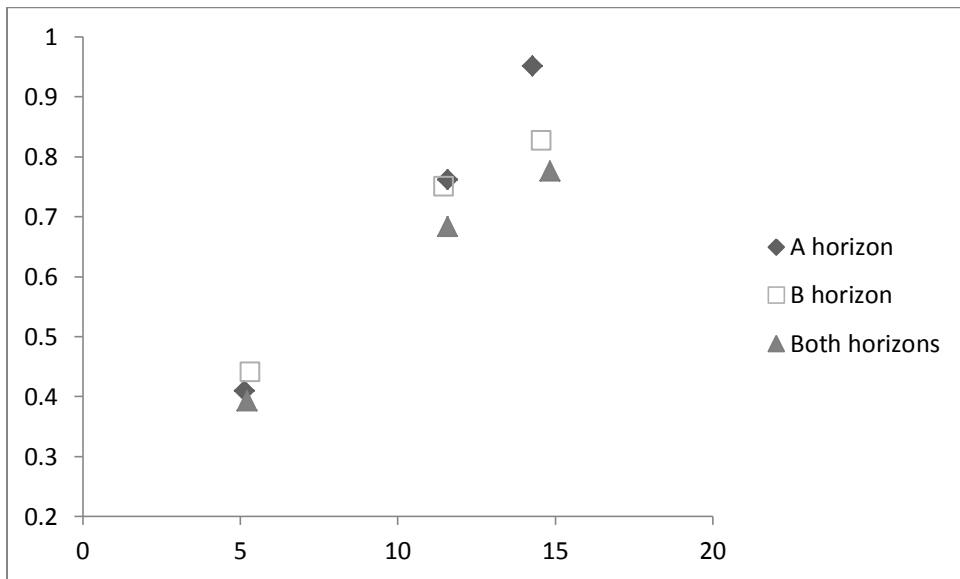
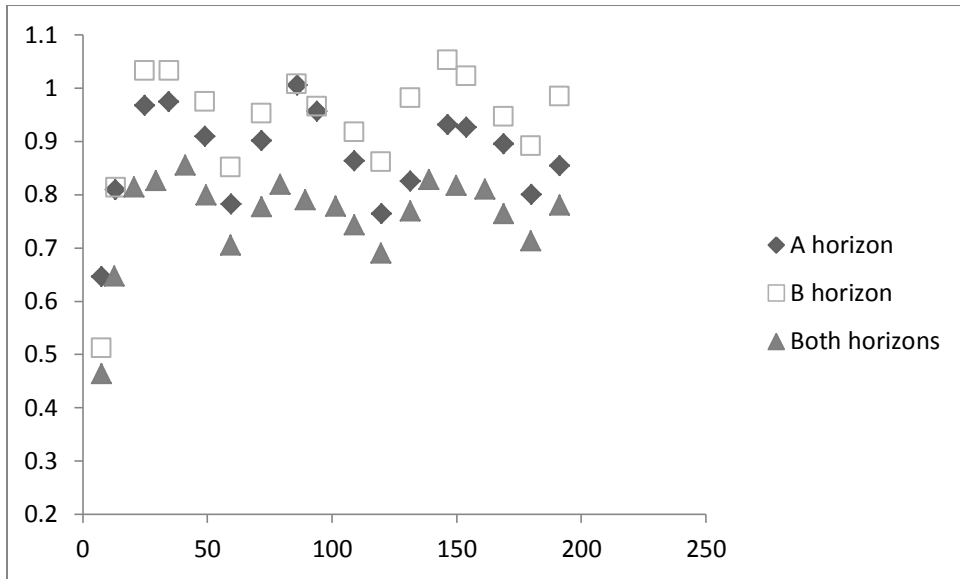


Figure 3-2: Estimated empirical variogram for α

a) horizontal



b) vertical

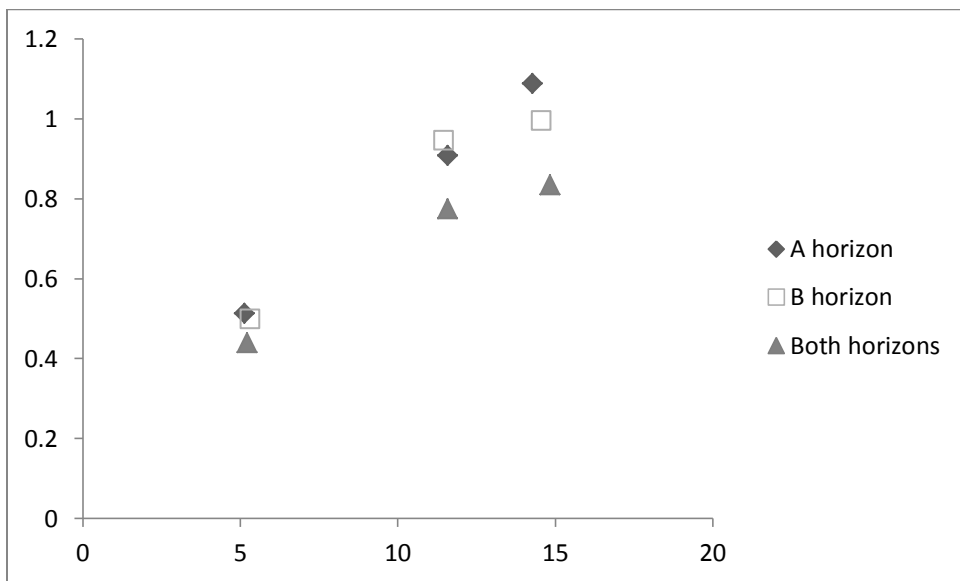
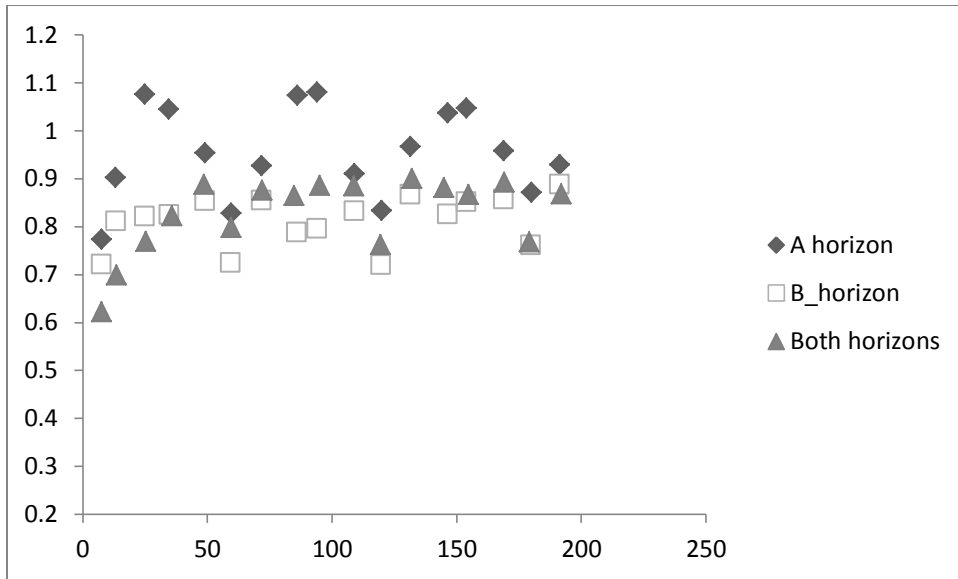


Figure 3-3: Estimated empirical variogram for n

a) horizontal



b) vertical

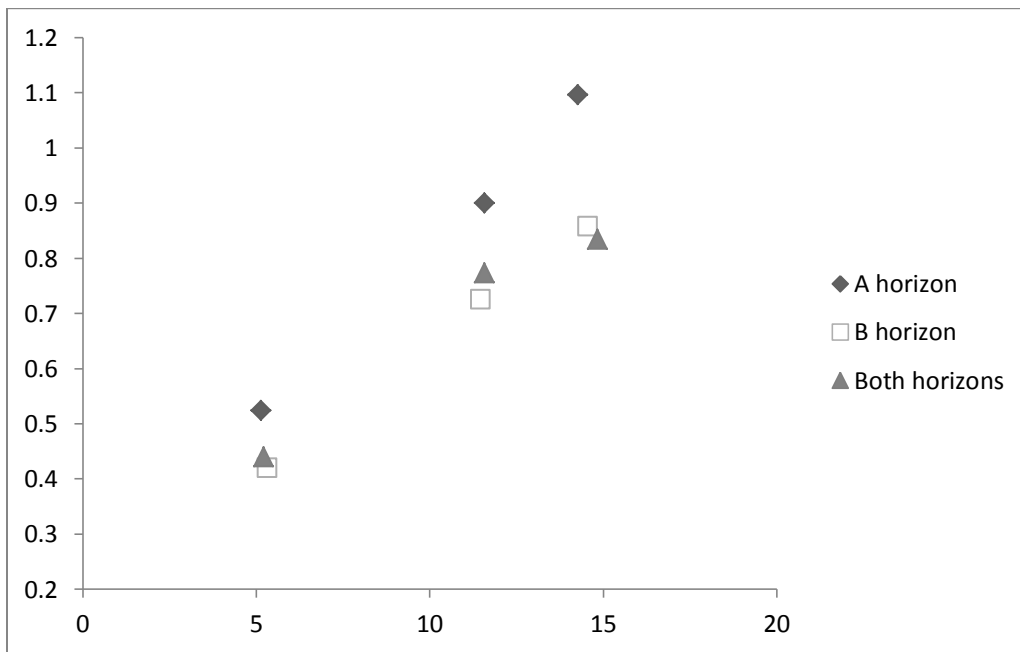


Figure 3-4: Estimated empirical variogram for θ_s

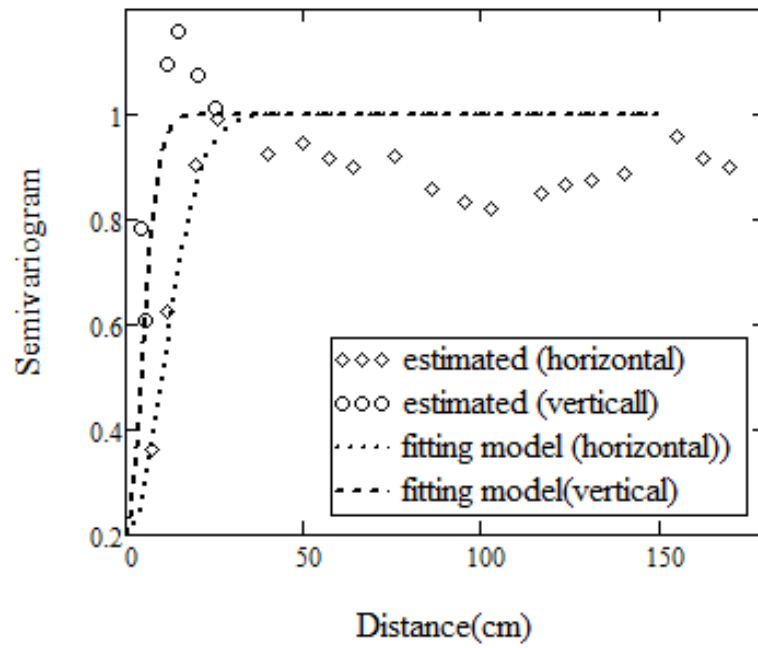


Figure 3-5: parametric variogram model for Ks

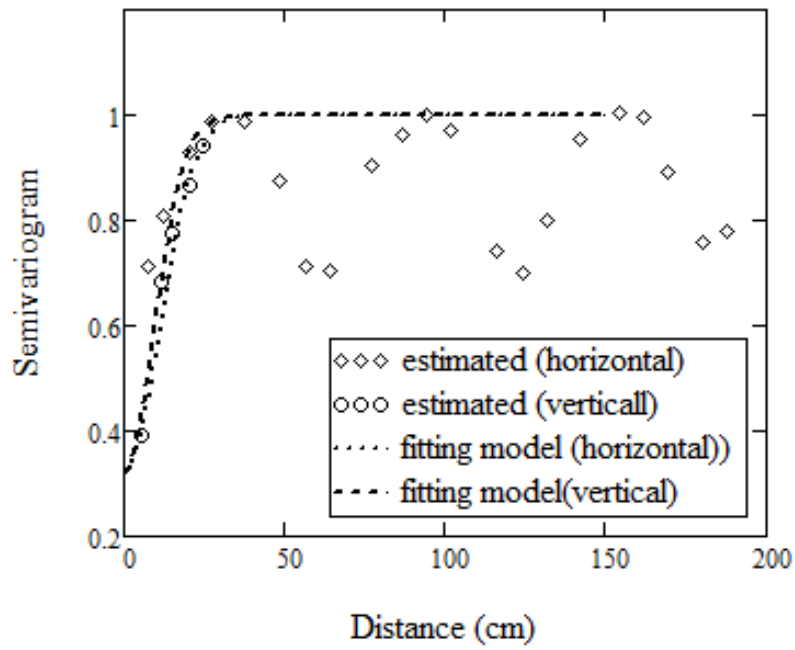


Figure 3-6: Parametric variogram model for α

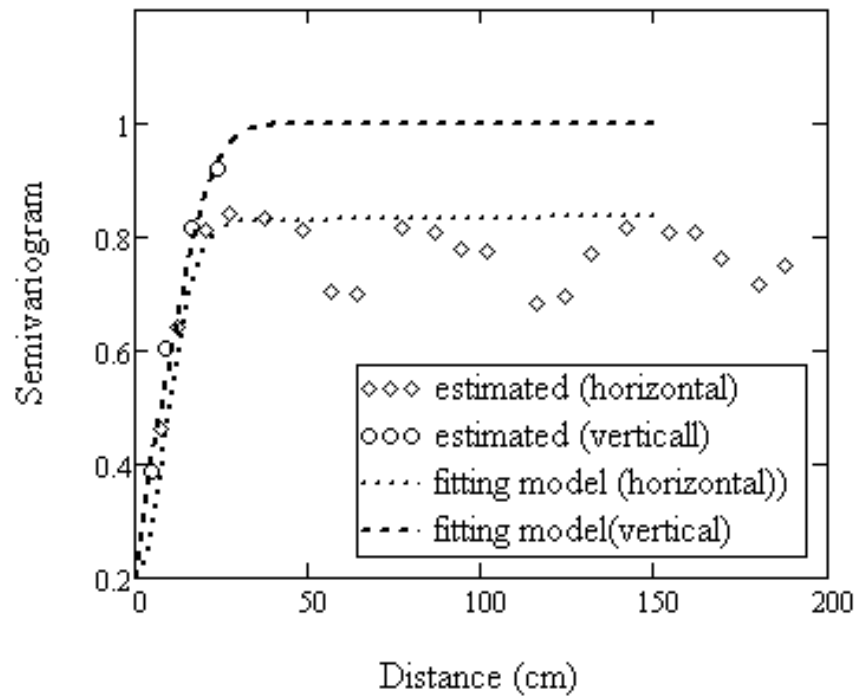


Figure 3-7: Parametric variogram model for n

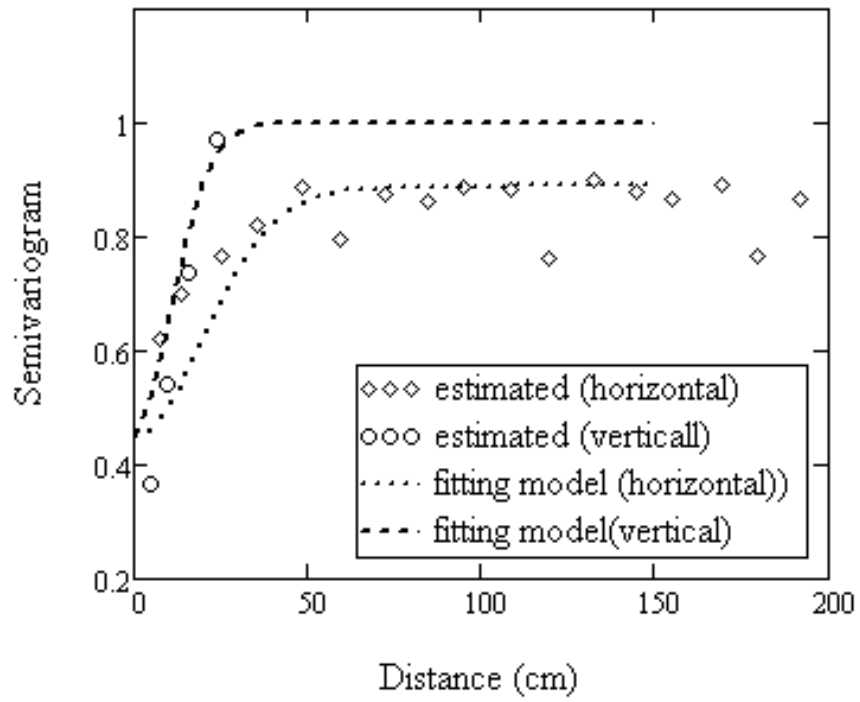


Figure 3-8: Parametric variogram model for saturated water content θ_s

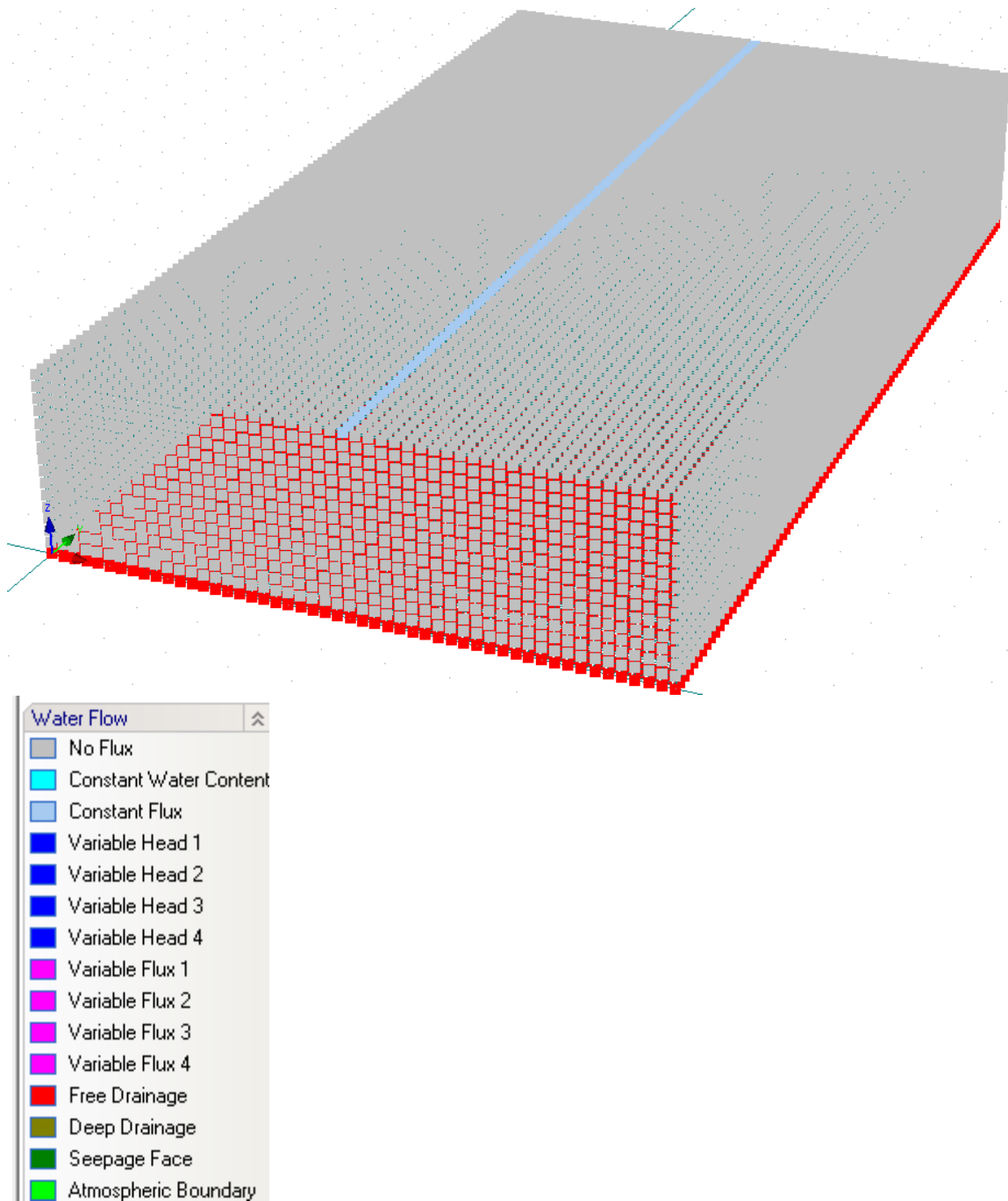


Figure 3-9: Boundary condition of the numerical model (HYDRUS)

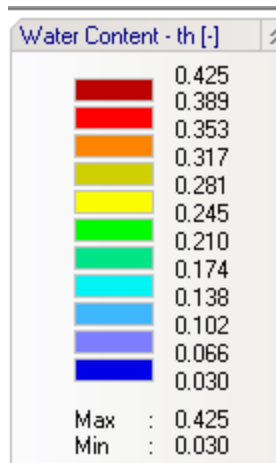
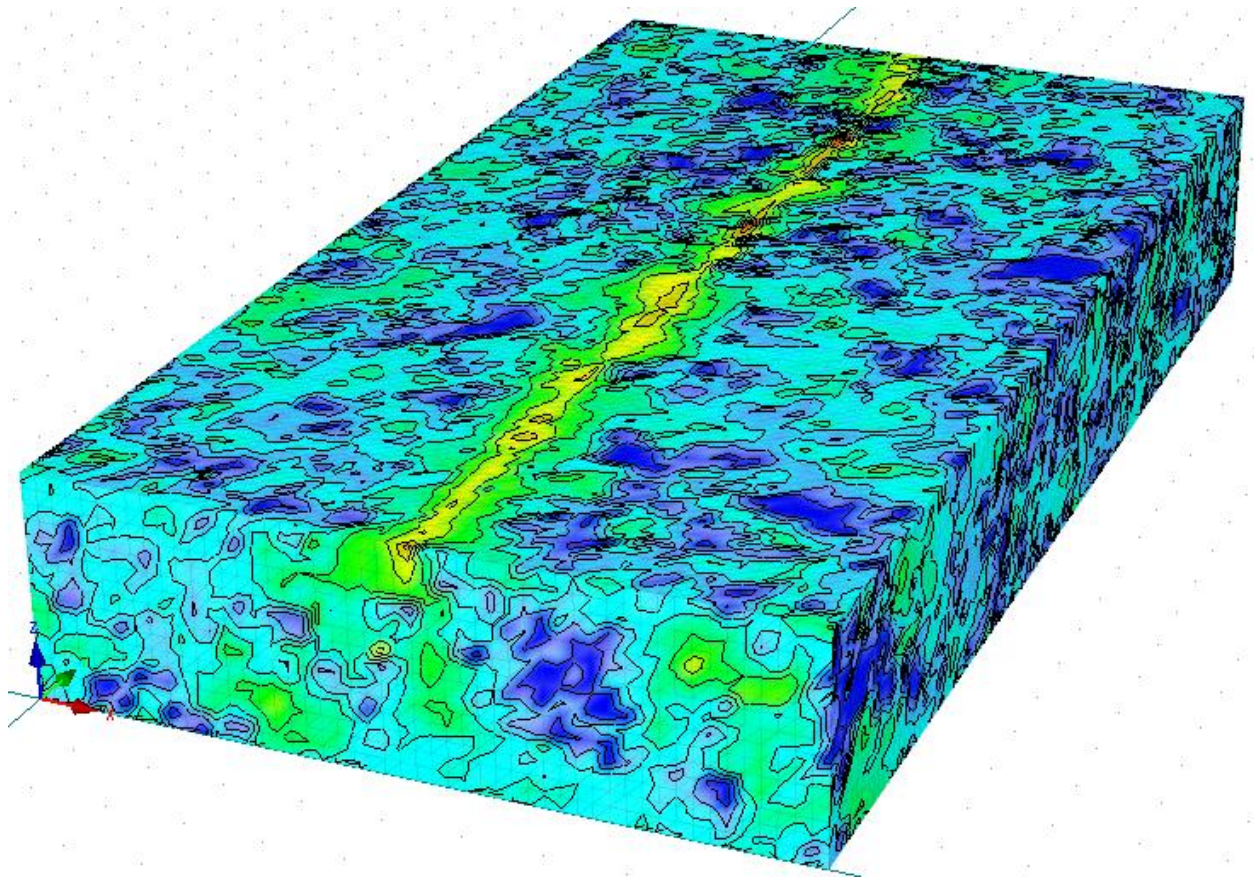


Figure 3-10: Output results after 10 days of simulation (HYDRUS)

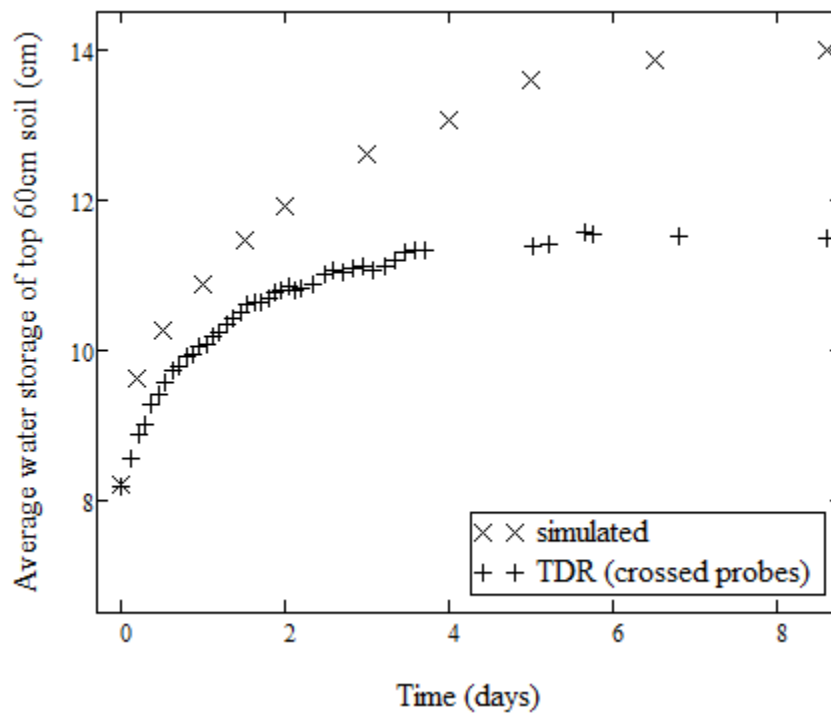
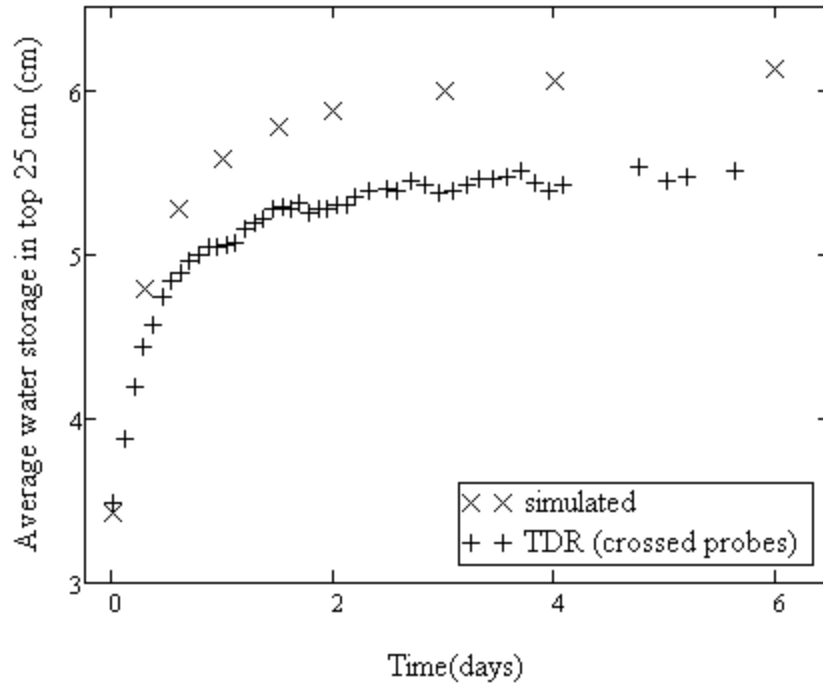


Figure 3-11: Comparison of average water in top 25 cm and 60 cm of simulated output versus field measurement

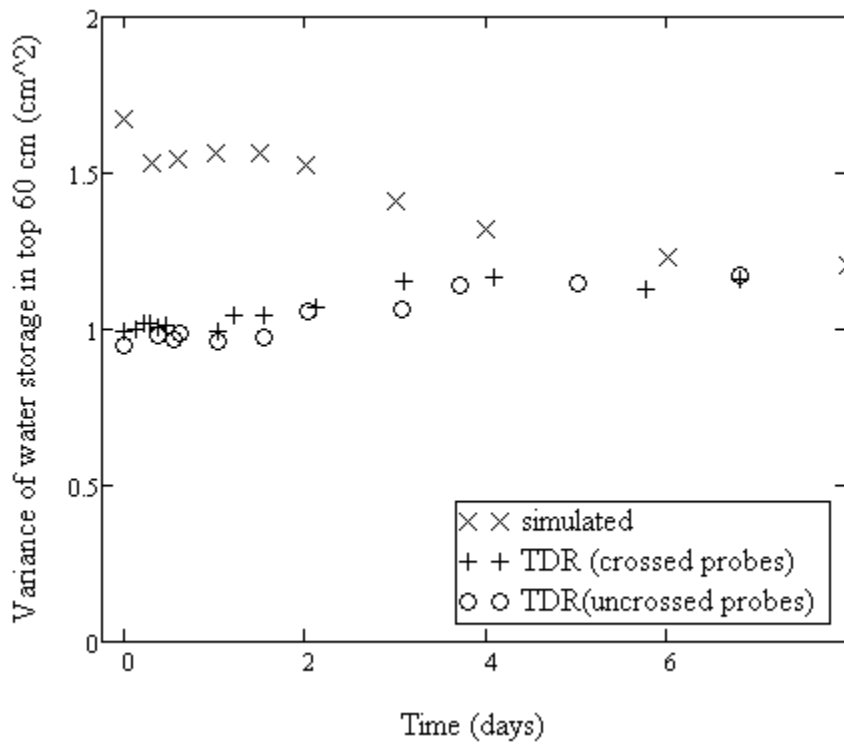
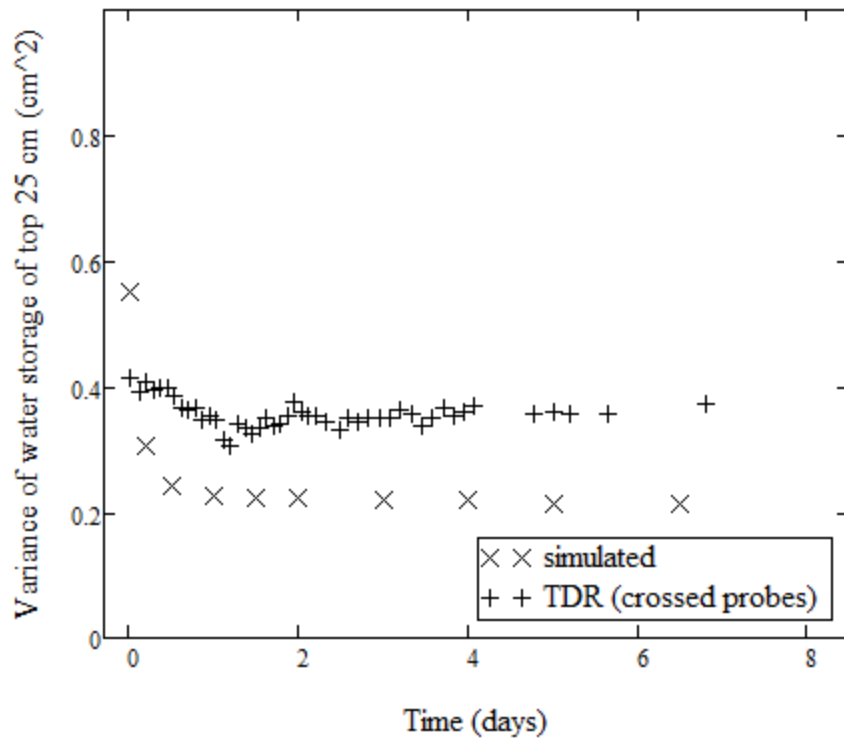


Figure 3-12: Comparison of water storage variance in top 25 cm and 60 cm of simulated output versus field measurement

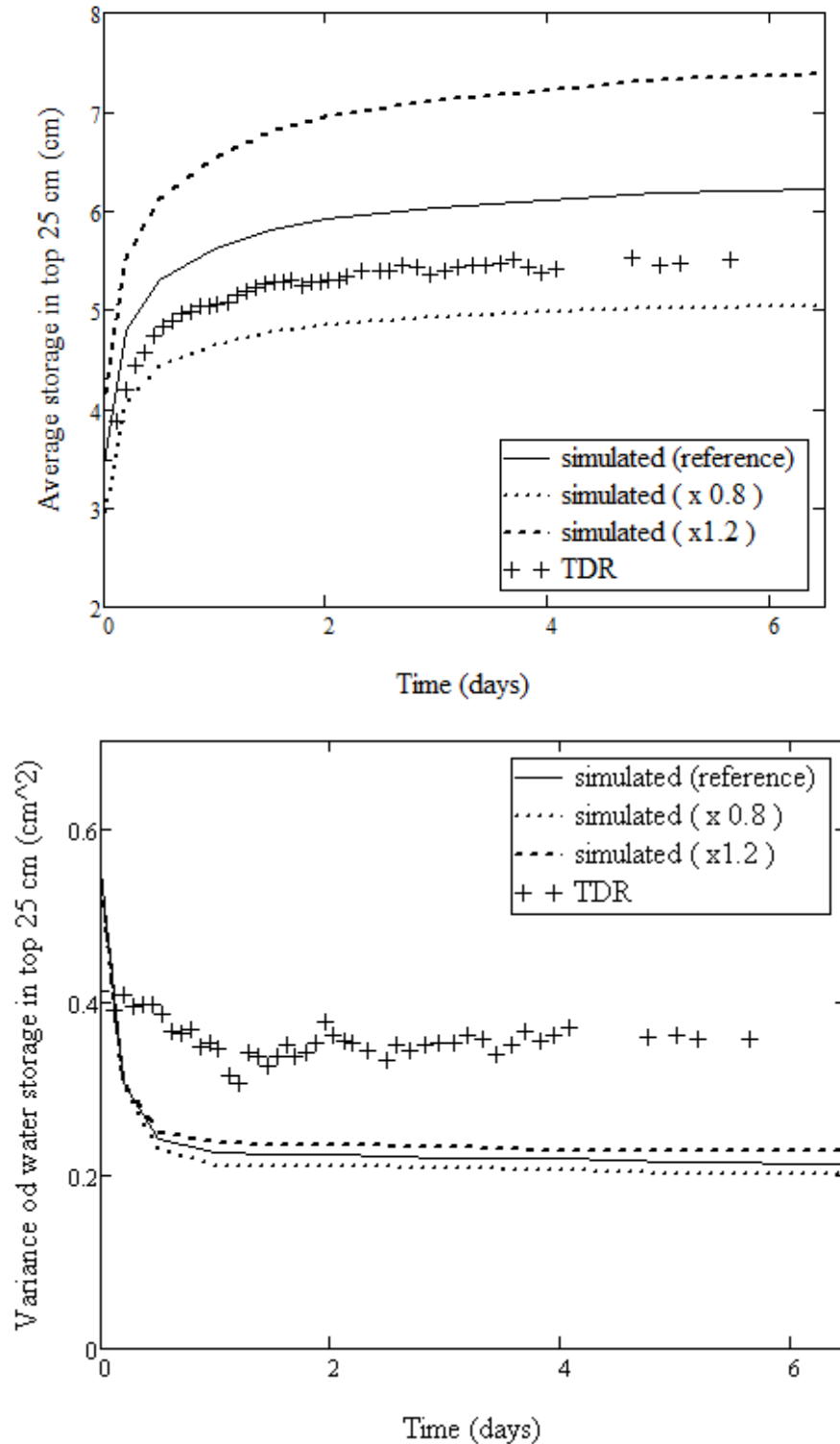


Figure 3-13: Soil water storage from numerical simulations with input VG parameter $\theta_s \pm 20\%$, and TDR measured field data. The simulation corresponding to unmodified VG parameters is utilized as a reference

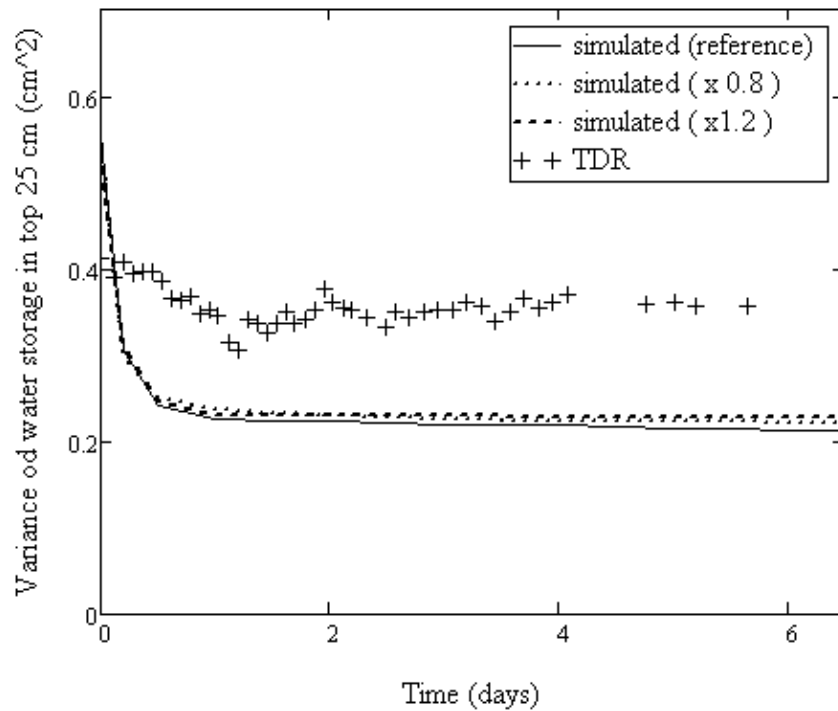
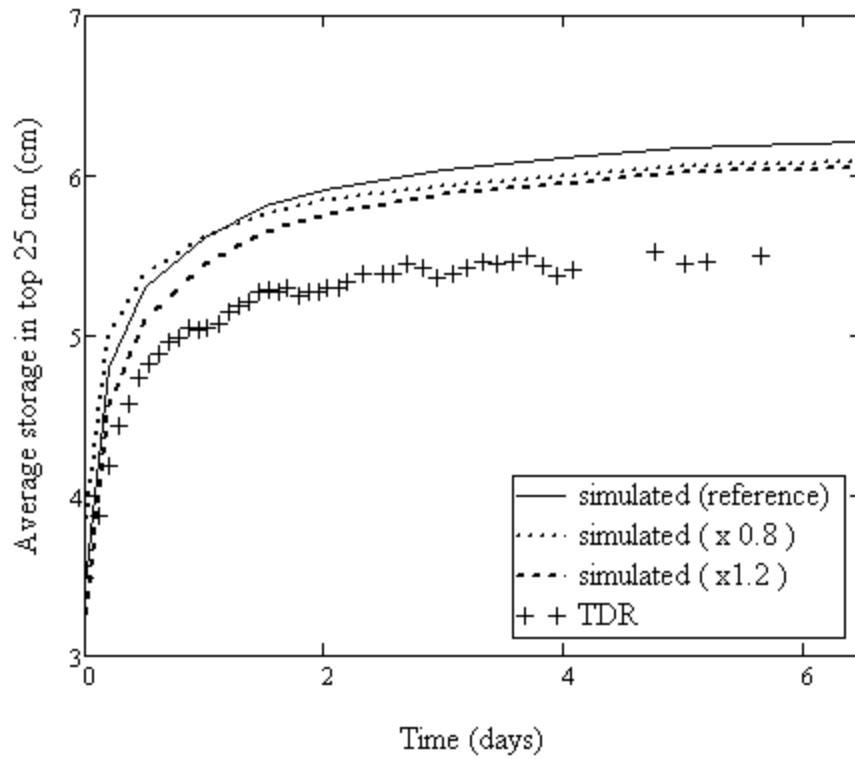


Figure 3-14: Soil water storage from numerical simulations with input VG parameter $\pm 20\%$, and TDR measured field data. The simulation corresponding to unmodified VG parameters is utilized as a reference

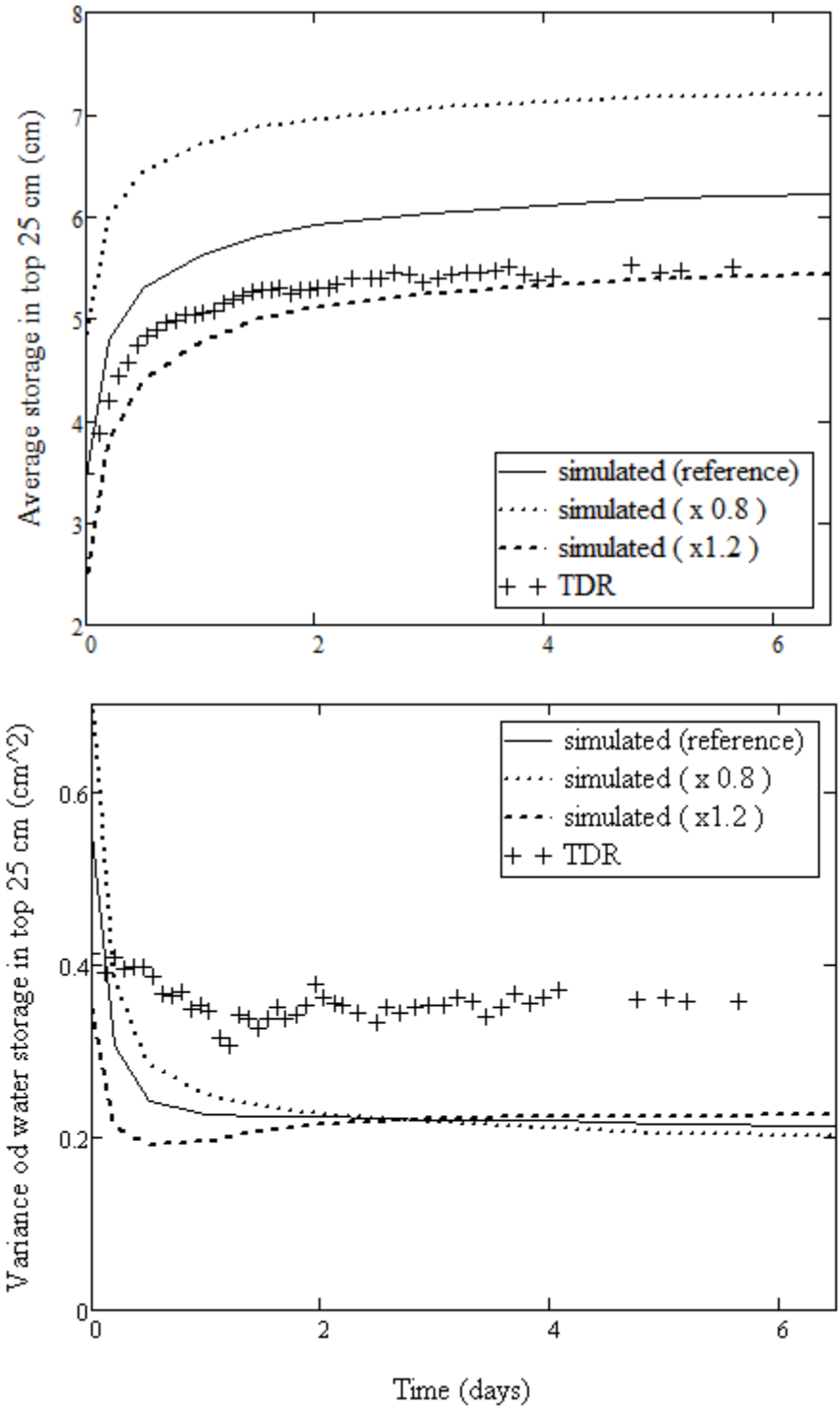


Figure 3-15: Soil water storage from numerical simulations with input VG parameter $\pm 20\%$, and TDR measured field data. The simulation corresponding to unmodified VG parameters is utilized as a reference

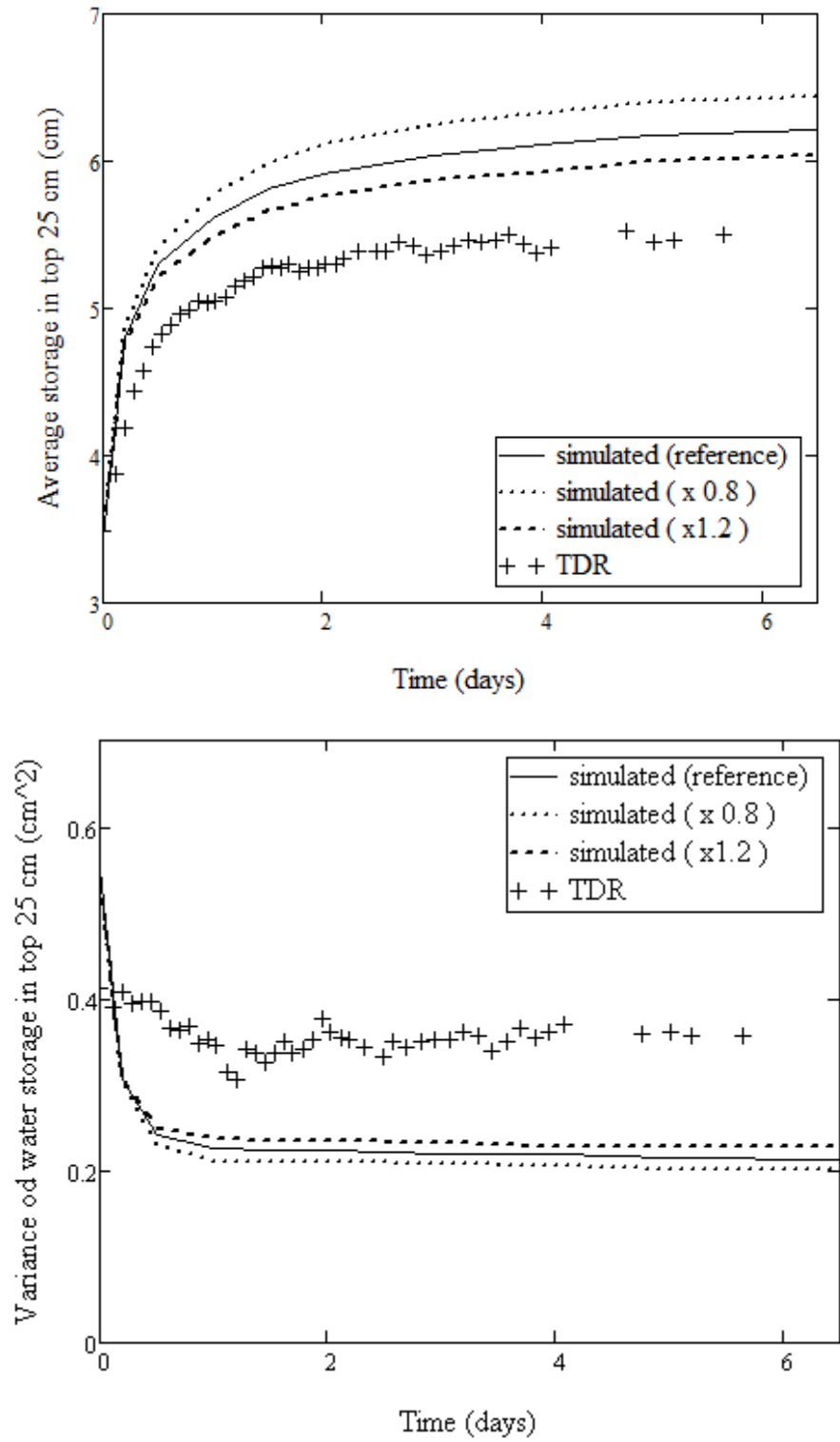


Figure 3-16: Soil water storage from numerical simulations with input VG parameter $K_s \pm 20\%$, and TDR measured field data. The simulation corresponding to unmodified VG parameters is utilized as a reference

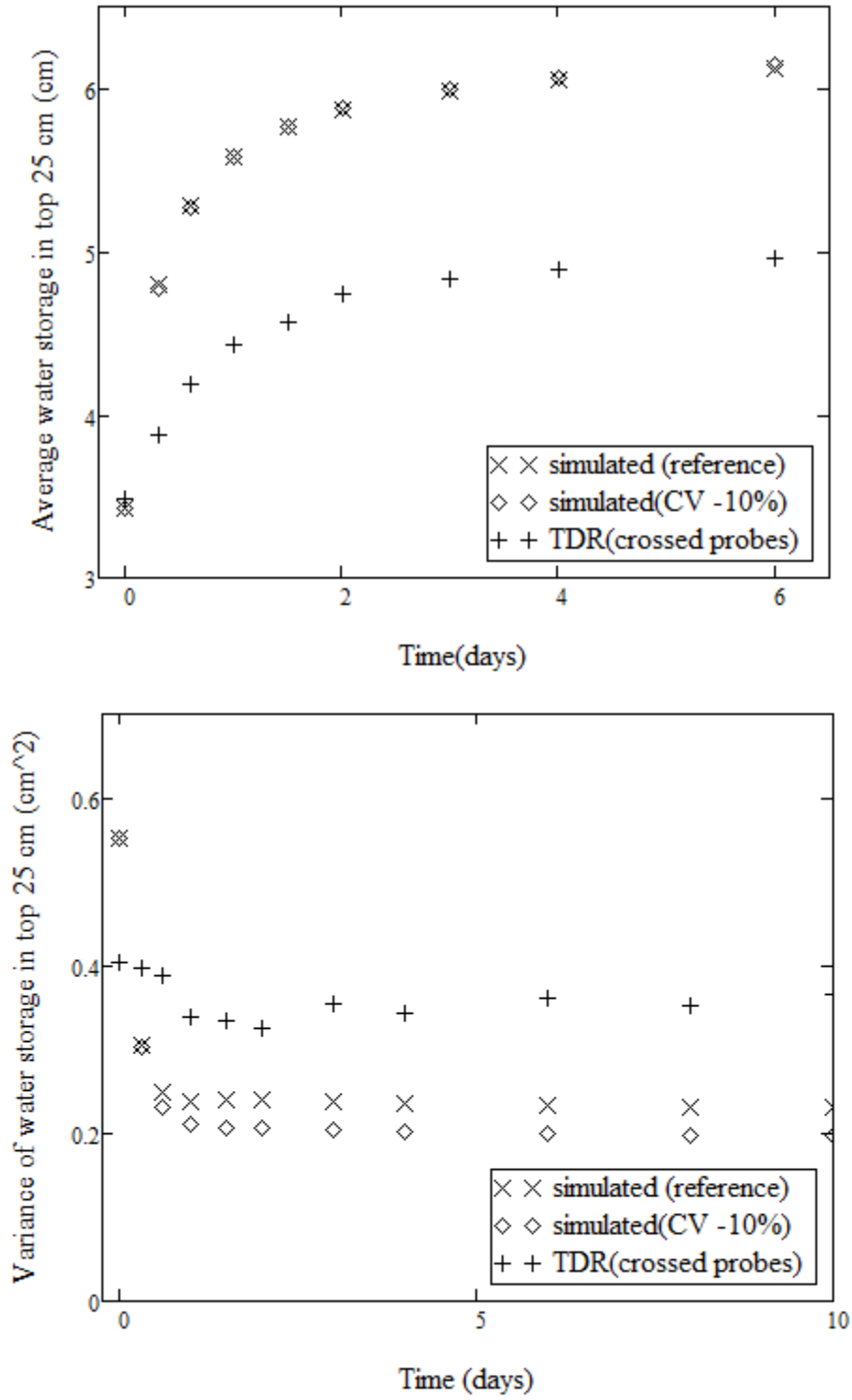


Figure 3-17: Soil water storage from numerical simulations with CV of the input VG parameter Ks decreased by 10%, and TDR measured field data. The simulation corresponding to unmodified VG parameters is utilized as a reference

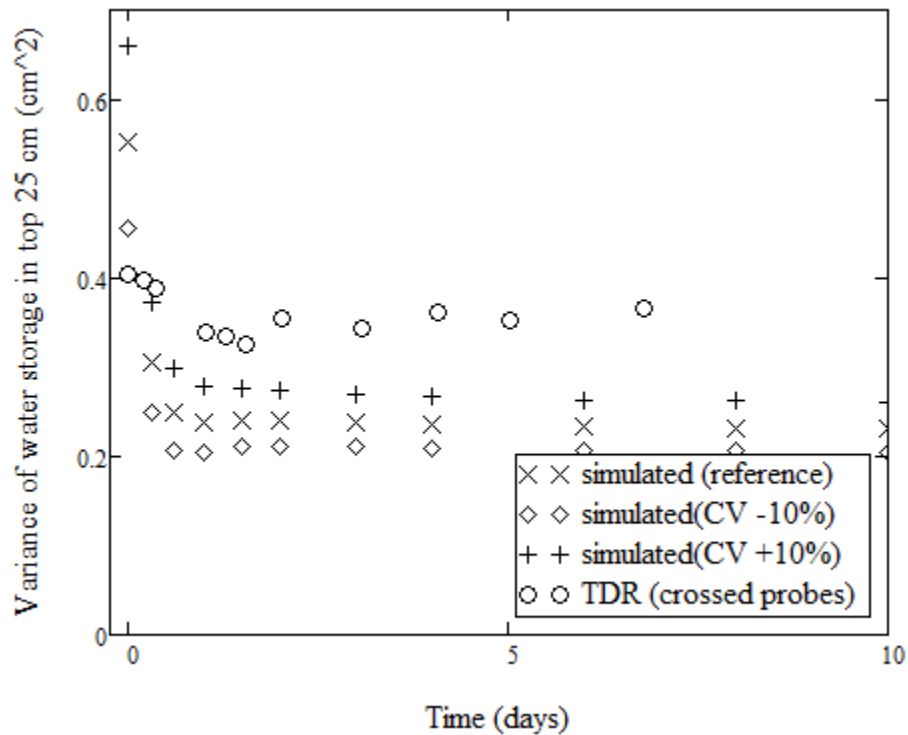
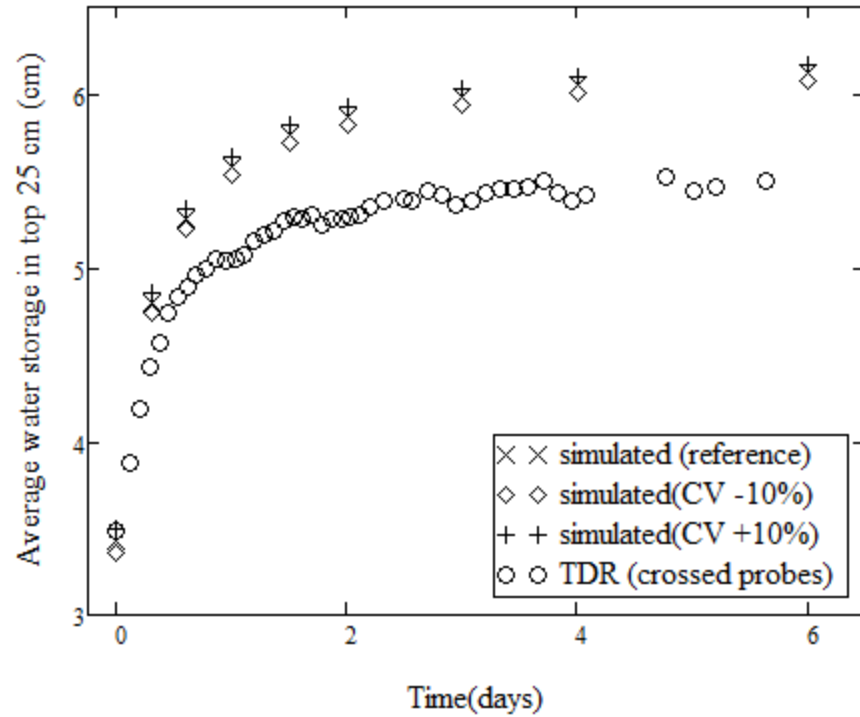


Figure 3-18: Soil water storage from numerical simulations with CV of the input VG parameter $n \pm 10\%$, and TDR measured field data. The simulation corresponding to unmodified VG parameters is utilized as a reference

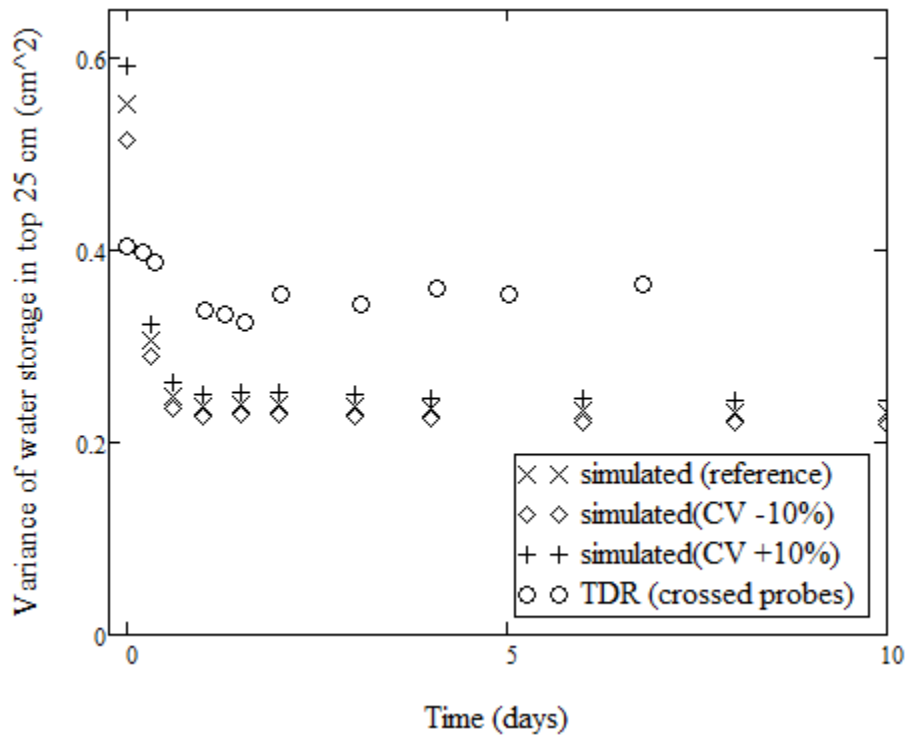
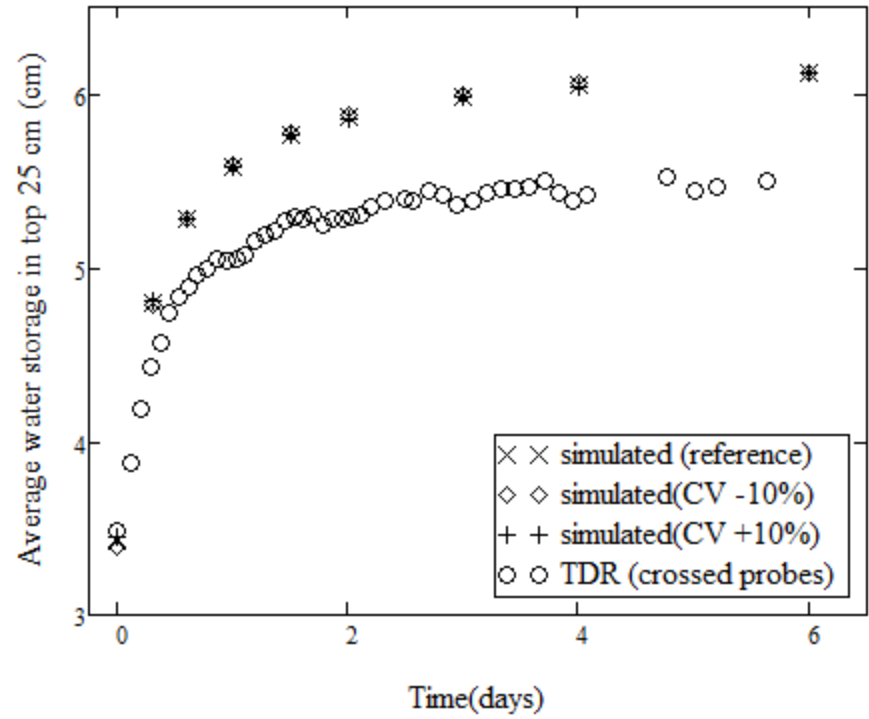


Figure 3-19: Soil water storage from numerical simulations with CV of the input VG parameter $\alpha \pm 10\%$, and TDR measured field data. The simulation corresponding to unmodified VG parameters is utilized as a reference

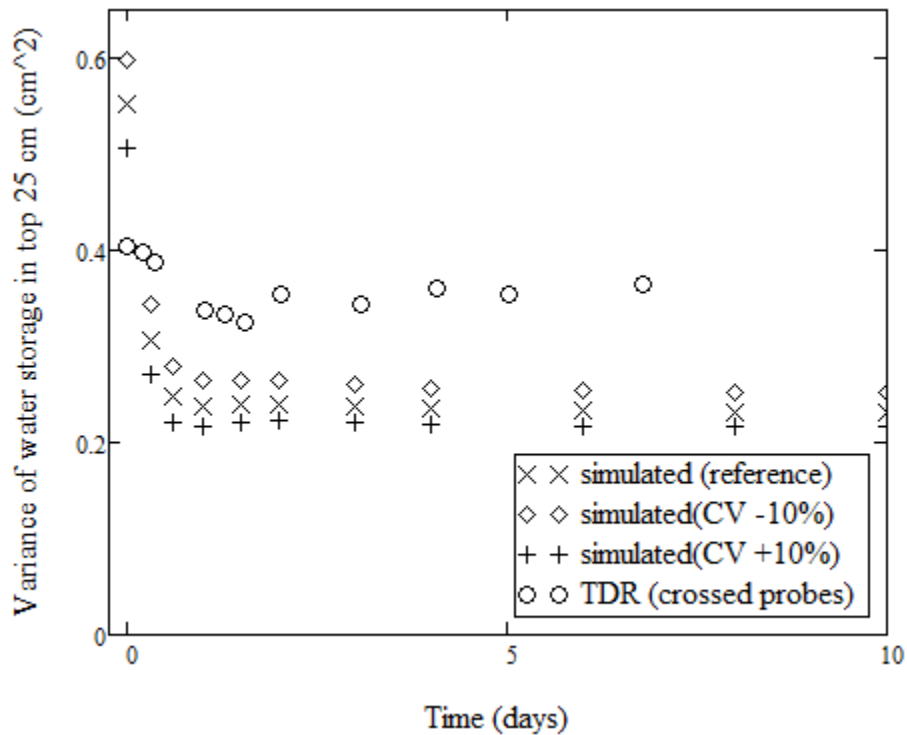
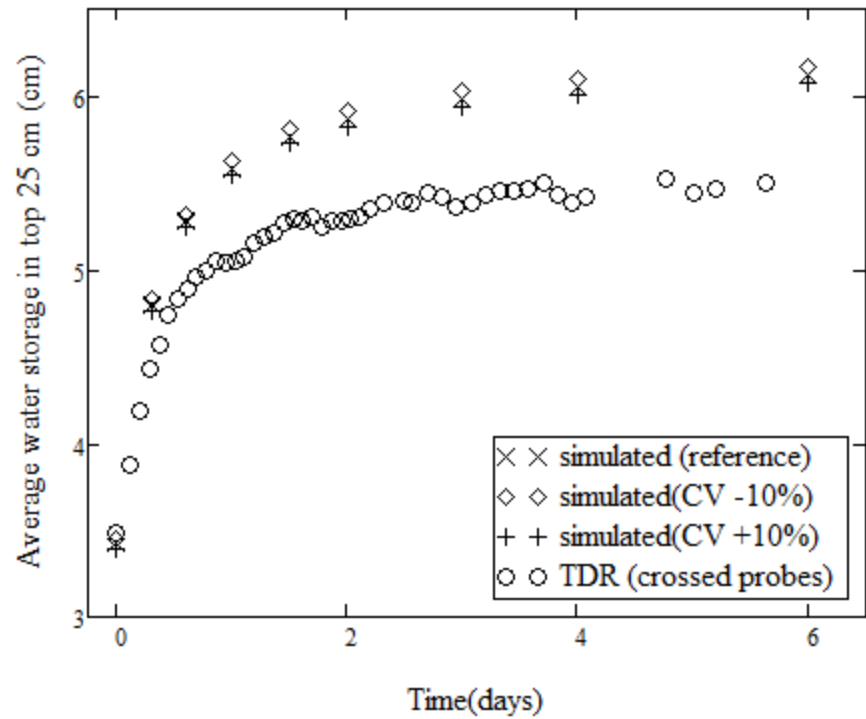


Figure 3-20: Soil water storage from numerical simulations with CV of the input VG parameter $\theta_s \pm 10\%$, and TDR measured field data. The simulation corresponding to unmodified VG parameters is utilized as a reference

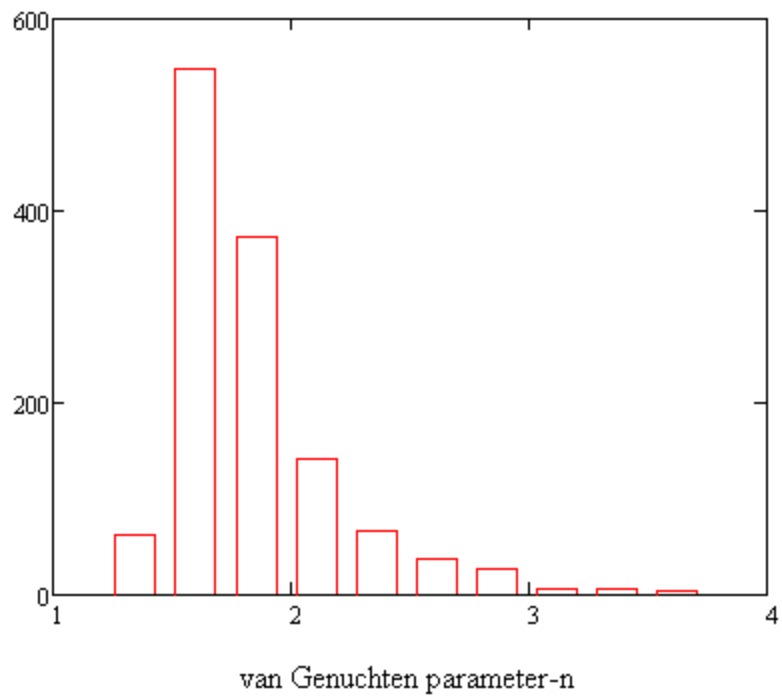
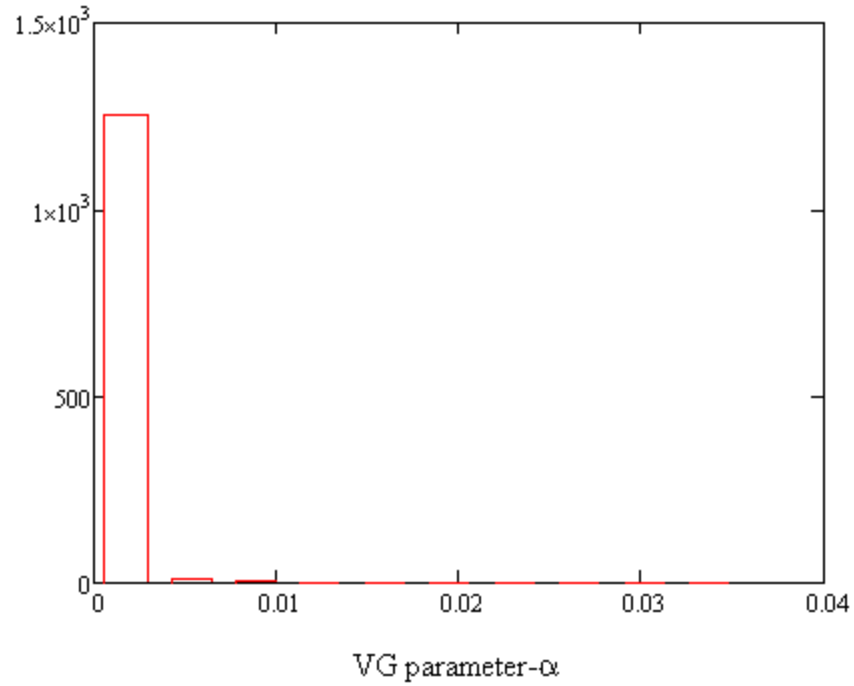


Figure 3-21: Histogram of lab-measured α and n distributions

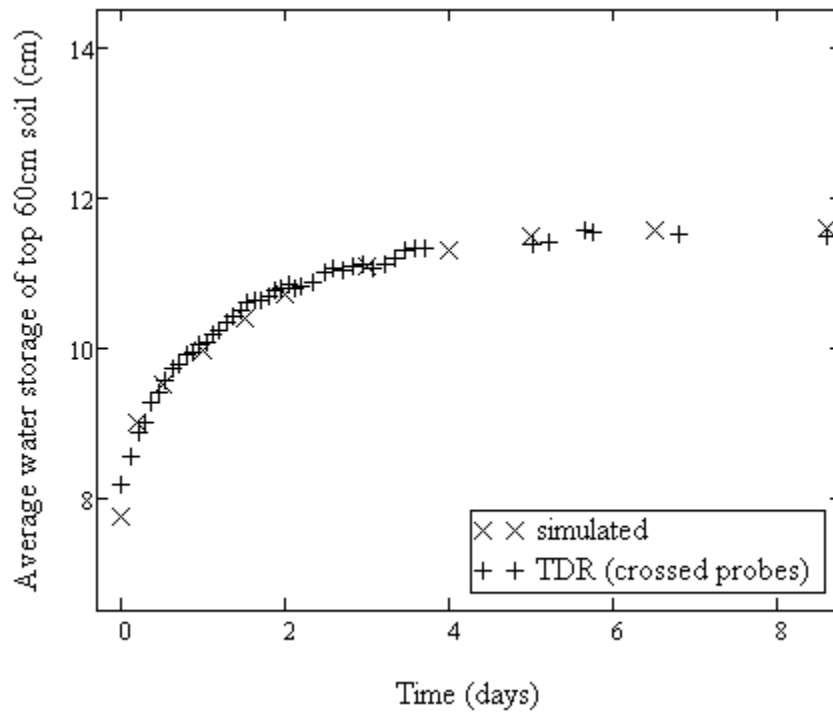
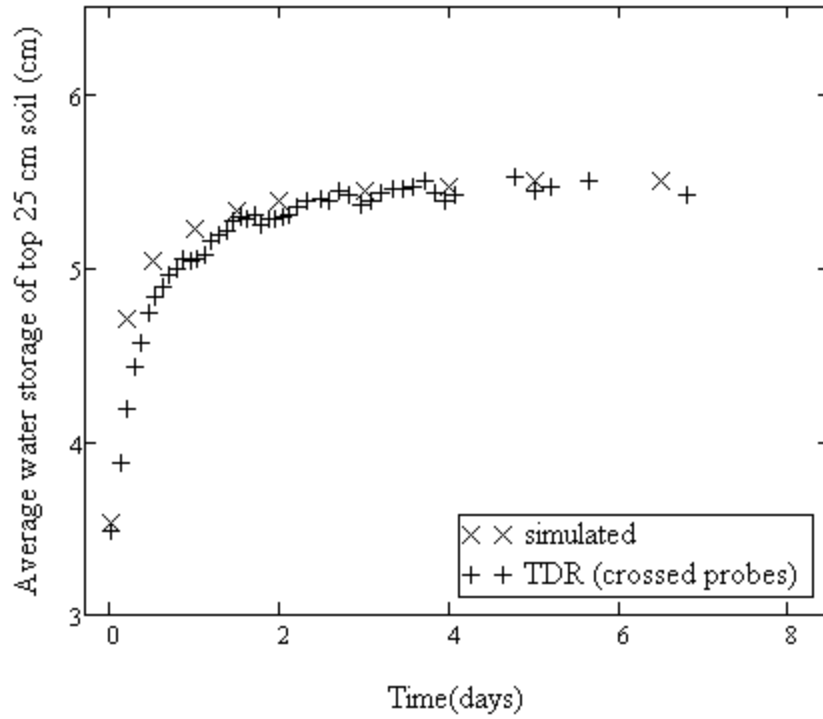


Figure 3-22: Comparison of average water storage from numerical simulations with optimum input VG parameters versus TDR measured field data

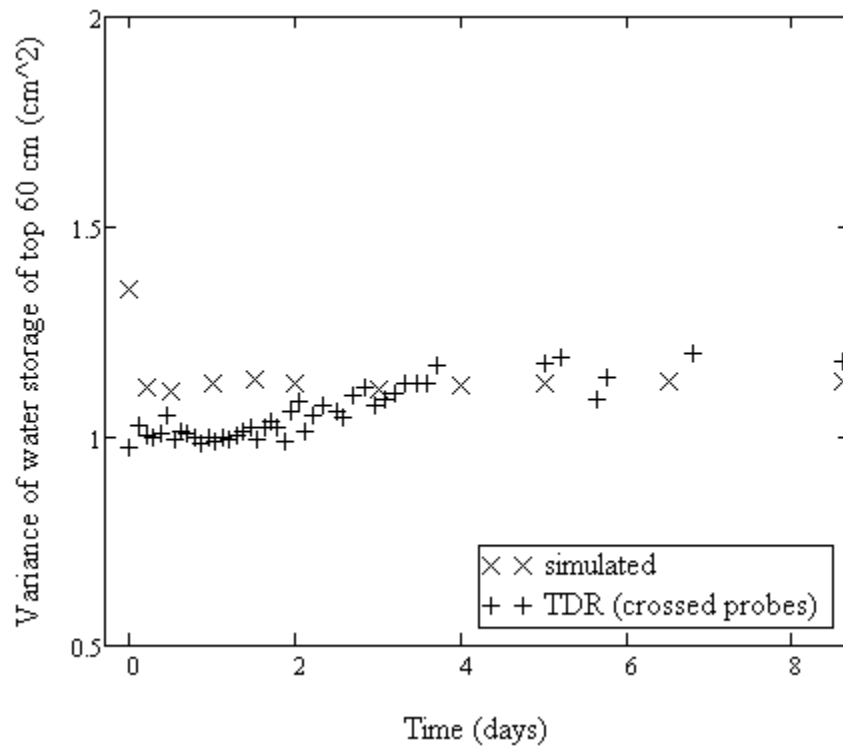
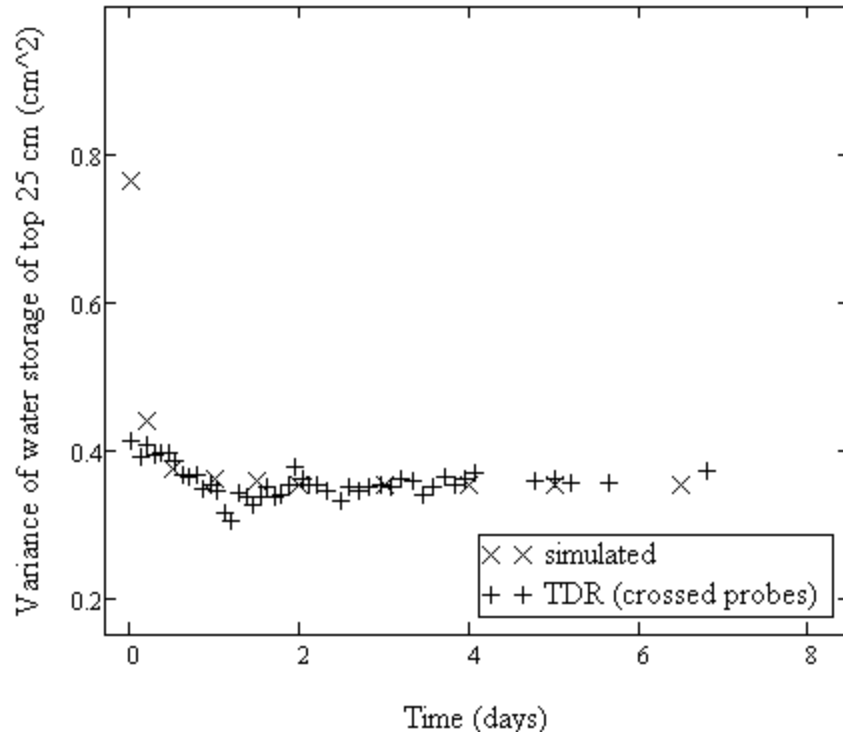


Figure 3-23: Comparison of average soil water storage from numerical simulations with optimum input VG parameters versus TDR measured field data

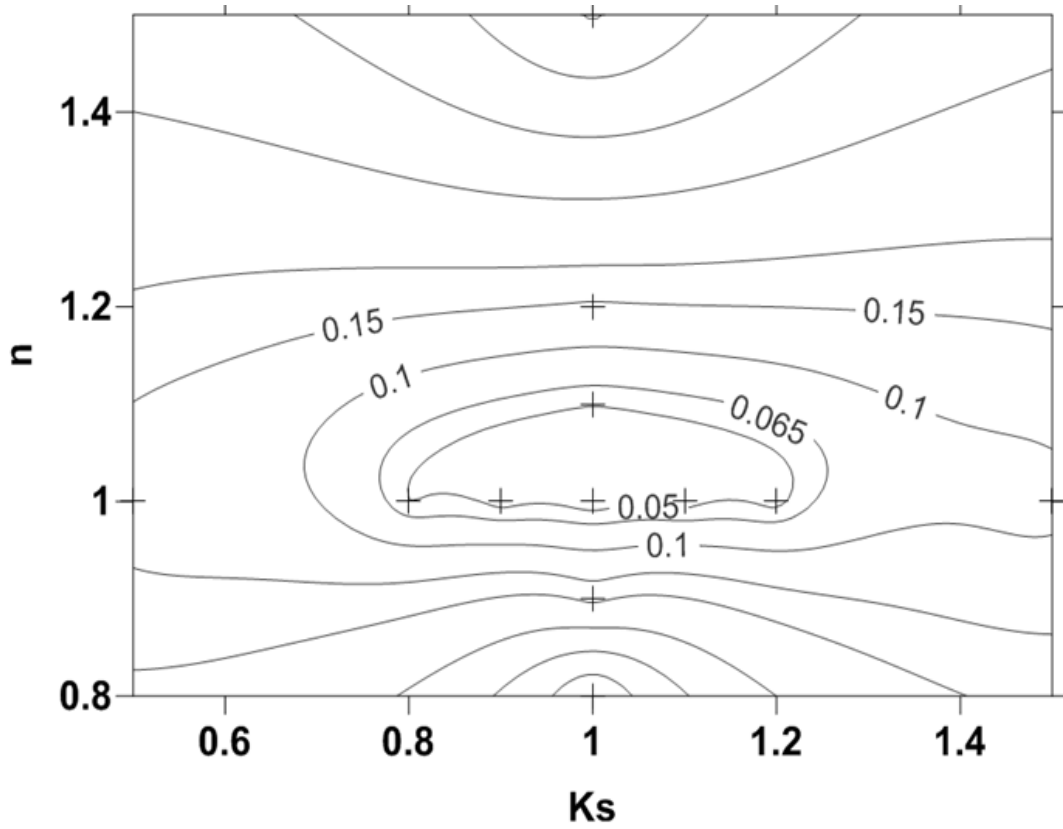


Figure 3-24: Contour maps of sum of square errors (SSE) of average water storage and the corresponding variance.

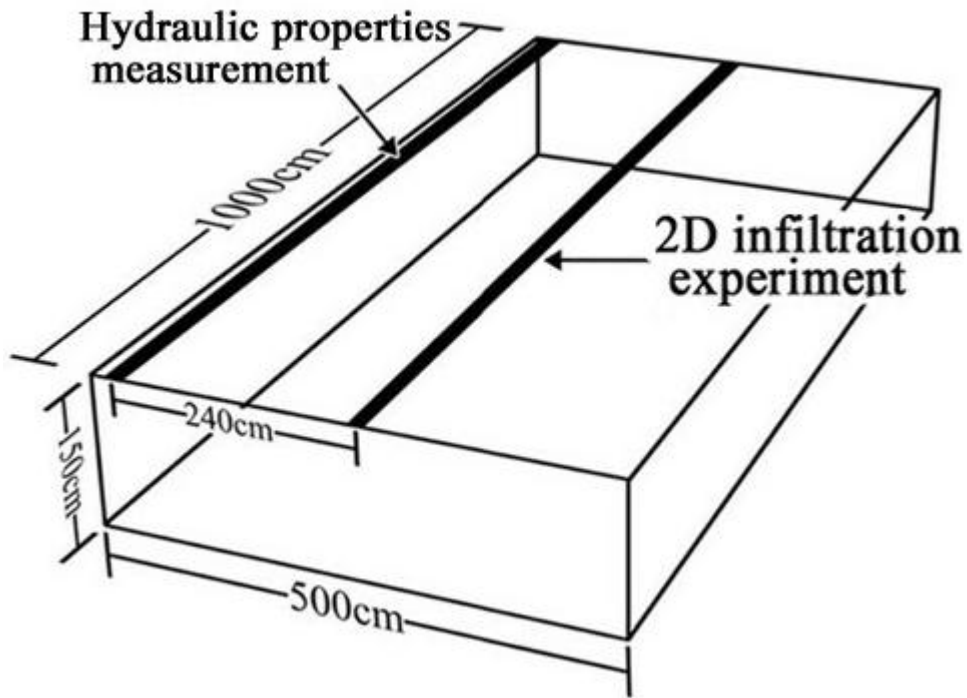


Figure 3-25: Indication of the transect corresponding to the hydraulic properties measurement and transect of the 2D infiltration experiment.

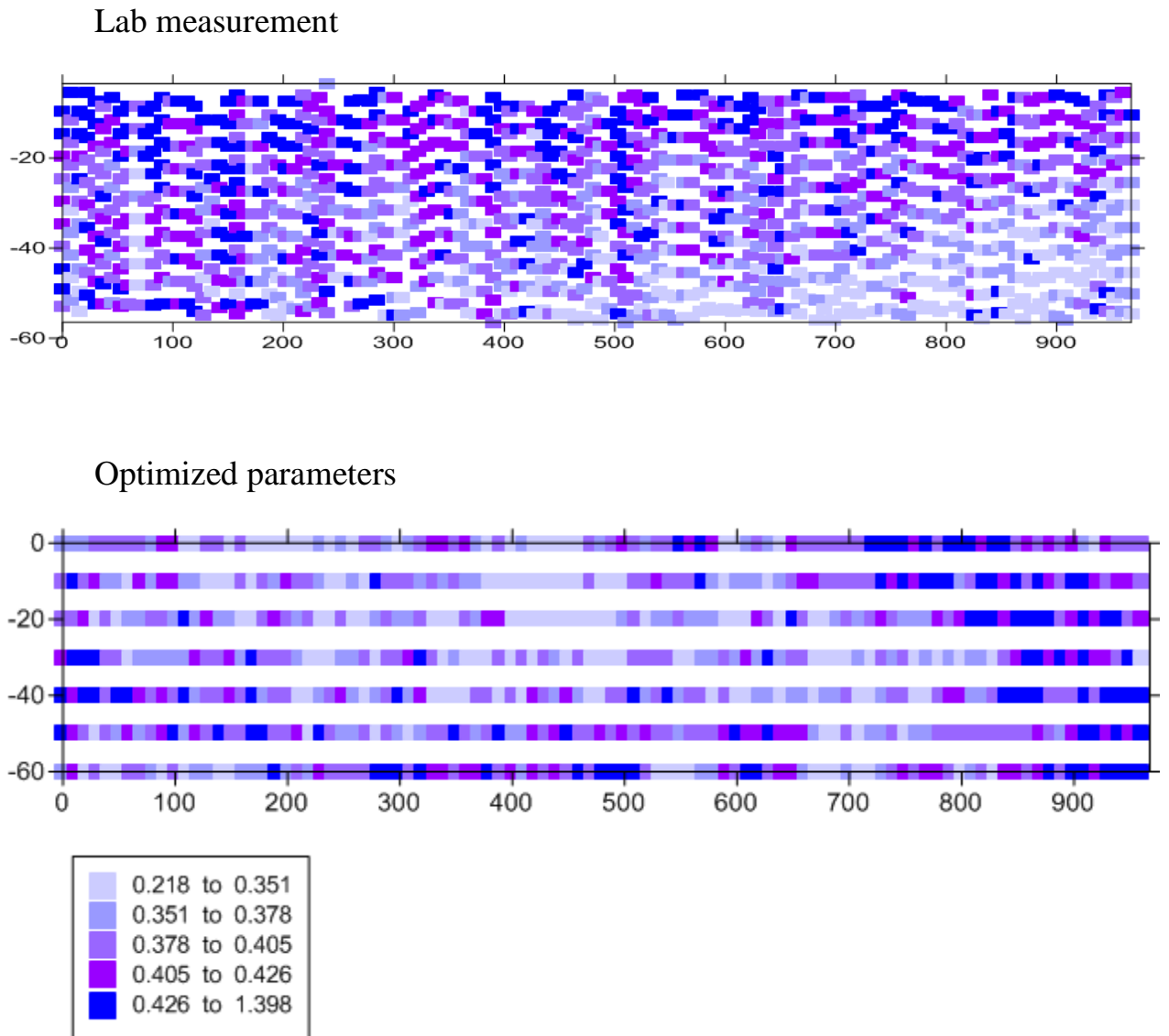


Figure 3-26: Classed post maps of lab-measured θ s and the optimized θ s along the line source transect

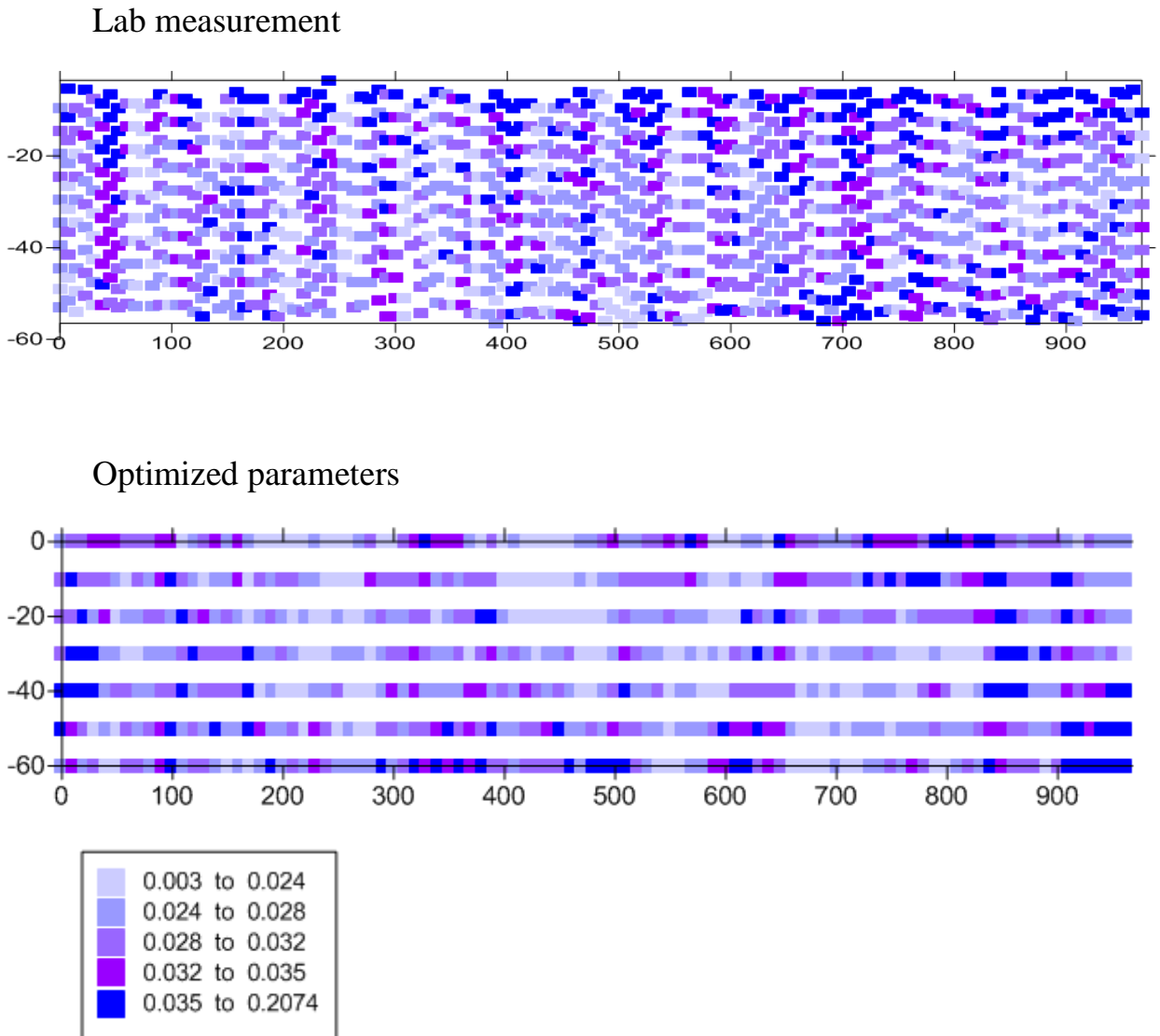
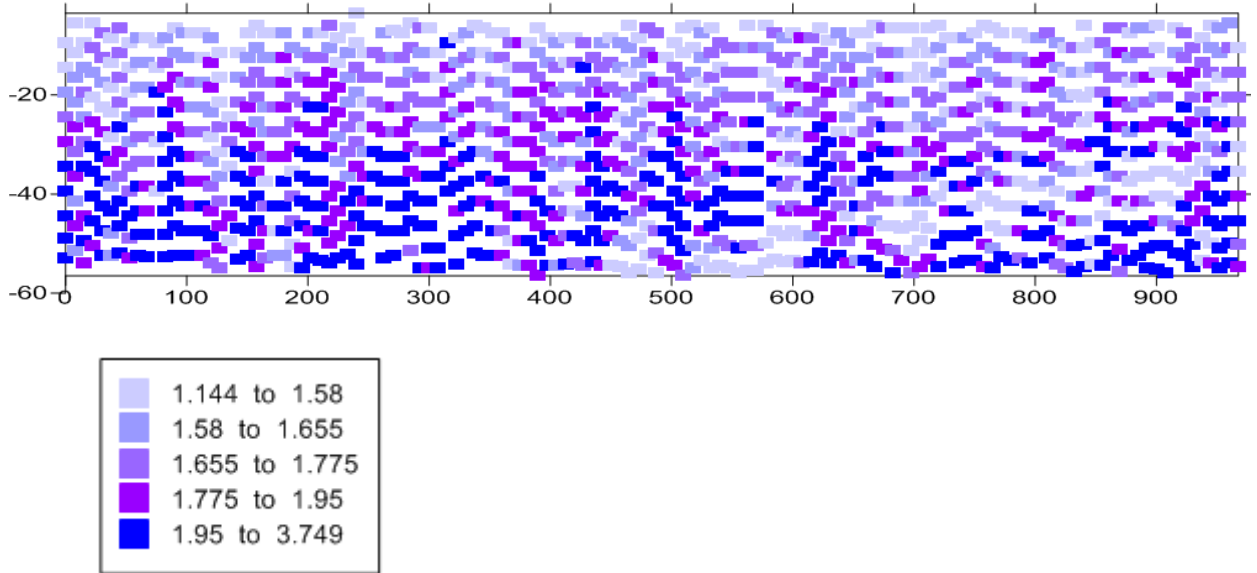


Figure 3-27: Classed post maps of lab-measured α and the optimized α along the line source transect

Lab measurement



Optimized parameters

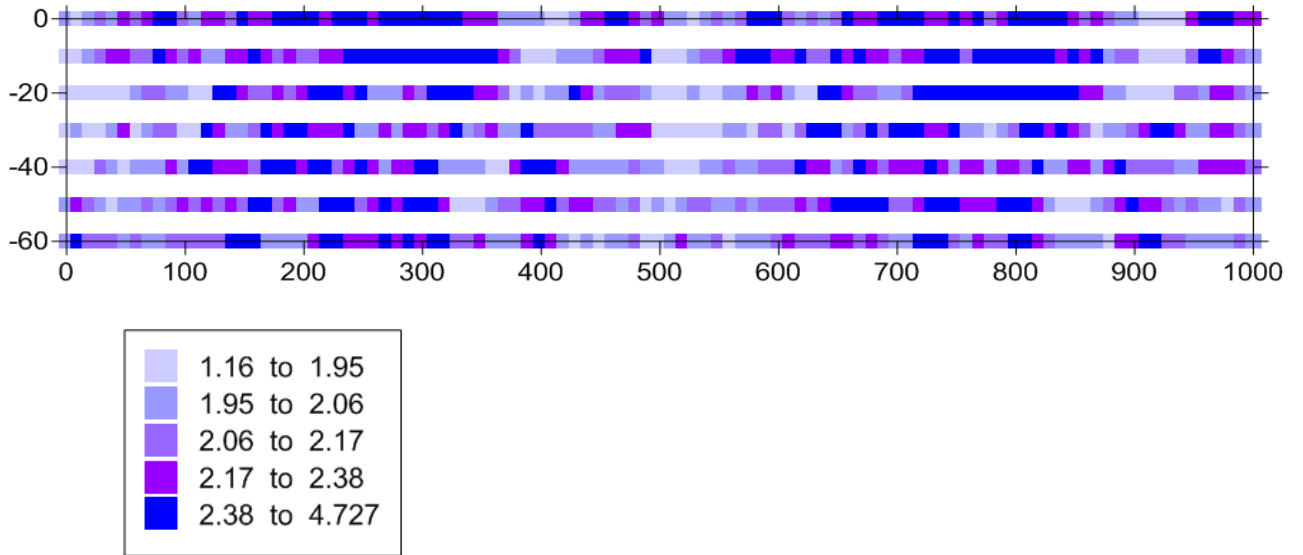
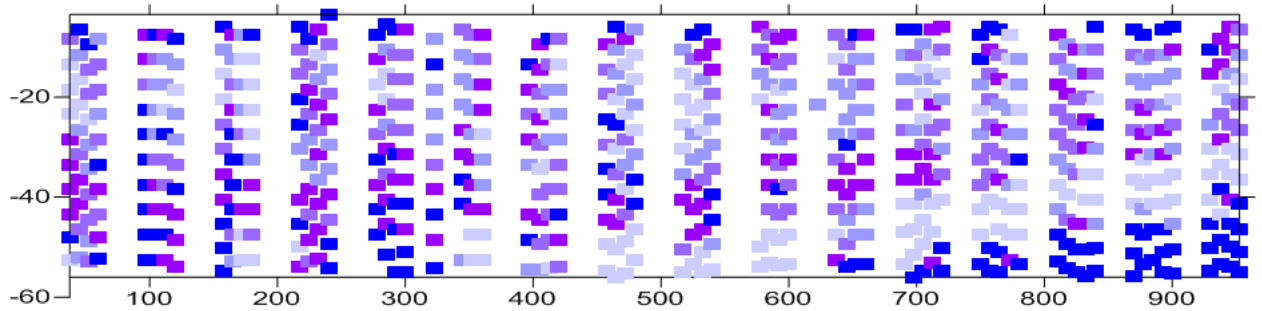


Figure 3-28: Classed post maps of lab-measured n and the optimized n along the line source transect

Lab measurement



Optimized parameters

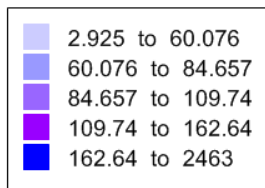
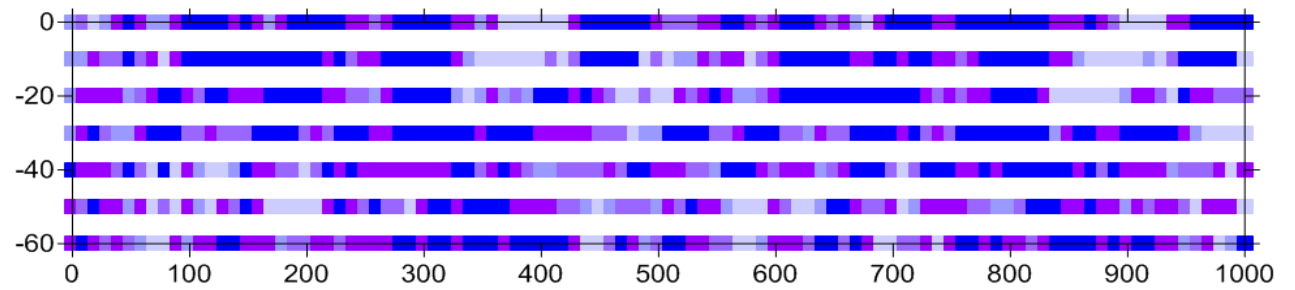


Figure 3-29: Classed post maps of lab-measured n and the optimized K_s along the line source transect

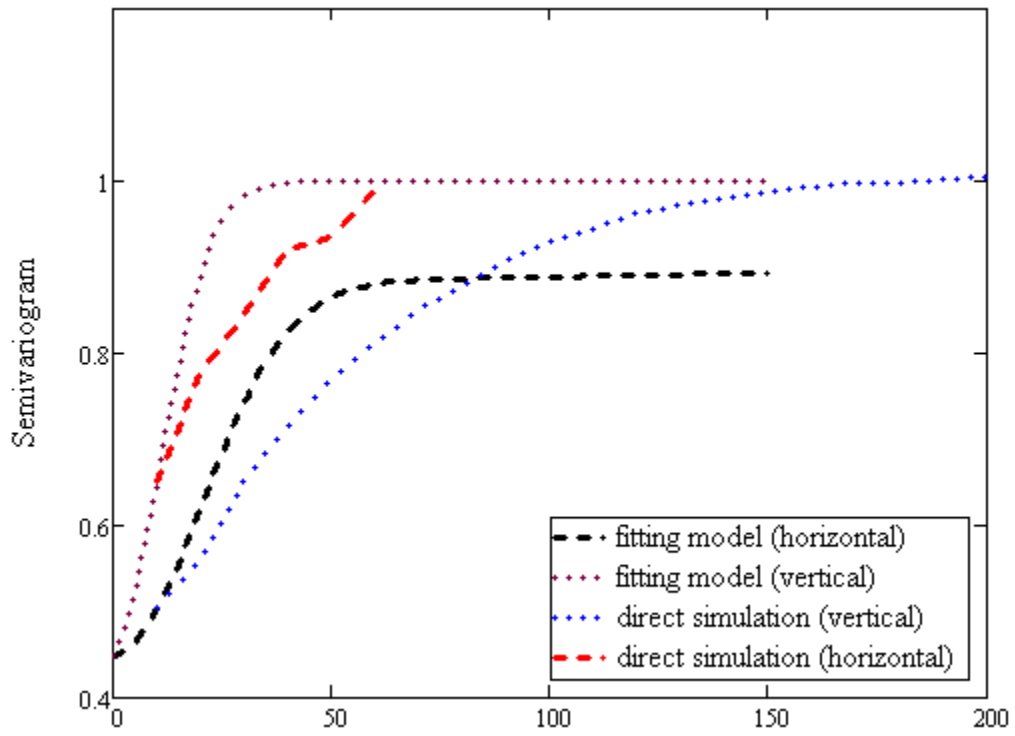


Figure 3-30: Comparison of the parametric variogram models and the corresponding empirical variograms of the simulated VG parameter θ_s

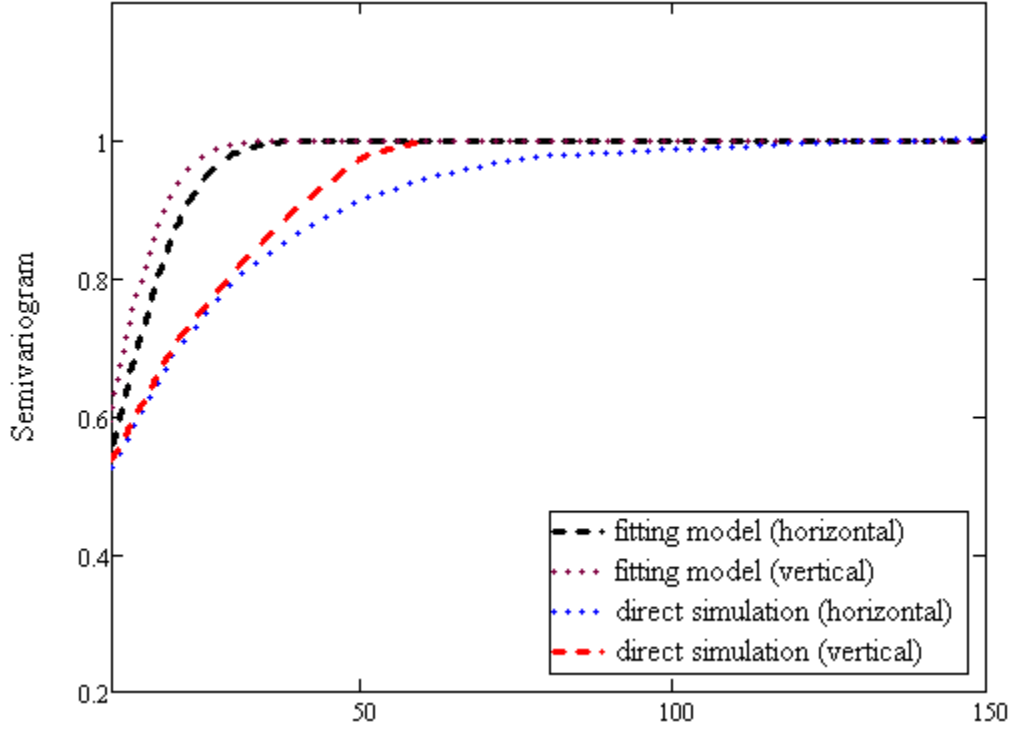


Figure 3-31: Comparison of the parametric variogram models and the corresponding empirical variograms of the simulated VG parameter α

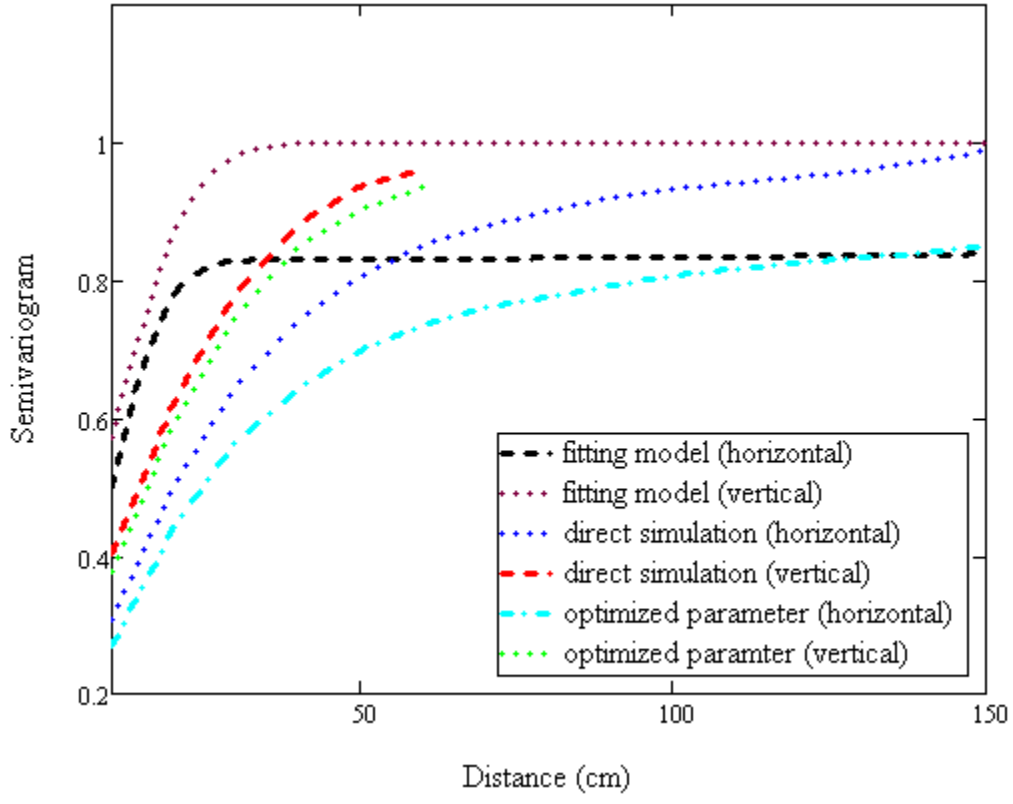


Figure 3-32: Comparison of the parametric variogram models and the corresponding empirical variograms of the simulated VG parameter n

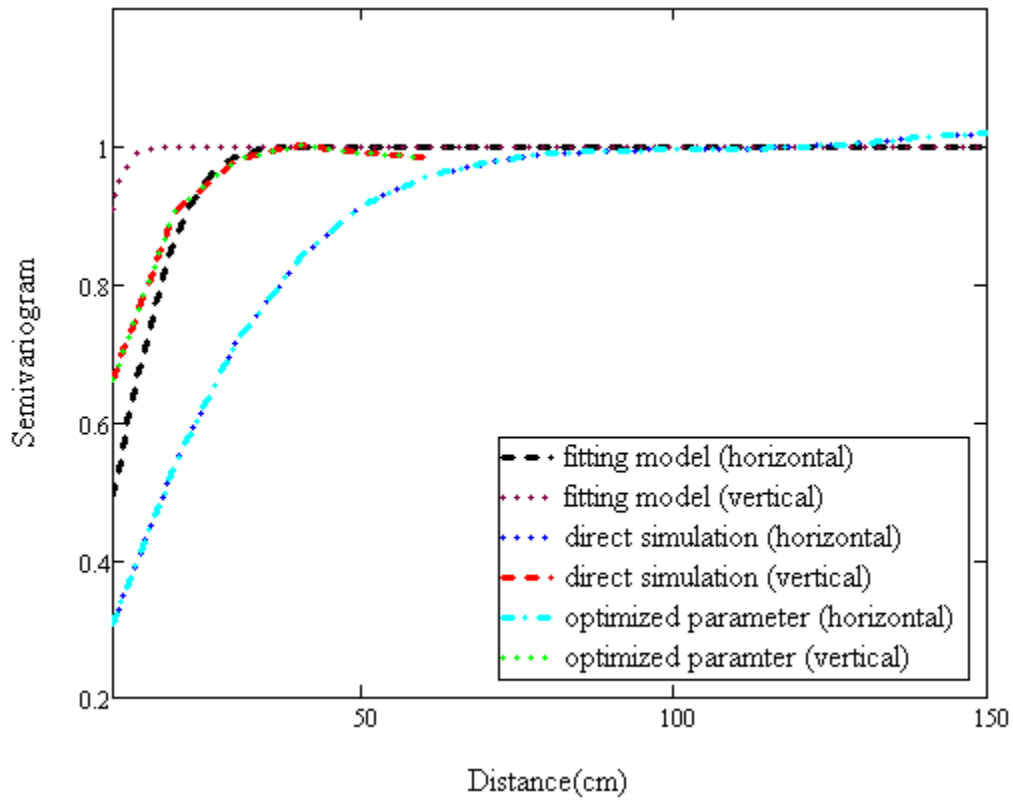


Figure 3-33: Comparison of the parametric variogram models and the corresponding empirical variograms of the simulated VG parameter K_s

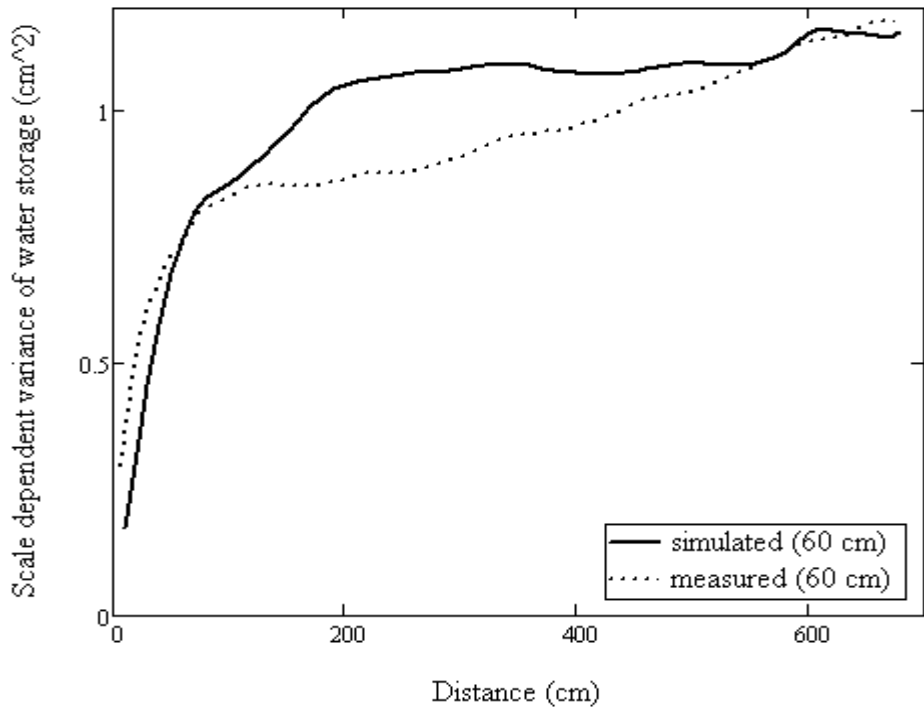
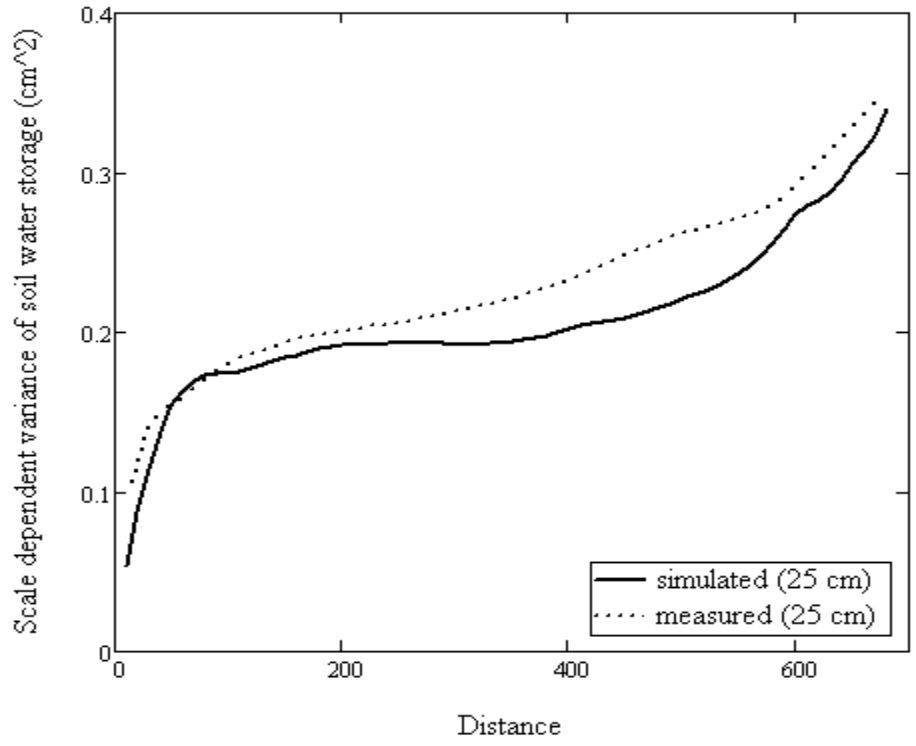


Figure 3-34: Spatial-scale dependent variance of average water storage of both 25 cm and 60 cm depth of both field measurement and numerical model simulation

4. General Discussion and Conclusion

4.1. Summary and contribution of this M.sc thesis

The main objective of this thesis was to get better understanding of the physics of infiltration into layered field soil for boundary condition typical for the onsite at-grade waste water treatment system (surface line source). In order to achieve this objective, numerical models were constructed to investigate flow and transport processes in heterogeneous soils. The heterogeneity of the field soil was simulated in two ways: in Section 2, the hydraulic properties were linearly scaled assuming Miller-similar media (Miller and Miller, 1956); in Section 3, the spatial pattern of the hydraulic properties of a field soil (Dyck and Kachanoski, 2009a, 2009b) was measured to generate the input van Genuchten parameters (van Genuchten, 1980) for the three-dimensional numerical model. The sensitivity of the input hydraulic heterogeneity on the hydraulic output of the numerical model was accessed. The major contributions and conclusions of this thesis are as following.

For the Miller-similar media (Section 2):

1. The Miller-similar scaling method (Miller and Miller 1956; Miller, 1980) was extended to layered soils. The cross-correlation between the hydraulic properties above and below the horizon was accounted by simulating the scaling factors continuously across the domain. This method can be used to verify the influence of cross-correlated horizons on the water flow process in a Miller-similar media.
2. Sensitivity analysis of the hydraulic heterogeneity and presence of layers on the hydraulic output of the numerical model, the vertical flux directly underneath the line source, corresponding water content, velocity and travel time, showed that the hydraulic heterogeneity and presence of layers had a significant influence on the hydraulic output. The hydraulic output of the soil was more sensitive to the hydraulic heterogeneity at the soil depth close to the surface line source than at greater depth.
3. The difference between the maximum and minimum solute travel time (10 days) directly underneath the surface line source due to different hydraulic heterogeneity was expected

to have significant influence on the remediation of the pathogenic bacteria and viruses.

For the input van Genuchten (vg) parameters generated from measured hydraulic properties (Section 3):

1. The soil hydraulic heterogeneity of the layered field soil was generated according to spatial pattern of the laboratory measured soil hydraulic properties from a two-dimensional transect. The spatial pattern of the hydraulic properties was extended to a three-dimensional domain and the properties of the two horizons were estimated simultaneously in order to account the cross-correlation of the hydraulic properties above and below the horizon interface. In this case, data from a surface line source experiment were available and the output of the numerical model could be compared with actual field measurements.
2. The simulated hydraulic outputs (average and variance of the water storage) were found to be sensitive to the variation of the input VG parameters.
3. The limitation of the model was found as: the numerical model failed to predict the variance of the field measured water

storage in the 60-cm depth at transient state. Reasons for discrepancies between observed and simulated flow may be: that the spatial pattern of the generated input VG parameters for the model was slightly different from the spatial pattern of the measured data because only one realization from the random field generation was used and the effect of horizon interface on the hydraulic process.

4.2. Future research

There are several approaches for the future research. For example, the numerical models (Section 2) can be utilized to further quantify the influence of spatial variance and correlation under different surface line source magnitudes boundary condition to water flow process. The influence of the shape of the soil horizon interface can be incorporated into the numerical model to test the influence of the horizon interface on the water flow process in transient state versus steady state.

4.3. References

- Dyck, M. F. and R. G. Kachanoski. 2009a. Measurement of transient soil water flux across a soil horizon interface. *Soil Sci. Soc. Am.J.* 73:1604-1613.
- Dyck, M. F. and R. G. Kachanoski. 2009b. Measurement of steady-state soil water flux across a Soil Horizon Interface. *Soil Sci. Soc. Am.J.* 73: 1786-1795.
- Miller, E. E., and R. D. Miller. 1956. Physics theory for capillary flow phenomena. *J. Appl. Phys.* 27:324-32.
- Miller, E. E., 1980. Similitude and scaling of soil water phenomena. In *Applications of soil Physics*, ed. D. Hillel, 300-318. New York: Academic Press.
- van Genuchten, M.Th, 1980. A closed-form equation for predicting the hydraulic conductivity of unsaturated soils. *Soil sci. Am.J.*, 44 (5): 892–898.

APPENDIX A: HYDRUS software package for simulating two and three-dimensional water flow, heat and solute transport

The numerical software packages, HYDRUS (two-dimensional or three-dimensional) simulate water flow, heat and solute transport in both saturated and unsaturated media with a large degree of complexity and dimensionality (Šimůnek, 2008). The HYDRUS software package consists of an easy-understand and interactive graphics-based user interface and numerical solver. The HYDRUS program can be used to predict water flow process and heat solute transport by numerically solving Richard's equation and advection-dispersion equation respectively. The water and solute movement can be analyzed with various types of hydraulic models, such as Van Genuchten's hydraulic model, Modified Van Genuchten hydraulic model, Gardner's hydraulic model, Brooks-Correy hydraulic model, etc.

The program of HYDRUS uses finite element spatial discretization, which may consider rectangular, or hexahedral finite element mesh and irregular shape of transport domain. These features make the program able to handle more complicated geometry, (Šimůnek and van Genuchten 2007) minimizes numerical error when

considering regions with sharp gradients. The orientation and geometry of the domain may be two-dimensional vertical or horizontal, or three-dimensional.

Depending on the specific type of simulation, the simulated results from the HYHRUS program may consist of the hydraulic output as a function of time (hydraulic pressure head, water content, velocity, and temperature), the run time information, mass balance information, the soil hydraulic properties, or inverse solution of an inverse problem, etc. The program presents the results of simulations in forms of contour maps isoclines, spectral maps and velocity vectors.

References

- Šimůnek, J., M. Šejna and M. Th. van Genuchten, 2007. The HYDRUS software package for simulating the two- and three-dimensional movement of water, heat and multiple solutes in variably-saturated media. User Manual, Version 1.02. PC Progress, Prague, Czech Republic.
- Šimůnek, J. and M. Th. van Genuchten, 2008. Modeling nonequilibrium flow and transport processes using HYDRUS Vadose Zone J. 7(2) pp782-797.